Application of Nanocrystalline-Graphite (GUITAR) in Electrochemical Energy Storage and Sensing

A Dissertation

Presented in Partial Fulfillment of the Requirements for the

Degree of Doctorate of Philosophy

with a

Major in Chemistry

in the

College of Graduate Studies

University of Idaho

by

Md Humayun Kabir

Major Professor: I. Francis Cheng, Ph.D.

Committee Members: Dean Edwards, Ph.D.; Vivek Utgikar, Ph.D.; Peter B. Allen, Ph.D.

Department Administrator: Ray von Wandruszka, Ph.D.

August 2019

Authorization to Submit Dissertation

This dissertation of Md Humayun Kabir, submitted for the degree of Doctor of Philosophy with a Major in Chemistry and titled "Application of Nanocrystalline-Graphite (GUITAR) in Electrochemical Energy Storage and Sensing," has been reviewed in final form. Permission, as indicated by the signatures and dates given below, is now granted to submit final copies to the College of Graduate Studies for approval.

Major Professor:

_____ Date: _____

I. Francis Cheng, Ph.D.

Committee Members:

_____ Date: _____

Dean Edwards, Ph.D.

_____ Date: _____

Vivek Utgikar, Ph.D.

_____ Date: _____

Peter B. Allen, Ph.D.

Department Administrator:

_____ Date: _____

Ray von Wandruszka, Ph.D.

Abstract

Nanocrystalline-graphite produced from pyrolyzed vegetable oil has properties that deviate from typical graphites, but is similar to the previously reported Graphite/Graphene from the University of Idaho Thermolyzed Asphalt Reaction (GUITAR). GUITAR has the classical basal and edge plane morphology similar to graphite and graphene with similar X-ray photoelectron spectroscopy (XPS), Raman and IR characteristics. However, GUITAR is electrochemically different from both graphite and graphene. GUITAR has (i) faster heterogeneous electron transfer rate across its basal plane, (ii) an electrochemical window that exceeds graphitic materials by 1 V and (iii) higher corrosion resistance beyond graphitic materials. To discover the structural basis for these properties, characterization of GUITAR was investigated with Raman and X-ray photoelectron spectroscopies, density, X-ray diffraction (XRD), thermogravimetric and elemental analyses (see Chapter-1). These characteristics established GUITAR as a new form of carbon different from previous forms. The aforementioned beneficial electrochemical properties of GUITAR are examined for application in different fields like as electrochemical energy storage (vanadium redox flow battery – VRFB, chapter-2) and electrochemical sensing of important electroactive analytes (chemical oxygen demand – COD and free chlorine – HOCl and ClO^-, see chapter 3 and 4, respectively). The results explained in this dissertation show that GUITAR is an excellent alternative material for the negative electrode in the vanadium redox flow battery and an effective sensor material for determination of chemical oxygen demand and free chlorine.

Acknowledgements

My deepest appreciation goes to Dr. I. Francis Cheng, for his guidance and mentorship throughout my Ph.D. study. Words can neither qualify nor quantify how helpful his guidance and advice have been. He helped shape my career and professional life. I am forever grateful for his myriad support. I would also like to appreciate my committee members: Dr. Dean Edwards, Dr. Vivek Utgikar and Dr. Peter B. Allen for dedicating their time, knowledge and experience to help shape my academic pursuit.

I am very thankful to the faculty and staff, who have created a friendly research environment at the Chemistry department, University of Idaho in diverse ways. In addition, I would like to thank Dr. and Mrs. Renfrew, Mr. Thomas F. Harland and Mr. Rao for all the scholarships. Many thanks to UI Chemistry graduate students, Bangladesh communities of UI and WSU, former and current lab mates, specially Dr. Isaiah Gyan and Dr. Haoyu Zhu. It was really great knowing each other and working together.

Dedication

This dissertation is dedicated to my elder brother (Md Hanif) and my wife (Kulsuma Akter).

Thank you for your countless support.

Table of Contents

List of Figures

List of Tables

Chapter 1: Introduction to GUITAR

"The sp^2-sp^3 carbon hybridization content of nanocrystalline graphite from pyrolyzed vegetable oil, comparison of electrochemistry and physical properties with other carbon forms and allotropes." CARBON 2019, vol. 144, pp. 831-840.

Abstract

Nanocrystalline (nc) graphite produced from pyrolyzed vegetable oil has properties that deviate from typical graphites but is similar to the previously reported Graphite from the University of Idaho Thermolyzed Asphalt Reaction (GUITAR). These properties include (i) fast heterogeneous electron transfer (HET) at its basal plane and (ii) corrosion resistance beyond graphitic materials. To discover the structural basis for these properties, characterization of this nc-graphite was investigated with Raman and X-ray photoelectron spectroscopies, nano-indentation, density, X-ray diffraction (XRD), thermogravimetric and elemental analyses. The results indicate that this nc-graphite is in Stage-2 of Ferrari's amorphization trajectory between amorphous carbon (a-C) and graphite with a sp^2/sp^3 carbon ratio of 85/15. The nanocrystallites size of 1.5 nm from XRD is consistent with fast HET rates as this increases the density of electronic states at the Fermi-level. However, d-spacing from XRD is 0.350 nm vs. 0.335 for graphite. This wider distance does not explain its corrosion resistance. Literature trends suggest that increasing sp2 content in a-C's increase both HET and corrosion rates. While nc-graphite's HET rate follows this trend, it exhibits higher than predicted corrosion resistance. In general, this form of nc-graphite matches the best examples of boron-doped diamond in HET and corrosion rates.

1.1 Introduction

Carbon electrodes offer the promise of low cost and high performance relative to other materials. The element itself is capable of forming many types of allotropes, each with a unique set of physicochemical properties. In electrochemical applications, the aqueous potential window and heterogeneous electron transfer (HET) kinetics with dissolved redox species are important from the standpoint of sensors and with electrochemical energy conversion and storage. [1,2,3,4] At the anodic potential limits, corrosion processes and water oxidation predominate (Reactions 1.1a and 1.1b).

$C + 2H_2O \rightarrow CO_2 + 4H^+ + 4e^-$ $E^0_{red} = 0.207$ V (1.1a)

$2H_2O \rightarrow O_2 + 4H^+ + 4e^-$ $E^0_{red} = 1.23$ V (1.1b)

On the other hand, at the cathodic potential limits, H_2 (g) evolution comes into consideration (Reaction 1.1c).

$2H^+ + 2e^- \rightarrow H_2$ $E^0_{red} = 0.00$ V (1.1c)

Slow electrode kinetics for the reactions above can increase effective stability up to a 2 V potential window on most graphitic electrodes. [5,6] In general, sp^3-C containing boron-doped diamond (BDD) and amorphous carbon (a-C) electrodes offer greater stability to corrosion than pure sp^2 carbon materials. [7,8,9,10] The sp^2/sp^3 ratio governs the chemical and physical characteristics of the carbon electrodes. In general, literature results suggest that increasing the sp^2 content will increase both rates of corrosion and HET kinetics. [5,6,7] The hybridization content (sp^2/sp^3 ratio) would also be important in determining atomic arrangement. Graphitic stacking would be expected of pure sp^2 materials, while structures with no layering would result from pure sp^3 materials. Most micrographs indicate that with

mixed sp^2-sp^3 a-C materials do not exhibit layered morphology. [11,12,13,14,15] However, in a computational study, Galli and coworkers examined an a-C consisting of 85% sp^2 and 15% sp^3, and predicted that the C atoms would form into a layered material. [16] The simulation also indicated that this a-C will have an increased density of electronic states at the Fermi level relative to crystalline graphite, which is expected to increase HET rates. [16,17]

The previously reported material, graphite (or graphene) from the University of Idaho Thermolyzed Asphalt Reaction (GUITAR) was initially mistaken for a graphite, as it has some physical and morphological similarities with sp^2-hybridized carbon materials. [18,19] Those initial characterizations best described this material as nanocrystalline (nc) graphite. In the search for increasing yields and scalability, the precursors for this material has varied. In this contribution, we examined a nc-graphite produced from pyrolyzed vegetable oil rather than the previously reported precursors. However, given that this material exhibits identical electrochemical, Raman spectroscopic, and x-ray diffraction characteristics as the previous GUITAR materials from this group, it will be referred to from this point on as GUITAR. [18,19,20,21]

Due to the combination of GUITAR's resistance to corrosion and fast HET rates, several investigations are underway examining applications in ultracapacitors, fuel cells, batteries and sensors. [4,20,21] In order to understand the stark differences in electrochemical characteristics between graphite and GUITAR, cyclic voltammetry, X-ray photoelectron spectroscopy (XPS), X-ray diffraction (XRD), and Raman studies were conducted to assess the sp^2/sp^3 carbon content and d-spacing of GUITAR with the goal of determining both shared and distinct structural characteristics with other forms of carbon. Density measurements,

elemental, thermogravimetric (TGA), and hardness analyses were conducted to augment those studies. These measurements allow the placement of GUITAR in the sp^2-sp^3 carbon-H ternary phase diagram so that its electrochemical characteristics be compared to the carbons of similar compositions. Quantitative measurements of corrosion were conducted by Tafel studies to ascertain any correlation with sp^3 content, and for comparison with anodically stable carbon electrodes with similar sp^2/sp^3 ratios.

1.2 Experimental

1.2.1 Chemicals

Deposition targets were constructed from quartz tubes (Technical Glass Products, Inc., Painesville Twp., OH, USA) cut into 2 cm x 0.5 cm wafers. The precursor for GUITAR deposition was vegetable (soybean) oil obtained from WinCo Foods grocery store in Moscow, Idaho, USA. The tube furnace was a Hevi Duty Electric Co., type M-3024. The peristaltic pump, steel injection needle, tubing, and thermocouple were acquired from McMaster-Carr (IL, USA). Nitrogen gas (>99.5 %) was supplied from Oxarc (WA, USA). Paraffin wax and high vacuum grease were obtained from Royal Oak Enterprises (GA, USA) and Dow Corning (MI, USA) respectively. Pyrolytic graphite foil (Lot # 157161) and graphite felt (KFD 2.5 EA) were obtained as gift from SGL Carbon Company (PA, USA). Highly ordered pyrolytic graphite (HOPG, ZYA) was obtained from SPI Supplies (PA, USA), with a mean step density 0.5±0.1 $\mu m/\mu m^2$, as reported by Unwin et al. [22] Sulfuric acid (96.3%) was purchased from J.T. Baker (NJ, USA). All aqueous stock solutions were prepared with deionized water, which was further purified by passage through an activated carbon purification cartridge (Barnstead, model D8922, Dubuque, IA).

1.2.2 GUITAR Synthesis from Vegetable Oil and Electrode Preparation

GUITAR samples were prepared via a chemical vapor deposition (CVD) method with the apparatus shown in Figure 1.1. This revised method obviates the need for sulfur as required in previous studies. [18,19,23] The tube furnace was heated to a temperature of 900 ^{o}C and the carrier gas (N_2) purifier was preheated to 400 ^{o}C in a gas chromatograph gas purifier oven

(Supelco, PA, USA). The deposition targets (2 cm x 0.5 cm, quartz slides) were positioned inside the quartz tube and the end was plugged with a small exhaust tube wrapped in ceramic wool to prevent O_2 from entering the chamber. The system was purged with preheated N_2 at a flow rate of 4.2 L/minute for 5 min prior to the start of run. Vegetable oil precursor was injected into the tube furnace at a rate of 5 mL/min for a total deposition time of 30 min. The tube furnace was then allowed to cool down under N_2 before the GUITAR coated substrates were removed.

Preparation of GUITAR working electrodes is described in previous publications [18,23]. GUITAR coated quartz slides were waxed leaving an exposed basal plane area of 0.1-0.2 cm^2. The graphite foil working electrodes were prepared by the same method.

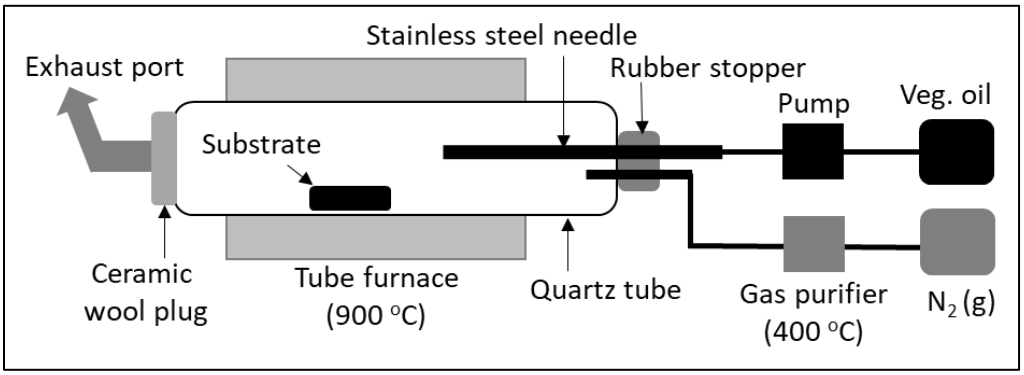

Figure 1.1. Schematic of GUITAR synthesis via chemical vapor deposition (CVD) method.

1.2.3 Characterization of GUITAR

Scanning electron microscope (SEM) images were obtained with a Zeiss Supra 35 SEM (Carl Zeiss, Germany). Density analyses were conducted by Micromeritics Particle Testing Authority (Norcross, GA, USA). Midwest Microlab (Indianapolis, IN, USA) did the elemental analysis for C, H, N and O. The XPS apparatus was built in-house at Oklahoma State University

and performed in a vacuum chamber with a base pressure of 1×10^{-10} Torr. Measurements were made with the Al Kα emission line (1486.6 eV) and a hemispherical energy analyzer with a resolution of 0.025 eV. All spectra were acquired at room temperature. The XPS peaks were fit with a Gaussian curve after performing a Shirley background subtraction. The FWHM were held at a constant value for all peaks. Raman spectrum was acquired with a Horiba LabRAM HR Evolution Raman microscope (Irvine, California) using a laser excitation wavelength of 514.5 nm. Hardness values were measured using a Hysitron TS 75 TriboScope nanoindenter head mounted on a Bruker Dimension 3100 AFM. A diamond tip Berkovich probe (Hysitron TI-0039) with a 100 nm nominal radius of curvature was used to create the indents. A series of indentations were carried out at loads varying from 0.3-25 mN.

Thermogravimetric analyses (TGA, Perkin Elmer TGA-7, Waltham, MA, USA) were conducted under air atmosphere (21 standard cubic centimeters per minute, or SCCM, flow rate) from ambient temperature to 900 °C with a heating rate of 10 °C/min. Samples used in TGA consisted of 1-2 mg of particles with a size <1 mm. Powder X-ray diffraction (XRD) was conducted on a Siemens D5000 Diffractometer (Germany) equipped with an FK 60-04 air insulated XRD tube and a Cu anode. The spectra were taken with Cu K-alpha radiation (0.154 nm) at 40 kV and 30 mA in the range of 2θ = 0-80° at room temperature. Electrochemical measurements were carried out at room temperature using a Gamry PCI4/750 potentiostat (Gamry Instruments, Warminster, PA, USA). The reference electrode was an Ag/AgCl/3 M NaCl system (0.209 V vs. SHE). A KFD graphite felt (15 cm x 10 cm) served as the counter electrode. Tafel polarization measurements were carried out in N_2 saturated 1.0 M H_2SO_4 using a single compartment 1.0 L volume cell. The working electrodes were allowed to

equilibrate in electrolyte solutions for ≥ 1 hour to attain an equilibrium or open circuit potential (E_{ocp}) prior to the start of polarization. The working electrodes were scanned from -0.5 to +1.0 V vs. Ag/AgCl at a scan rate of 1 mV/s. These experiments were performed under vigorously stirred conditions. The standard HET rate constants (k^0, cm/s) for $Fe(CN)_6^{3-/4-}$ on GUITAR and other carbon electrodes were calculated using the Nicholson method as described in reference 24, and also determined by modeling with DigiSim version 3.03b (Bioanalytical Systems, Inc. West Lafayette, IN, USA). The k^0 values obtained from modeling agreed with the Nicholson method. Above a cyclic voltammetric potential peak separation (ΔE_p) greater than 212 mV, only DigiSim was used for the determination of k^0 for literature carbon materials, as Nicholson's analysis is limited to ΔE_p 212 mV. The transfer coefficient (α) and diffusion coefficient (D) for $Fe(CN)_6^{3-/4-}$ are assumed as 0.5 and 6×10^{-6} cm^2/s respectively, as reported in literature. [25,26,27]

1.3 Results and Discussion

1.3.1 Micrographs of the *nc-Graphite, GUITAR and Highly Ordered Pyrolytic Graphite (HOPG)*

Optical and scanning electron micrographs show GUITAR has clearly discernable basal and edge planes with a layered structure, similar to previous synthetic methods and to graphites and graphenes. [18,19] Figure 1.2 illustrates these configurations and similarities between GUITAR and highly ordered pyrolytic graphites (HOPG). However, an important feature observed with graphites is missing with GUITAR as its basal plane is flat and featureless to the resolution of SEM. On the other hand, the basal plane of HOPG exhibits its characteristic step defects. The mean step density of the HOPG (ZYA) is calculated as 0.5±0.2 μm/μm^2 using SEM images. This value agrees with the result reported by Unwin et al. (0.5±0.1 μm/μm^2, using atomic force microscopy). [22]. No step defects have been observed on the basal plane of GUITAR in over 200 SEM images over several years (2010-2018).

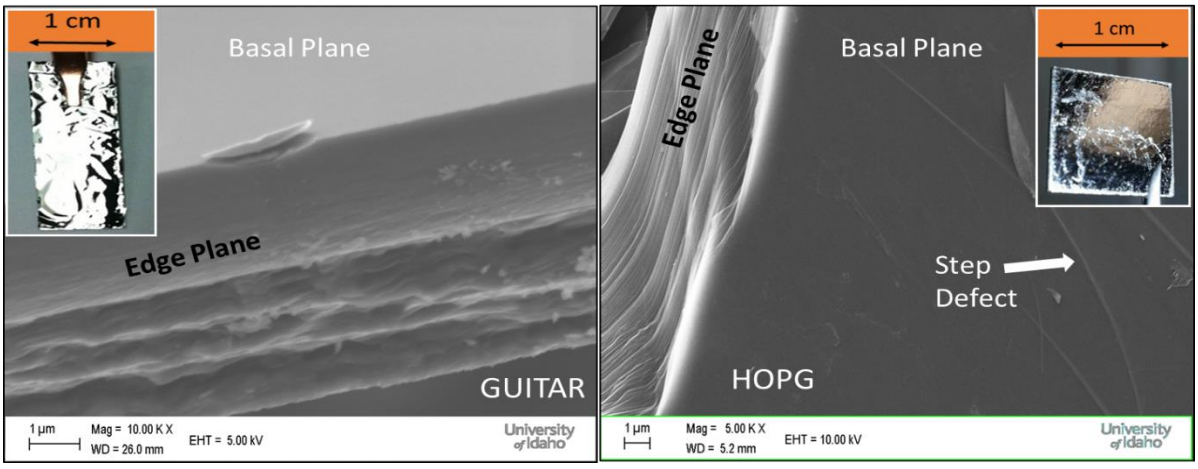

Figure 1.2. Photographs (insets) and scanning electron micrographs illustrating morphological similarities between GUITAR and highly ordered pyrolytic graphite (HOPG). Both show clear basal and edge plane configurations.

1.3.2 Electrochemical Properties of GUITAR

Despite the morphological similarities, GUITAR has electrochemical properties that diverge from graphites and graphenes. These include fast HET rate across its basal plane (BP) and resistance to corrosion as measured by cyclic voltammetry. The results obtained with the newest and simplified synthetic process of this contribution are in concordance with previous studies. [19,20,21,28] The $Fe(CN)_6^{3-/4-}$ redox probe is often employed to measure these rates on carbon materials (Reaction 1.2). [29,30,31]

$$Fe(CN)_6^{3-} + e^- \rightleftharpoons Fe(CN)_6^{4-} \qquad E^0_{red} = 0.430\ V \qquad (1.2)$$

Cyclic voltammetric experiments were conducted on GUITAR electrode with 1 mM $Fe(CN)_6^{3-}$ in 1 M KCl at 50 mV/s with a measured ΔEp of 65 mV. This replicates previous studies of GUITAR with various synthetic methods. [19,20,21] That ΔEp corresponds to a standard rate constant (k^0) of 0.03 cm/s as calculated from the Nicholson method as well as determination by modelling with DigiSim software. This exceeds the basal planes of other graphites and graphenes by 2-6 orders of magnitude [19,29,32,33]. Slow kinetics on the BP of crystalline graphites is attributed to the low density of electronic states (DOS) at the Fermi-level. [29,30] On the other hand, the defect-rich nanocrystallinity of GUITAR would increase that DOS. [19,30] The measured 200 $\mu A/cm^2$ anodic limit of 1.9 V vs. Ag/AgCl in 1.0 M H_2SO_4 at 50 mV/s matches previous studies. [19,20] This is 300 to 500 mV greater than graphites in various electrolytes. [5,6,19,20] This resistance to corrosion is attributed to the lack of electrolyte intercalation through the edge and basal planes of GUITAR as discussed in previous studies. [19] The total potential window at 200 $\mu A/cm^2$ in 1 M H_2SO_4 is 3 V, which surpasses graphites by 1 V. [19,20,21]

1.3.3 Density of GUITAR is Consistent with Graphites and Amorphous Carbons

Skeletal and bulk densities of GUITAR were measured as 1.95 and 0.57 g/cm^3 respectively. This is consistent with literature graphites that have skeletal and bulk densities of 1.6-2.3 g/cm^3 and 0.22-0.59 g/cm^3 respectively. [34,35,36] It is also similar to the skeletal densities of a-C and hydrogenated amorphous carbons (a-C:H) which range between 1.6-2.2 and 1.2-2.4 g/cm^3 respectively. [35,36,37,38] The skeletal density of GUITAR lies well below that of diamond (3.51 g/cm^3) and DLC (2.35-3.26 g/cm^3), but above that of glassy carbon (1.3-1.5 g/cm^3). [36,39,40] Also of interest is the agreement of the skeletal density for GUITAR with the computational value for an a-C consisting of 15% sp^3-C reported by McKenzie (see Figure 21 therein). [41] Based on density, GUITAR can be placed in the range expected of graphitic to a-C materials.

1.3.4 Elemental Analysis Indicates GUITAR is a Hydrogenated Carbon Material

The results of this study yield 98.72% C, 0.20% O and 1.08% H by mass (88.35% C, 0.14% O and 11.51% H by mole) for GUITAR. This matches results obtained with XPS analysis below. It is noteworthy that GUITAR is one of the purest carbon films grown by a CVD method, and significantly, shows no metal contamination and negligible oxygen content. Literature CVD-grown graphenes typically contain metal contamination and 5-30 wt% oxygen. [42,43,44] Furthermore, elemental analysis indicates that GUITAR possesses more hydrogen content that would be expected of most graphites but within the range of graphite-like hydrogenated a-C (GLCH, <20 atomic %). [45]

1.3.5 XPS Analysis Indicates that GUITAR is 15% sp^3-Carbon

Figure 1.3A shows the full scan XPS spectrum of GUITAR, where only the C1s peak is observed. This agrees with the results from elemental analysis. In Figure 1.3B the deconvolved C1s peak reveals 3 components: sp^2-C (284.2 eV) at 85.0% abundance, sp^3-C (285.4 eV) at 15.0%, and a satellite peak typical of sp^2 carbon at 286.9 eV. [46] The sp^2 content of GUITAR is close to, but slightly below that of literature graphites, which range from 90 to 100%. [47,48] In contrast, the sp^2 carbon content of a-C and DLC electrodes varies from 10-75%. [7,49,50,51] Another graphite-like material, turbostratic carbon consists of 70% sp^2 carbon. [52] This places GUITAR's sp^2 content midway between the lower bound of graphites and the upper end of a-C.

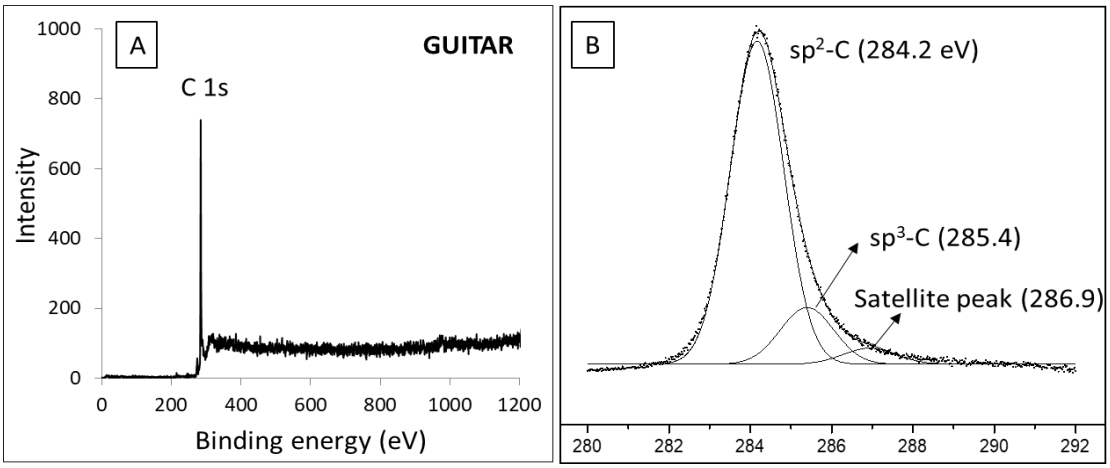

Figure 1.3. (A) Wide scan XPS spectra of GUITAR and (B) Deconvolved peaks of the C1s signal.

1.3.6 Raman Studies of GUITAR Indicate that it has Characteristics of Nanocrystalline Graphite and Graphite-Like Hydrogenated a-C

Figure 1.4 illustrates the Raman spectrum of GUITAR obtained with a laser excitation wavelength of 514.5 nm. In graphitic materials the G-band (1575-1600 cm^{-1}) is associated with the E_{2g} vibrational mode within the graphene lattice, while the D-band (1350-1380 cm^{-1}) is associated with a breathing mode that appears due to defects in that lattice. [53,54] For GUITAR, the ratio of the intensities, I(D)/I(G) = 1.16 with the D and G band positions at 1359 and 1591 cm^{-1} respectively. Using that data in the Raman analysis of Figure 5 in reference [45] yields a H atomic % of ~10% which is in good agreement with the elemental analysis of this study (11.51% H). In Figure 5 of reference [49], the G-band position of GUITAR (1591 cm^{-1}) is found to be intermediate to nano-crystalline graphite (nc-G, 1600 cm^{-1}) and graphite-like hydrogenated a-C (GLCH, 1560 cm^{-1} and 16% H).

A Raman spectrum of GLCH with 12% atomic H that could not be located in literature. GLCH with 16% H differs significantly from GUITAR with reported D and G band positions at 1385 and 1569 cm^{-1} respectively, and I(D)/I(G) = 0.60. [14] Another carbon material with exposed nc-graphene edges and an sp^2-C content of 85-87% has similar Raman and electrochemical characteristics (see Section 1.3.11) with GUITAR. [55] Ferrari's amorphization trajectory offers further insights based on the placement of carbon materials in one of three stages, (1) graphite to nanocrystalline graphite (nc-G, 100% sp^2), (2) nc-G to a-C (up to 20% sp^3) and (3) a-C to tetrahedral a-C (ta-C, up to 85% sp^3). Based on G-positions and I(D)/I(G) ratios, GUITAR is in Ferrari's Stage 2, near the transition with Stage 1. The reported GLCH with 16% H is again in Stage 2 but near the transition to Stage 3. [56,57] The full width at half

maximum (FWHM) of the G-band in Figure 1.4 of 79 cm^{-1} gives an L_a (crystal grain size) of 2-5 nm based on an analysis by Ferrari and Robertson. [57] This is consistent with a previous investigation of GUITAR that gave a L_a of 1.5 nm and the XRD results below (see Section 1.3.10). [58 (manuscript submitted)]

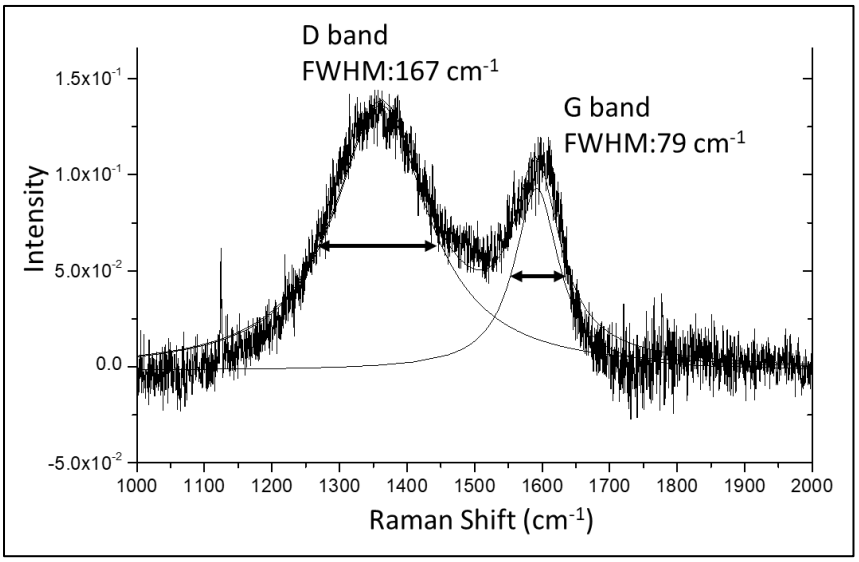

Figure 1.4. Raman spectrum of GUITAR at 514.5 nm laser excitation wavelength. The D and G bands peaks are at 1359 and 1591 cm^{-1} respectively with I(D)/I(G) intensity ratio of 1.16. The deconvolved peaks are shown with the FWHM of the D and G bands at 167 and 79 cm^{-1} respectively.

1.3.7 Hardness Analysis of GUITAR is Consistent with 15% sp^3-C Content

The hardness of carbon increases with increasing sp^3-C content with the transition from graphite to diamond covering 0 to 100 gigapascals (GPa). [59,60] For GUITAR the hardness is 5.6 ± 1 (n = 20) GPa as measured via nanoindentations. Figure 1.5 illustrates that GUITAR, with its 15% sp^3-C content as obtained by XPS, lies along the linear trend between 0-100% sp^3 when compared with other carbon materials in the literature. [14,59,60,61,62,63,64]

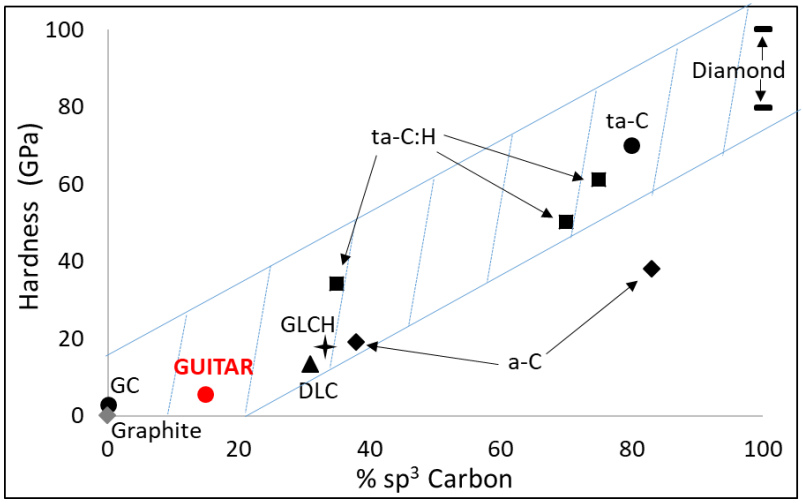

Figure 1.5. Hardness (GPa) vs. sp^3-C content for different carbon forms. Abbreviations: a-C = Amorphous Carbon, ta-C = Tetrahedral a-C, ta-C:H = Hydrogenated tetrahedral a-C. GLCH = Graphite like hydrogenated a-C, DLC = Diamond like Carbon, GC = Glassy Carbon.

1.3.8 Thermogravimetric analysis (TGA) of GUITAR Indicates a Graphite-like Homogeneous Mixture

From the analyses presented up to this point, GUITAR appears to be mostly graphitic in nature with some hydrogenated a-C content. Carbon materials with a heterogeneous mixture of graphitic and a-C exhibit two decomposition temperatures (T_d), one for each type of carbon. [65,66] To investigate this possibility in GUITAR, thermogravimetric analysis of both GUITAR and HOPG were conducted under flowing air, with the results shown in Figure 1.6. The T_d onsets are 640 and 700 °C for GUITAR and HOPG powders respectively as determined by the first derivative method ($\Delta m/\Delta T$). [67] The T_d of GUITAR conforms with literature graphites which range from 610-680 °C. [66,68,69] For comparison, the decomposition temperatures of other carbon materials are: 525-600 °C for BDD and 250-410 °C for both a-C and DLC.

[65,70,71,7273,74] Significantly, the single T_d of GUITAR indicates a homogeneous composition of graphite-like carbon, rather than a mixture that includes a-C.

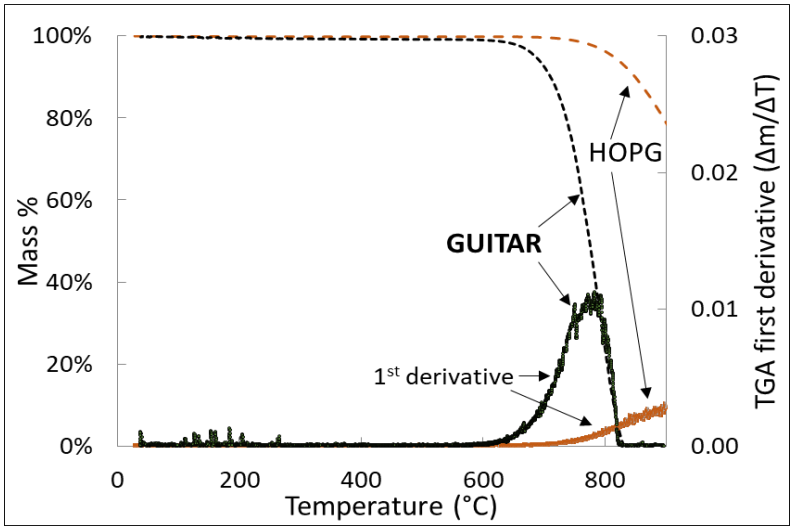

Figure 1.6. Thermogravimetric (TGA) curves of GUITAR and HOPG in the presence of air.

1.3.9 Placement of GUITAR in the sp^2-sp^3 Carbon-Hydrogen Phase Diagram is between Graphite and GLCH

Figure 1.7 illustrates the carbon ternary phase diagram. [45] Based on the analyses thus far, the position of GUITAR is in the border region of GLCH (graphite like hydrogenated amorphous carbon) using the Ferrari and coworkers classification system. These materials have less than 20 atomic % H with high sp^2-C content. [45] This placement is consistent with the Raman spectrum, indicating that GUITAR is intermediate between nc-graphite and GLCH.

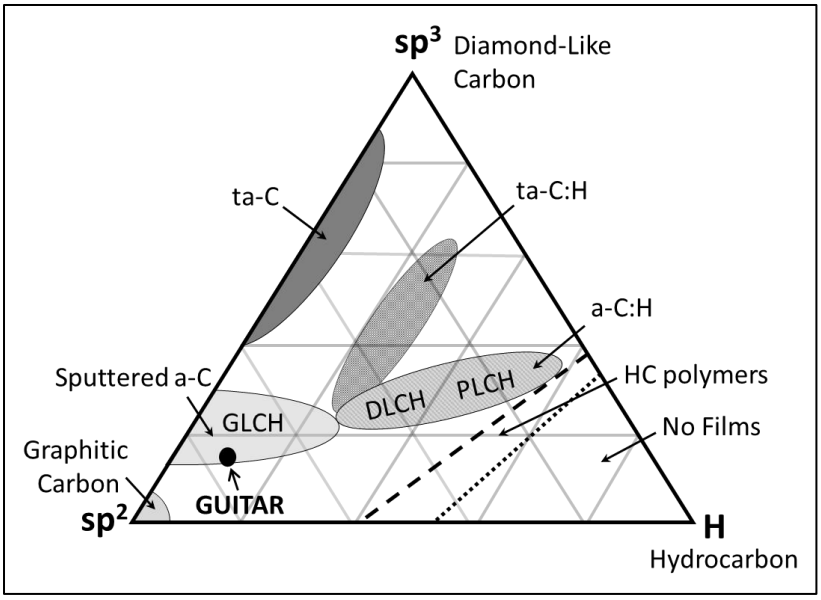

Figure 1.7. Placement of GUITAR (75.1% sp^2-C, 13.2% sp^3-C and 11.5% H by mole) in the sp^2-sp^3-H ternary phase diagram for carbon. Abbreviations: a-C = Amorphous Carbon, a-C:H = Hydrogenated a-C, ta-C = Tetrahedral a-C, ta-C:H = Tetrahedral a-C:H, GLCH = Graphite like a-C:H, DLCH = Diamond like a-C:H and PLCH = Polymer like a-C:H.

1.3.10 Measurement of Crystallite Grain Size (L_a) and d-spacing by X-ray Diffraction, Relationships with Fast HET Rates and Resistance to Corrosion

Crystalline graphites typically exhibit relatively slow $Fe(CN)_6^{3-/4-}$ HET kinetics, although some studies indicate an initial fast rate with degradation after a few hours. [33,75] Sluggish HET kinetics is attributed to the low density of electronic states (DOS) near the Fermi-level of graphite [29,30]. The DOS increases with disorder in the graphite lattice, which increases the HET rate. This feature is hypothesized to be the basis of the relatively fast HET rate observed for BP-GUITAR (k^0 = 0.03 cm/s). The standard rate constant (k^0) for $Fe(CN)_6^{3-/4-}$ on BP-GUITAR matches that of edge plane HOPG, while surpassing the kinetics of BP HOPG by 10^6 [29,32]. Furthermore, GUITAR maintains excellent stability for k^0 over 24 hours. [19] The crystal grain

size (L_a) for HOPG is 100-1000 nm with $k^0 \approx 10^{-6}$ to 10^{-9} cm/s. [19,33] Based on $Fe(CN)_6^{3-/4-}$ HET rates the L_a for GUITAR is expected to be much smaller.

Figure 1.8 shows the XRD spectra of GUITAR and HOPG. GUITAR exhibits a strong basal reflection (002) peak at $2\theta = 25.4°$ which is close to classical graphites ($2\theta = 26.5\text{-}27°$). [76,77] A previous Raman study of GUITAR indicated a nano-crystallite grain size (L_a) of ~1.5 nm. [58] This is in good agreement with X-ray diffraction-based estimates of L_a = 1.6 nm as calculated in this study from Scherrer's law ($L_a = (K\lambda)/(B \cos\theta)$, where K is the crystallite shape factor = 0.94, λ is the X-ray wavelength, B is the full width at half maximum of the peak, and θ the Bragg angle. [78] The XRD analysis was also used to obtain the d-spacing of GUITAR and the reference HOPG material.

Generally, wider d-spacing enhances electrolyte intercalation, the initial step leading to electrode corrosion. [79,80,81] However, the d-spacing in GUITAR is calculated as 0.350 nm from Bragg's Equations ($n\lambda = 2d \sin(\theta)$, with n = 1), while the reference HOPG gives 0.335 nm, in agreement with the literature. [] It is apparent that GUITAR's d-spacing is wider than both graphites (0.335-0.340 nm) and glassy carbons (0.335-0.342 nm). [82,83,84,85] On multiwall carbon nanotubes (MWCNT) and onion-like carbons the d-spacing is 0.340-0.390 nm and 0.336 nm respectively. [86,87,88] GUITAR's d-spacing is most similar to turbostratic carbons (0.342-0.365 nm), coals (0.334-0.362 nm) and graphites with AA stacking (0.352-0.366 nm). [89,90,91,92,93,94] It is significant to note that micrographs of turbostratic carbon do not exhibit discernable layered structures as does GUITAR (Figure 1.2). [52] This increased d-spacing relative to graphites might be expected of nanocrystalline GUITAR as predicted by a

computational analysis by Belenkov, which calculates increase of d-spacing from 0.338 to 0.352 nm as L_a decreases from infinity to 0.6 nm. [95]

As increased d-spacing is associated with more facile electrolyte intercalation, the measured d-spacing runs contra to previous cyclic voltammetric studies of GUITAR which indicated no such behavior (Figure 4 in Ref. 19). [19,79] Computational models of a-C with the same sp^3 carbon composition of 15% as GUITAR predict the formation of inter-planar bonds in a layered graphite-like morphology. [16,17] Thus a possible hypothesis is that decreased electrolyte intercalation is from inter-planar bonds that prevent this process from occurring, increasing the corrosion resistance of GUITAR relative to graphites. [19] Future investigations will examine this hypothesis.

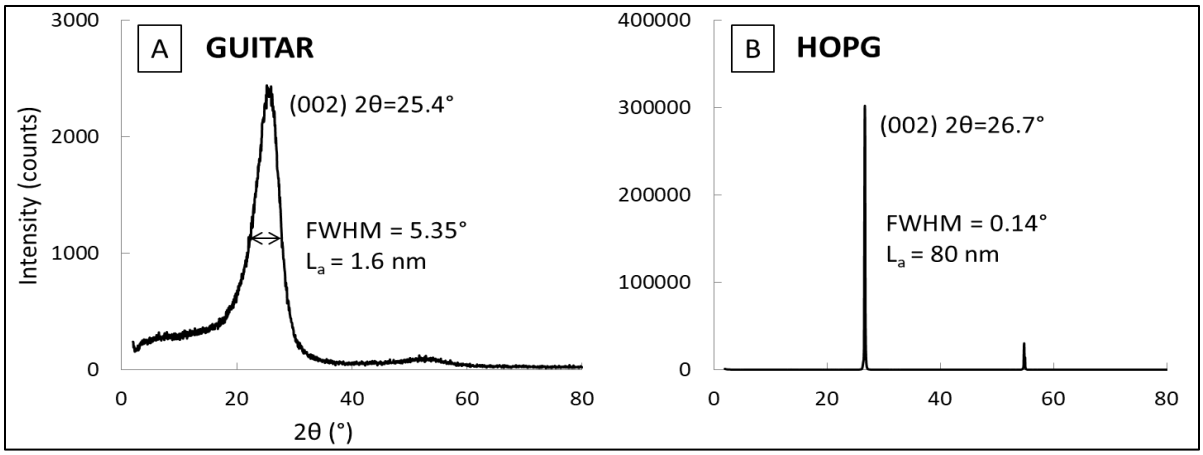

Figure 1.8. X-ray diffraction (XRD) analysis of (A) GUITAR and (B) Highly ordered pyrolytic graphite (HOPG).

1.3.11 The Role of Carbon Hybridization in the Corrosion of GUITAR: Tafel Studies

In contrast to graphene and graphites, the anodic potential limit of GUITAR is similar to materials containing sp^3-hybridized carbon. These include BDD, diamond-like carbons (DLC) which are primarily sp^3-C, and a-C which have various ratios of sp^2 and sp^3 carbons.

[5,6,7,19,96,97,98,99,100] The sp^2/sp^3 ratio plays a strong role in the electrochemical behavior of a-C electrodes. [5,7,97] As discussed in the Introduction, as that ratio increases, the HET kinetics for $Fe(CN)_6^{3-/4-}$ improve. On the other hand, increasing sp^2/sp^3 typically decreases resistance to corrosion. [5,7] The sp^2 content of GUITAR was established above as 85% by XPS. Relative to other anodically stable carbon materials, this is high and thus GUITAR would be expected to have lower resistance to corrosion relative to high sp^3 carbon materials, albeit with superior HET rates. Classical Tafel studies allow for the quantitative assessment of corrosion. Tafel studies were therefore conducted on GUITAR in 1.0 M H_2SO_4 using BP-pyrolytic graphite as a control, with the results shown in Figure 1.9.

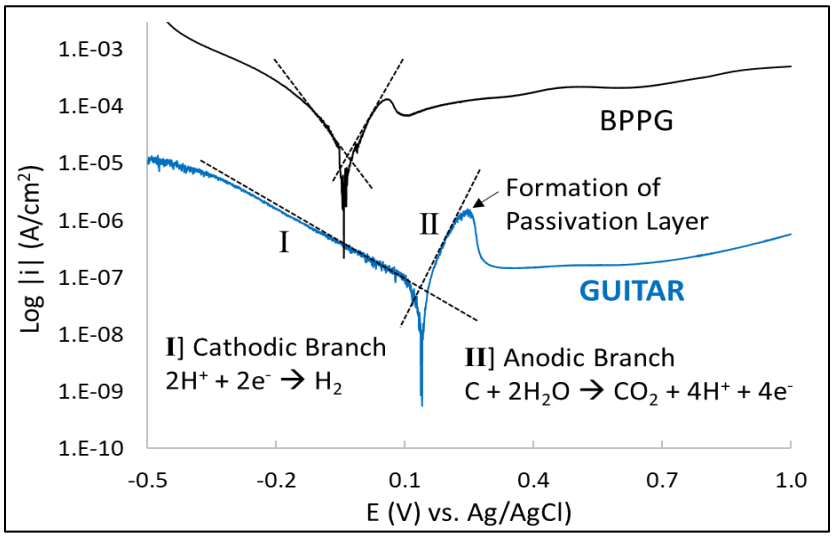

Figure 1.9. Tafel plots obtained at 1 mV/s for basal plane pyrolytic graphite (BPPG) and basal plane GUITAR in 1.0 M H_2SO_4. Extrapolation of Tafel plot to give i_{corr} and E_{corr} are shown along with the electrochemical reactions for the anodic and cathodic branches. Both BPPG and GUITAR exhibit the formation of a passivation layer.

Extrapolations of the Tafel plots for GUITAR in 1.0 M H_2SO_4 give an i_{corr} (corrosion current) of $2.4 \pm 1.5 \times 10^{-8}$ A/cm^2 and E_{corr} (corrosion potential) of 126 ± 15 mV vs. Ag/AgCl (both i_{corr} and E_{corr} are given as average ± standard deviation for 5 measurements). For comparison, the

BPPG sample gave i_{corr} of 1.9 x 10^{-5} A/cm^2 and E_{corr} of -40 mV vs. Ag/AgCl respectively, these values are typical of graphite electrodes. [10,101,102] The rate of corrosion for GUITAR is three orders of magnitude lower than the pure sp^2 material. The passivation layers evident in the Tafel plots for BPPG and GUITAR arise from the formation of oxide layers that inhibit electron transfer. These behaviors are typical for carbon electrodes. [10,101,102,103]

Figure 1.10A demonstrates the trend of corrosion rates increasing with sp^2 content for GUITAR and literature a-C and graphitic electrodes. [8,9,14,104,105,106,107,108]

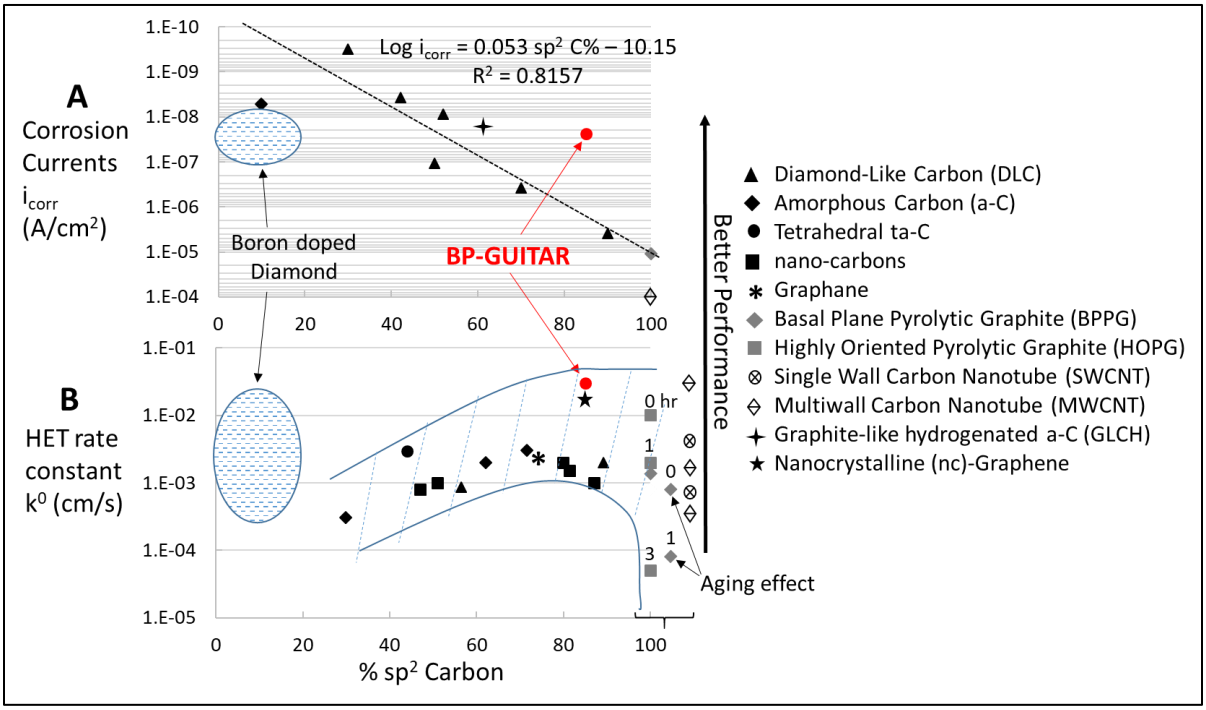

Figure 1.10. A) Corrosion currents (i_{corr}) vs. sp^2-C content for carbon electrodes. A linear trend for log (i_{corr}) vs % sp^2-C in amorphous carbon is noted. GUITAR is an outlier in that trend. B) HET rates for $Fe(CN)_6^{3-/4-}$ expressed as k^0 (cm/s). The outlined region is the observed trend for amorphous (30-85% sp^2) and graphitic (100% sp^2) carbons. HOPG and BPPG age over time in air or solution, which eventually lowers the HET rates.

A linear relationship between log i_{corr} and % sp^2-C is evident from the trend for amorphous and graphitic carbons. BDD (sp^3-C) electrodes do not conform to this trend. GUITAR is an outlier relative to that linear trend, exhibiting more resistance to corrosion than expected. Its

deviation from that trend is about 1.5 orders lower than what would be predicted for an a-C of GLCH with 15% sp^3-C content. This is unexpected given its wider d-spacing (0.350 nm) relative to graphite (0.335 nm).

Figure 1.10B illustrates the trend between the extent of sp^2 hybridization and literature $Fe(CN)_6^{3-/4-}$ HET rates (k^0, cm/s), which reach a maximum at 85% sp^2-C. [5,6,25,31,55,98108,109,110,111,112,113,114,115,116]. The literature values were obtained by Nicholson's method or DigiSim software as explained in the Experimental. [24] The BDD electrodes again fall outside the trends associated with the a-C to graphite series. The wide variation of the performance of the 100% sp^2-C material is based on aging effects that lower HET rates with exposure time to air or solution. [32] It is noteworthy that such effects are much less pronounced with the BP of GUITAR. [19] The MWCNT closest to the k^0 of BP-GUITAR (0.03 cm/s) is an edge plane material, and edge plane materials are known to exhibit faster HET rates compared to basal plane materials. [30,31] The nc-graphene electrode close to the k^0 of GUITAR also consists of ~85/15 sp^2/sp^3, in that case the investigators attribute that behavior to edge planes exposed to solution. [55] The investigators did not conduct Tafel i_{corr} analyses of their materials, but it is expected to match the performances of GUITAR based on their potential window of 3.2 V at 500 $\mu A/cm^2$ in 0.05 M H_2SO_4. Overall, in the literature search of this contribution, GUITAR maintains excellent performance matching BDD for its combination of excellent HET rate and high resistance to corrosion. Furthermore, it is expected that GUITAR will have lower production costs than many of the other carbon materials of Figure 1.10.

1.4 Conclusions

Relative to other methods of depositing a-C films, the method described in this contribution is significantly less expensive and simpler. It is expected that GUITAR will prove to be more economically viable for large-scale implementation relative to BDD. The latter requires high cost substrates, while GUITAR utilizes an inexpensive starting material (vegetable oil) that can be deposited on a variety of common substrates, including carbon fiber and stainless steel. It produces a graphitic film referred to as GUITAR, which, based on density measurements, elemental analysis, XPS, Raman spectroscopy, hardness, TGA, and XRD, indicates that GUITAR is a material intermediate of nc-Graphite and GLCH. It maintains the layered configuration of graphite, a morphology not seen with other amorphous carbons, but predicted by a 1989 computational analysis of a material with the identical composition of GUITAR. Significantly, that model predicts a higher DOS at the Fermi-level for this type of material than crystalline graphites, which may form the basis for the observed higher HET rates at its BP over graphites and graphenes. The XRD and a previous Raman analysis indicate that GUITAR has a grain size (L_a) of about 1.5 nm. This would increase the disorder within the BP and the DOS in GUITAR. Both the sp^2-C content of 85% and the wider d-spacing (0.350 nm) relative to graphites (0.335 nm), seem to run contra to the observed low rate of corrosion by Tafel analysis, which gave 2.4×10^{-8} A/cm^2. This is one of the lowest rates measured on any electrode material. An unexplored hypothesis is the formation of inter-planar bonds that would limit the intercalation of electrolytes, which is the nascent phase of corrosion. Compared to existing materials greater than 30% sp^2-C (a-C to graphite), GUITAR offers the highest performance in

terms of both resistance to corrosion and HET kinetics, matching the best examples of BDD in performance, with added versatility and lower cost.

1.5 References

1) Liangsheng Hu, Xiang Peng, Kaifu Huo, Rongsheng Chen, Jijiang Fu, Yong Li, Lawrence Y.S. Lee, Kwok Y. Wong, Paul K. Chu. Dominant Factors Governing the Electron Transfer Kinetics and Electrochemical Biosensing Properties of Carbon Nanofiber Arrays. ACS Applied Materials & Interfaces 2016, 8, 28872-28879.

2) Shengli Chen, Yuwen Liu, Junxiang Chen. Heterogeneous electron transfer at nanoscopic electrodes: importance of electronic structures and electric double layers. Chemical Society Reviews 2014, 43, 5372-5386.

3) P. Suvarnaphaet, S. Pechprasarn. Graphene-Based Materials for Biosensors: A Review. Sensors 2017, 17(10), 2161.

4) H. Kabir, I.O. Gyan, I.F. Cheng. Electrochemical modification of a pyrolytic graphite sheet for improved negative electrode performance in the vanadium redox flow battery. Journal of Power Sources 2017, 342, 31-37.

5) Y. Tanaka, M. Furuta, K. Kuriyama, R. Kuwabara, Y. Katsuki, T. Kondo, A. Fujishima, K. Honda. Electrochemical properties of N-doped hydrogenated amorphous carbon films fabricated by plasma-enhanced chemical vapor deposition methods. Electrochimica Acta 2011, 56(3), 1172-1181.

6) H.B. Martin, A. Argoitia, U. Landau, A.B. Anderson, J.C. Angus. Hydrogen and oxygen evolution on Boron-Doped Diamond electrodes. Journal of the Electrochemical Society 1996, 143(6), L133-L136.

7) K. Honda, H. Naragino, Y. Shimai. Control of Electric Conductivity and Electrochemical Activity of Hydrogenated Amorphous Carbon by Incorporating Boron Atoms. Journal of The Electrochemical Society 2014, 161(10), B207-B215.

8) Renhui Zhang, Juan Zhao, Yingchang Yang. A novel diamond-like carbon film. Surfaces and Interfaces 2017, 7, 1-5.

9) Renhui Zhang, Liping Wang, Wei Shi. Variable corrosion behavior of a thick amorphous carbon coating in NaCl solution. RSC Advances 2015, 5, 95750-95763.

10) F. Beck, H. Krohn, E. Zimmer. Corrosion of graphite intercalation compounds. Electrochimica Acta 1986, 31(3), 371-376.

11) C. Louro, C.W. Moura, N. Carvalho, M. Stueber, A. Cavaleiro. Thermal stability in oxidative and protective environments of a-C:H cap layer on a functional gradient coating. Diamond & Related Materials 2011, 20, 57-63.

12) T. Frauenheim, G. Jungnickel, T. Kohler, U. Stephan. Structure and electronic properties of amorphous carbon: from semimetallic to insulating behaviour. Journal of Non-Crystalline Solids 2011, 182, 186-197.

13) M.H. Kim, J.Y. Lee. Thermal analysis of hydrogenated amorphous carbon films prepared by plasma enhanced chemical vapour deposition. Journal of Materials Science 1991, 26, 4787-4794.

14) T.M. Manhabosco, A.P.M. Barboza, R.J.C. Batista, B.R.A. Neves, I.L. Müller. Corrosion, wear and wear–corrosion behavior of graphite-like a-C:H films deposited on bare and nitrided titanium alloy. Diamond & Related Materials 2013, 31, 58-64.

15) Meidong Huang, Xueqian Zhang, Peiling Ke, Aiying Wang. Graphite-like carbon films by high power impulse magnetron sputtering. Applied Surface Science 2013, 283, 321-326.

16) Giulia Galli, Richard M. Martin, Roberto Car, Michele Parrinello. Structural and Electronic Properties of Amorphous Carbon. Physical Review Letter 1989, 62, 555-558.

17) Giulia Galli, Richard M. Martin, Roberto Car, Michele Parrinello. Ab initio calculation of properties of carbon in the amorphous and liquid states. Physical Review B 1990, 42, 7470-7482.

18) I.F. Cheng, Y.Q. Xie, R.A. Gonzales, P.R. Brejna, J.P. Sundararajan, B.A.F. Kengne, D.E. Aston, D.N. McIlroy, J.D. Foutch, P.R. Griffiths. Synthesis of graphene paper from pyrolyzed asphalt. Carbon 2011, 49(8), 2852-2861.

19) I.O. Gyan, P.M. Wojcik, D.E. Aston, D.N. McIlroy, I.F. Cheng. A Study of the Electrochemical Properties of a New Graphitic Material: GUITAR, ChemElectroChem 2015, 2(5), 700-706.

20) I.O. Gyan, I.F. Cheng. Electrochemical study of biologically relevant molecules at electrodes constructed from GUITAR, a new carbon allotrope. Microchemical Journal 2015, 122, 39-44.

21) H. Kabir, I.O. Gyan, J.D. Foutch, H. Zhu, I.F. Cheng. Application of GUITAR on the negative electrode of the Vanadium redox flow battery: improved $V^{3+/2+}$ heterogeneous electron transfer with reduced hydrogen gassing. Journal of Carbon Research C 2016, 2(2), 13.

22) A.N. Patel, M.G. Collignon, M.A. O'Connell, W.O.Y. Hung, K. McKelvey, J.V. Macpherson, P.R. Unwin. A New View of Electrochemistry at Highly Oriented Pyrolytic Graphite. Journal of American Chemical Society 2012, 134(49), 20117-20130.

23) Y.Q. Xie, S.D. McAllister, S.A, Hyde, J.P. Sundararajan, B.A. Fouetio-Kengne, D.N. McIlroy, I.F. Cheng. Sulfur as an important co-factor in the formation of multilayer graphene in the thermolyzed asphalt reaction. Journal of Materials Chemistry 2012, 22(12), 5723-5729.

24) R.S. Nicholson. Theory and Application of Cyclic Voltammetry for Measurement of Electrode Reaction Kinetics. Analytical Chemistry 1965, 37(11), 1351-1355.

25) S.J. Konopka, B. McDuffie. Diffusion Coefficients of Ferri- and Ferrocyanide Ions in Aqueous Media, Using Twin-Electrode Thin-Layer Electrochemistry. Analytical Chemistry 1970, 42(14), 1741-1746.

26) P.H. Daum, C.G. Enke. Electrochemical Kinetics of the Ferri-Ferrocyanide Couple on Platinum. Analytical Chemistry 1969, 41(4), 653-656.

27) M.E.G. Lyons, G.P. Keeley. The Redox Behaviour of Randomly Dispersed Single Walled Carbon Nanotubes both in the Absence and in the Presence of Adsorbed Glucose Oxidase. Sensors 2006, 6, 1791-1826.

28) C.C.Villarreal, T. Pham, P. Ramnani, A. Mulchandani. Carbon allotropes as sensors for environmental monitoring. Current Opinion in Electrochemistry 2017, 3(1), 106-113.

29) Kristin K. Cline, Mark T. McDermott, Richard L. McCreery. Anomalously Slow Electron Transfer at Ordered Graphite Electrodes: Influence of Electronic Factors and Reactive Sites. Journal of Physical Chemistry, 1994, 98, 5314-5319.

30) Richard L. McCreery, Mark T. McDermott. Comment on Electrochemical Kinetics at Ordered Graphite Electrodes. Analytical Chemistry 2012, 84, 2602-2605.

31) [1] Xiaobo Ji, Craig E. Banks, Alison Crossley, Richard G. Compton. Oxygenated Edge Plane Sites Slow the Electron Transfer of the Ferro-/Ferricyanide Redox Couple at Graphite Electrodes. ChemPhysChem 2006, 7, 1337-1344.

32) A.N. Patel, M.G. Collignon, M.A. O'Connell, W.O.Y. Hung, K. McKelvey, J.V. Macpherson, P.R. Unwin. A New View of Electrochemistry at Highly Oriented Pyrolytic Graphite. Journal of the American Chemical Society 2012, 134(49), 20117-20130.

33) Richard L. McCreery. Advanced Carbon Electrode Materials for Molecular Electrochemistry. Chemical Reviews 2008, 108, 2646-2687.

34) J. Klett, R. Hardy, E. Romine, C. Walls, T. Burchell. High-thermal-conductivity, mesophase-pitch-derived carbon foams: effect of precursor on structure and properties. Carbon 2000, 38, 953-973.

35) S.H. Kim, G.W. Mulholland, M.R. Zachariah. Density measurement of size selected multiwalled carbon nanotubes by mobility-mass characterization. Carbon 2009, 47, 1297-1302.

36) J. Robertson. Diamond-like amorphous carbon. Materials science and engineering 2002, R37, 129-281.

37) L.J. Peng, J.R. Morris. Structure and hydrogen adsorption properties of low density nanoporous carbons from simulations. Carbon 2012, 50(3), 1394-1406.

38) T. Frauenheim, P. Blaudeck, U. Stephan, G. Jungnickel. Atomic structure and physical properties of amorphous carbon and its hydrogenated analogs. Physical review B 1993, 48(7), 4823-4834.

39) A. Libassi, A.C. Ferrari, V. Stolojan, B.K. Tanner, J. Robertson, L.M. Brown. Density and sp^3 content in diamond-like carbon films by x-ray reflectivity and electron energy loss spectroscopy. Materials Research Society symposia proceedings 2000, 593, 293-298.

40) M. Hu, J. He, Z. Zhao, T.A. Strobel, W. Hu, D. Yu, H. Sun, L. Liu, Z. Li, M. Ma, Y. Kono, J. Shu, H. Mao, Y. Fei, G. Shen, Y. Wang, S.J. Juhl, J.Y. Huang, Z. Liu, B. Xu, Y. Tian. Compressed glassy carbon: An ultrastrong and elastic interpenetrating graphene network. Science Advances 2017, 3, e1603213.

41) D.R. McKenzie. Tetrahedral bonding in amorphous carbon. Reports on Progress in Physics 1996, 59, 1611-1664.

42) D.A.C. Brownson, M.G. Mingot, C.E. Banks. CVD graphene electrochemistry: biologically relevant molecules. Physical Chemistry Chemical Physics 2011, 13, 20284-20288.

43) R. Hawaldar, P. Merino, M.R. Correia, I. Bdikin, J. Gracio, J. Mendez, J.A. M. Gago, M.K. Singh. Large-area high-throughput synthesis of monolayer graphene sheet by Hot Filament Thermal Chemical Vapor Deposition. Scientific Reports 2012, 2, 682.

44) R. John, A. Ashokreddy, C. Vijayan, T. Pradeep. Single- and few-layer graphene growth on stainless steel substrates by direct thermal chemical vapor deposition. Nanotechnology 2011, 22, 165701.

45) C. Casiraghi, A.C. Ferrari, J. Robertson. Raman spectroscopy of hydrogenated amorphous carbons. Physical Review B 2005, 72, 085401.

46) R. Blume, D. Rosenthal, J.P. Tessonnier, H. Li, A.K. Gericke, R. Schlogl. Characterizing Graphitic Carbon with X-ray Photoelectron Spectroscopy: A Step-by-Step Approach. ChemCatChem 2015, 7, 2871-2881.

47) W. Xie, K.M. Ng, L.T. Weng, C.M. Chan. Characterization of hydrogenated graphite powder by X-ray photoelectron spectroscopy and time-of-flight secondary ion mass spectrometry. RSC Advances 2016, 6, 80649-80654.

48) S.K. Jerng, D.S. Yu, J.H. Lee, C. Kim, S. Yoon, S.H. Chun. Graphitic carbon growth on crystalline and amorphous oxide substrates using molecular beam epitaxy. Nanoscale Research Letters 2011, 6(1), 565.

49) F. Atchison, T. Bryś, M. Daum, P. Fierlinger, A. Foelske, M. Gupta, R. Henneck, S. Heule, M. Kasprzak, K. Kirch, R. Kötz, M. Kuźniak, T. Lippert, C.F. Meyer, F. Nolting, A. Pichlmaier, D. Schneider, B. Schultrich, P. Siemroth, U. Straumann. Structural characterization of diamond-like carbon films for ultracold neutron applications. Diamond & Related Materials 2007, 16, 334-341.

50) J.C. Lascovich, R. Giorgi, S. Scaglione. Evaluation of the sp^2/sp^3 ratio in amorphous carbon structure by XPS and XAES. Applied Surface Science 1991, 47, 17-21.

51) R.J. Yeo. Ultrathin carbon-based overcoats for extremely high-density magnetic recording. 2017, ISBN 978-981-10-4881-4.

52) A. Wollbrink, K. Volgmann, J. Koch, K. Kanthasamy, C. Tegenkamp, Y. Li, H. Richter, S. Kamnitz, F. Steinbach, A. Feldhoff, J. Caro. Amorphous, turbostratic and crystalline carbon membranes with hydrogen selectivity. Carbon 2016, 106, 93-105.

53) A.M. Dimiev, S. Eigler. Graphene Oxide: Fundamentals and Applications. 2016, ISBN: 978-1-119-06940-9. DOI:10.1002/9781119069447.

54) A. Ochoa, B. Valle, D.E. Resasco, J. Bilbao, A.G. Gayubo, P. Castano. Temperature Programmed Oxidation Coupled with in situ Techniques Reveal the Nature and Location of Coke Deposited on a Ni/La_2O_3-αAl_2O_3 Catalyst in the Steam Reforming of Bio-oil. ChemCatChem 2018, 10, 2311-2321.

55) Liangliang Huang, Yuanyuan Cao, Dongfeng Diao. Nanosized graphene sheets induced high electrochemical activity in pure carbon film. Electrochimica Acta 2018, 262, 173-181.

56) A.C. Ferrari. Determination of bonding in diamond-like carbon by Raman spectroscopy. Diamond and Related Materials 2002, 11, 1053-1061.

57) Andrea Carlo Ferrari and John Robertson. Raman spectroscopy of amorphous, nanostructured, diamond-like carbon, and nanodiamond. Philosophical Transactions of the Royal Society London A 2004, 362, 2477-2512.

58) P.M. Wojcik, N. Rajabi, H. Zhu, D. Estrada, P. Davis, K. Livingston, K.M. Yocham, T. Pandhi, I.F. Cheng, D.N. McIlroy. The negative temperature coefficient, electrical resistivity, and surface morphology of single carbon coated silica nanospring. Materials Chemistry and Physics 2018 (Manuscript Submitted).

59) B.K. Gupta, Bharat Bhushan. Mechanical and tribological properties of hard carbon coatings for magnetic recording heads. Wear 1995, 190, 110-122.

60) Aiping Zeng, Victor F. Neto, Jose J. Gracio, Qi Hua Fan. Diamond-like carbon (DLC) films as electrochemical electrodes. Diamond & Related Materials 2014, 43, 12-22.

61) A. Singha, A. Ghosh, A. Roy, N.R. Ray. Quantitative analysis of hydrogenated diamond like carbon films by visible Raman spectroscopy. Journal of Applied Physics 2006, 100, 044910.

62) T. Frauenheim, G. Jungnickel, U. Stephan, P. Blaudeck, S. Deutschmann, M. Weiler, S. Sattel, K. Jung, H. Ehrhardt. Atomic-scale structure and electronic properties of highly tetrahedral hydrogenated amorphous carbon. Physical Review B 1994, 50(11), 7940-7945.

63) Sergey Dub, Petro Lytvyn, Viktor Strelchuk, Andrii Nikolenko, Yurii Stubrov, Igor Petrusha, Takashi Taniguchi, Sergey Ivakhnenko. Vickers Hardness of Diamond and cBN Single Crystals: AFM Approach. Crystals 2017, 7, 369.

64) R. Jarosova, P.M.D.S. Bezerra, C. Munson, G.M. Swain. Assessment of heterogeneous electron-transfer rate constants for soluble redox analytes at tetrahedral amorphous carbon, boron-doped diamond, and glassy carbon electrodes. Physica Status Solidi A 2016, 213(8), 2087-2098.

65) S. Chen, Y. Xin, Y. Zhou, F. Zhang, Y. Ma, H. Zhou, L. Qi. Branched CNT@SnO_2 nanorods@carbon hierarchical heterostructures for lithium ion batteries with high reversibility and rate capability. Journal of Materials Chemistry A 2014, 2, 15582-15589.

66) S.Y. Kim, J. Lee, B.H. Kim, Y.J. Kim, K. S. Yang, M.S. Park. Facile Synthesis of Carbon-Coated Silicon/Graphite Spherical Composites for High-Performance Lithium-Ion Batteries. ACS Applied Materials & Interfaces 2016, 8, 12109-12117.

67) S.K. Sharma, J. Prakash, P.K. Pujari. Effects of the molecular level dispersion of graphene oxide on the free volume characteristics of poly (vinyl alcohol) and its impact on the thermal and mechanical properties of their nanocomposites. Physical Chemistry Chemical Physics 2015,17, 29201-29209.

68) F. Cataldo. A study on the thermal stability to 1000°C of various carbon allotropes and carbonaceous matter both under nitrogen and in air. Fullerenes, Nanotubes and carbo nanostructures 2006, 10, 293-311.

69) X. Li, S. Feng, S. Liu, Z. Li, L. Wang, Z. Zhanand, W. Lu. Fabrication of ZnO nanowires array with nanodiamond as reductant. RSC Advances 2016, 6, 96479-96483.

70) Y. Kado, T. Goto, R. Hagiwara. Stability of a boron-doped diamond electrode in molten chloride systems. Diamond & Related Materials 2009, 18, 1186-1190.

71) C. Louro, C.W. Moura, N. Carvalho, M. Stueber, A. Cavaleiro. Thermal stability in oxidative and protective environments of a-C:H cap layer on a functional gradient coating. Diamond & Related Materials 2011, 20, 57-63.

72) S.G. King, L. McCafferty, V. Stolojan, S.R.P. Silva. Highly aligned arrays of super resilient carbon nanotubes by steam purification. Carbon 2015, 84, 130-137.

73) S.H. Ng, J. Wang, K. Konstantinov, D. Wexler, J. Chen, H.K. Liu. Spray Pyrolyzed PbO-Carbon Nanocomposites as Anode for Lithium-Ion Batteries. Journal of The Electrochemical Society 2006, 153(4), A787-A793.

74) Ken Judai, Naoyuki Iguchi, Yoshikiyo Hatakeyama. Low-Temperature Production of Genuinely Amorphous Carbon from Highly Reactive Nanoacetylide Precursors. Journal of Chemistry 2016, 2016, 7840687.

75) Stanley C. S. Lai, Anisha N. Patel, Kim McKelvey, Patrick R. Unwin. Definitive Evidence for Fast Electron Transfer at Pristine Basal Plane Graphite from High-Resolution Electrochemical Imaging. Angewandte Chemie International Edition 2012, 51, 5405-5408.

76) M. Fang, K. Wang, H. Lu, Y. Yang, S. Nutt. Covalent polymer functionalization of graphene nanosheets and mechanical properties of composites. Journal of Material Chemistry 2009, 19, 7098-7105.

77) K. Zhang, Y. Zhang, S. Wang. Enhancing thermoelectric properties of organic composites through hierarchical nanostructures. Scientific Reports 2013, 3, 3448.

78) B. Andonovic, M. Temkov, A. Ademi, A. Petrovski, A. Grozdanov, P. Paunović, A. Dimitrov. Laue functions model vs scherrer equation in determination of graphene layers number on the ground of XRD data. Journal of Chemical Technology and Metallurgy 2014, 49(6), 545-550.

79) Tae-Hee Kim, Eun Kyung Jeon, Younghoon Ko, Bo Yun Jang, Byeong-Su Kim, Hyun-Kon Song. Enlarging the d-spacing of graphite and polarizing its surface charge for driving lithium ions fast. Journal of Materials Chemistry A 2014, 2, 7600.

80) Minzhen Cai, Daniel Thorpe, Douglas H. Adamson, Hannes C. Schniepp. Methods of graphite exfoliation. Journal of Materials Chemistry 2012, 22, 24992-25002.

81) Kevin W. Hathcock, Jay C. Brumfield, Charles A. Goss, Eugene A. Irene, Royce W. Murray Incipient Electrochemical Oxidation of Highly Oriented Pyrolytic Graphite: Correlation

between Surface Blistering and Electrolyte Anion Intercalation. Analytical Chemistry, 1995, 67, 2201-2206.

82) A.H.R. Palser. Interlayer interactions in graphite and carbon nanotubes. Physical Chemistry Chemical Physics 1999, 1, 4459-4464.

83) K. Spyrou, P. Rudolf. An Introduction to Graphene: Functionalization of Graphene. Wiley-VCH Verlag GmbH & Co. KGaA. 2014, ISBN: 9783527672790.

84) Yun Wu, Takeyoshi Okajima, Takeo Ohsaka. Lithium Intercalation into Graphene Ribbons of Glassy Carbon. International Journal of Electrochemical Science 2017, 12, 1004-1013.

85) Meng Hu, Julong He, Zhisheng Zhao, Timothy A. Strobel, Wentao Hu, Dongli Yu, Hao Sun,1 Lingyu Liu, Zihe Li, Mengdong Ma, Yoshio Kono, Jinfu Shu, Ho-kwang Mao, Yingwei Fei, Guoyin Shen, Yanbin Wang, Stephen J. Juhl, Jian Yu Huang, Zhongyuan Liu, Bo Xu, Yongjun Tian. Compressed glassy carbon: An ultrastrong and elastic interpenetrating graphene network. Science Advances 2017, 3, e1603213.

86) O.V. Kharissova, B. I. Kharisov. Variations of interlayer spacing in carbon nanotubes. RSC Advances 2014, 4, 30807-30815.

87) K.B. Teo, C. Singh, M. Chhowalla, W.I. Milne. Catalytic Synthesis of Carbon Nanotubes and Nanofibers. Encyclopedia of Nanoscience and Nanotechnology. American Scientific Publisher 2003, X, 1–22.

88) R. Bajpai, L. Rapoport, K. Amsalem, H.D. Wagner. Rapid growth of onion-like carbon nanospheres in a microwave oven. CrystEngComm 2016, 18, 230-239.

89) B. Manoj, A.G. Kunjomana. Study of Stacking Structure of Amorphous Carbon by X-Ray Diffraction Technique. International Journal of Electrochemical Science 2012, 7, 3127-3134.

90) L.M. Malard, M.A. Pimenta, G. Dresselhaus, M.S. Dresselhaus. Raman spectroscopy in graphene. Physics Reports 2009, 473, 51-87.

91) Y. Hishiyama, M.Nakamura. X-ray diffraction in oriented carbon films with turbostratic structure. Carbon 1995, 33, 1399-1403.

92) C.J. Thambiliyagodage, S. Ulrich, P.T. Araujo, M.G. Bakker. Catalytic graphitization in nanocast carbon monoliths by iron, cobalt and nickel nanoparticles. Carbon 2018, 134, 452-463.

93) A. Vuong, T. Trevethan, C.D. Latham, C.P. Ewels, D. Erbahar, P.R. Briddon, M.J. Rayson, M.I. Heggie. Interlayer vacancy defects in AA-stacked bilayer graphene: density functional theory predictionsJournal of Physics: Condensed Matter 2017, 29, 155304.

94) M. Yoon, J. Howe, G. Tibbetts, G. Eres, Z. Zhang. Polygonization and anomalous graphene interlayer spacing of multi-walled carbon nanofibers. Physical Review B 2007, 75, 165402.

95) E.A. Belenkov. Formation of Graphite Structure in Carbon Crystallites. Inorganic Materials 2001, 37(9), 928-934.

96) T. Watanabe, T.K. Shimizu, Y. Tateyama, Y. Kim, M. Kawai, Y. Einaga. Giant electric double-layer capacitance of heavily boron-doped diamond electrode. Diamond & Related Materials 2010, 19, 772-777.

97) H. Naragino, K. Yoshinaga, A. Nakahara, S. Tanaka, K. Honda. Enhancement of electrical conductivity and electrochemical activity of hydrogenated amorphous carbon by incorporating boron atoms. Journal of Physical Chemistry Conference Series 2013, 441, 12042.

98) Q. Xue, D. Kato, T. Kamata, S. Umemura, S. Hirono, O. Niwa, Electron Cyclotron Resonance-Sputtered Nanocarbon Film Electrode Compared with Diamond-Like Carbon and Glassy Carbon Electrodes as regards Electrochemical Properties and Biomolecule Adsorption. Japanese Journal of Applied Physics 2012, 51, 90124.

99) K.S. Yoo, B. Miller, R. Kalish, X. Shi. Electrodes of nitrogen-incorporated tetrahedral amorphous carbon - A novel thin-film electrocatalytic material with diamond-like stability. Electrochemical and Solid-State Letters 1999, 5, 233-235.

100) A.P. Zeng, M.M. Bilek, D.R. McKenzie, P.A. Lay, A. L. Fontaine, V.J. Keast. Correlation between film structures and potential limits for hydrogen and oxygen evolutions at a-C:N film electrochemical electrodes. Carbon 2008, 46(4), 663-670.

101) W. Wang, Z. Wei, W. Su, X. Fan, J. Liu, C. Yan, C. Zeng. Kinetic investigation of vanadium (V)/(IV) redox couple on electrochemically oxidized graphite electrodes. Electrochimica Acta 2016, 205, 102-112.

102) B. Caglar, J. Richards, P. Fischer, J. Tuebke. Conductive polymer composites and coated metals as alternative bipolar plate materials for all-vanadium redox-flow batteries. Advanced Materials Letters 2014, 5(6) 299-308.

103) W.L. Wang, S.M. Heb, C.H. Lan. Protective graphite coating on metallic bipolar plates for PEMFC applications. Electrochimica Acta 2012, 62(15), 30-35.

104) S. Viswanathan, L. Mohan, P. Bera, V. P. Kumar, Harish C. Barshilia, C. Anandan. Corrosion and Wear Behaviors of Cr-Doped Diamond-Like Carbon Coatings. Journal of Materials Engineering and Performance 2017, 26(8), 3633-3647.

105) Mingjun Cui, Jibin Pu, Jun Liang, Liping Wang, Guangan Zhang, Qunji Xue. Corrosion and tribocorrosion performance of multilayer diamond-like carbon film in NaCl solution. RSC Advances 2015, 5, 104829-104840.

106) J. Bautista-Ruiz, J.C. Caicedo, W. Aperador. Tribocorrosion Behavior of Amorphous Carbon-Silicon Coated Titanium in Biological Medium. Tribology in Industry 2018, 40(2), 326-334.

107) M. Madej, D. Ozimina, K. Kurzydlowski, T. Plocinski, P. Wiecinski, P. Baranowicz. Diamond-like carbon coatings in biotribological applications. Kovove Materialy 2016, 54(3), 185-194.

108) R.K. Das, Y. Wang, S.V. Vasilyeva, E. Donoghue, I. Pucher, G. Kamenov, H.P. Cheng, A.G. Rinzler. Extraordinary Hydrogen Evolution and Oxidation Reaction Activity from Carbon Nanotubes and Graphitic Carbons. ACS Nano 2014, 8(8), 8447-8456.

109) M.C. Oliveira, A.S. Viana, A.M.B. Rego, A.M. Ferraria, P.B. Tavares, A.D. Veloso, R.A. Videira. Dual Behaviour of Amorphous Carbon Released Electrochemically from Graphite. ChemistrySelect 2016, 1, 4126-4130.

110) Xingyi Yang, Lars Haubold, Gabriel DeVivo, Greg M. Swain. Electroanalytical Performance of Nitrogen-Containing Tetrahedral Amorphous Carbon Thin-Film Electrodes. Analytical Chemistry 2012, 84, 6240-6248.

111) Tomoyuki Kamata, Dai Kato, Hideo Ida, Osamu Niwa. Structure and electrochemical characterization of carbon films formed by unbalanced magnetron (UBM) sputtering method. Diamond & Related Materials 2014, 49, 25-32.

112) Tomoyuki Kamata, Dai Kato, Shigeru Hirono, Osamu Niwa. Structure and Electrochemical Performance of Nitrogen-Doped Carbon Film Formed by Electron Cyclotron Resonance Sputtering. Analytical Chemistry 2013, 85, 9845-9851.

113) Daniel Bousa, Jan Luxa, David Sedmidubsky, Stepan Huber, Ondrej Jankovsky, Martin Pumera, Zdenek Sofer. Nanosized graphane $(C_1H_{1.14})_n$ by hydrogenation of carbon nanofibers by Birch reduction method. RSC Advances 2016, 6, 6475-6485.

114) Jun Li, Alan Cassell, Lance Delzeit, Jie Han, M. Meyyappan. Novel Three-Dimensional Electrodes: Electrochemical Properties of Carbon Nanotube Ensembles. Journal of Physical Chemistry B 2002, 106, 9299-9305.

115) Ryan R. Moore, Craig E. Banks, Richard G. Compton. Basal Plane Pyrolytic Graphite Modified Electrodes: Comparison of Carbon Nanotubes and Graphite Powder as Electrocatalysts. Analytical Chemistry 2004, 76, 2677-2682.

116) Irene Taurino, Sandro Carrara, Mauro Giorcelli, Alberto Tagliaferro, Giovanni De Micheli. Comparison of two different carbon nanotube-based surfaces with respect to potassium ferricyanide electrochemistry. Surface Science 2012, 606, 156-160.

Chapter 2: Application of GUITAR in Energy Storage

"Application of GUITAR on the Negative Electrode of the Vanadium Redox Flow Battery: Improved $V^{3+/2+}$ Heterogeneous Electron Transfer with Reduced Hydrogen Gassing." C - Journal of Carbon Research 2016, vol. 2, no. 13, pp. 1-10.

Abstract

GUITAR (Graphene from the University of Idaho Thermolyzed Asphalt Reaction) has the classical basal and edge plane morphology of graphites and thin layer graphenes with similar XPS, Raman and IR characteristics. However previous investigations indicated GUITAR is different electrochemically from graphenes and classical graphites. GUITAR has faster heterogeneous electron transfer across its basal plane and an electrochemical window that exceeds graphitic materials by 1 V. These beneficial properties are examined for application in the negative electrode of the vanadium redox flow battery (VRFB). Graphitic materials in this application suffer from hydrogen gassing and slow electron transfer kinetics for the $V^{2+/3+}$ redox couple. Cyclic voltammetry of the $V^{2+/3+}$ redox couple (0.05 M V^{3+} in 1 M H_2SO_4) on bare KFD graphite felt gives an estimated standard rate constant (k^0) of 8.2×10^{-7} cm/s. The GUITAR-coated KFD graphite felt improves that quantity to 8.6×10^{-6} cm/s. The total contribution of the cyclic voltammetric currents at -1.0 V vs. Ag/AgCl to hydrogen evolution is 3% on GUITAR-coated KFD graphite felt. On bare KFD graphite felt, this is 22%. These results establish GUITAR as an excellent alternative material for the negative electrode in the vanadium redox flow battery.

2.1 Introduction

GUITAR (Graphene from the University of Idaho Thermolyzed Asphalt Reaction) is a hypothesized new allotrope of carbon that offers many advantages over other conventional carbon-based materials in electrochemical applications [1,2]. When compared to graphite, graphene and other planar lamellar carbon materials, GUITAR possesses significantly faster electron transfer kinetics on the basal plane (BP), which serves as the most practical electrode surface in most applications [1]. Electron transfer at the surface of graphite is seen to be more favored at the terminating edges and grain boundaries as compared to the basal plane. This behavior is not observed with GUITAR. In previous work, we demonstrate that the kinetics of both the edges as well as the planar surfaces of GUITAR are equally fast in $Fe(CN)_6^{4-/3-}$, which is one of several properties which gives GUITAR a significant advantage over other carbon electrode materials in electrochemical applications [1]. The facile heterogeneous electron transfer (HET) rate of Basal Plane-GUITAR (BP-GUITAR) is attributed to increased density of electronic states (DOS) from the structural defects within its molecular planes [1]. Also of great interest is GUITAR's large potential window for operation [1]. On the cathodic side, GUITAR's overpotential for hydrogen evolution exceeds other graphitic materials [1]. On the anodic side, GUITAR exhibits high resistance to corrosion and oxygen gassing. Taken together, GUITAR has a 3 V aqueous electrochemical window at 200 $\mu A/cm^2$, which is similar to boron doped diamond electrodes and exceeds other graphitic materials by 1 volt [2–5]. These properties make GUITAR ideally suited for applications in batteries, fuel cells, ultracapacitors, water purification, solar energy conversion devices, and electrochemical sensors [2].

Redox flow batteries (RFB) offer economical advantages and will find applications in grid-level power buffering [6–8]. RFBs are also free from the constraints of cycle-life limitations and are ideally suited for electrical energy storage applications including frequency regulation, load following, peak shaving and energy time shift [6,8,9]. The all-vanadium redox flow battery (VRFB) is a promising RFB and is based on the reactions of $V^{3+/2+}$ and $V^{4+/5+}$ [10]. VRFB's possess high efficiency operation as evidenced by fast response rates, deep discharge levels, long life and high discharge rates, while maintaining very low self-discharge rates. One particular advantage over several other redox flow batteries is that the cross mixing of anolytes and catholytes will not result in severe catastrophic reactions, as both contain vanadium ions [10–13]. To increase power and energy densities, all flow batteries require both fast HET rates as well as minimized parasitic electrode reactions. In the negative cell of VRFB, two major issues are of concern: (i) slow HET rates with the $V^{3+/2+}$ redox couple and (ii) parasitic hydrogen evolution [14–16]. A consequence of the former is low power density and low energy efficiency whereas the latter results in a loss in both coulombic and energy efficiency of the battery [17]. Parasitic evolution of hydrogen gas can interrupt the electrolyte flow, lead to changes in the pH, increase the cell resistance and finally dissipate the total energy [11,17,18]. Formation of hydrogen gas bubbles on negative electrode also blocks the electrode surface for $V^{3+/2+}$ HET [14]. Approximately 5-25% of charging current is lost due to the parasitic hydrogen evolution at negative half of the VRBs. These hydrogen evolution percentages are calculated based on the given values/graphs in literature [17-21]. Therefore, minimization of parasitic hydrogen evolution in negative cells is critical for a durable and economically viable

VRB. It is notable that GUITAR has a hydrogen overpotential of 900 mV vs. SHE in 1 M H_2SO_4 which exceeds graphite by over 300-500 mV [22].

In order to increase $V^{3+/2+}$ HET rates, the electrode material should have a high surface area but also be mechanically and chemically stable [20,23,24]. Active research is going on to identify such materials with the greatest focus being on carbon and graphite felts [25–28]. These electrodes offer cost effectiveness but suffer from slow $V^{3+/2+}$ HET rates and from significant parasitic hydrogen evolution [17,29]. In previous investigations GUITAR exhibited facile HET rates with $Fe(CN)_6^{3-/4-}$ and $Ru(NH_3)_6^{2+/3+}$ redox couples [22,30]. In this investigation, we assess the HET rate constant for $V^{3+/2+}$ redox system and contribution of hydrogen evolution on the overall voltammetric current on GUITAR flake, KFD graphite felt and GUITAR coated KFD graphite felt electrodes.

2.2. Results and Discussion

2.2.1. GUITAR Coated Graphite Felt Electrode

Electrode materials used in the VRFB are often carbon and graphite felts, which have relatively high surface area and allow for electrolyte flow through the fibers [20,31-33]. In this investigation, KFD graphite felt (Figure 2.1A) was examined as an electrode material for VRFBs. Figure 2.1C shows the GUITAR-coated KFD graphite felt material (GUITAR/KFD), which has the metallic luster seen in previous studies using flat electrode configurations. Figure 2.1B is a photograph of graphite exposed to the same temperatures as the TAR but without roofing tar precursors, which shows noticeable contraction. In order to determine the depth of deposition, scanning electron microscopy (SEM) was conducted on as-received and GUITAR-coated KFD graphite felt (Figure 2.2). Fiber thickness of the bare felt measured in this work is within literature range and is measured as 8.70±0.46 μm (n=10) [34]. Deposition of GUITAR results in an increase in fiber thickness to 12.34±0.34 μm (n=10) indicating an estimated depth of the deposited GUITAR layer of 1.8 μm. Also notable is that deposition of GUITAR apparently fills pores and smoothens the graphite felt fibers (Figure 2.2). The “smooth” (or true) surface areas of the KFD graphite felt and GUITAR/KFD were calculated assuming the felt electrode is made up of cylindrical graphite fibers as considered in Smith et al. [35] (more detail in supporting information, Table 2.S1). The “smooth” surface area is found to be 64.4 cm^2 per cm^2 geometric area for KFD graphite felt and 61.6 cm^2 per cm^2 geometric area for GUITAR-coated KFD graphite felt. The electrochemical surface area (ECSA) of the KFD graphite felt and GUITAR/KFD felt electrodes were estimated from the Randles-Sevcik equation [36] using cyclic voltammograms on the electrodes in 1 mM $Fe(CN)_6^{3-/4-}$ (see Table 2.S2). The

electrochemical surface area (ECSA) of the KFD graphite felt was obtained as 61.5 cm^2 per cm^2 geometric area which is consistent with theoretical value. However, for GUITAR/KFD felt, the ECSA is 50.6 cm^2 per cm^2 geometric area which is around 15% less than the true surface area.

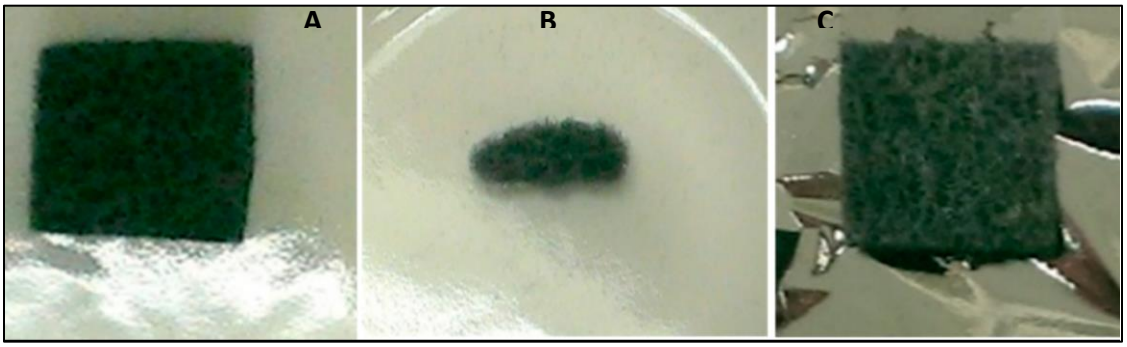

Figure 2.1. Photograph of (A) untreated graphite felt (geometric area 1 cm^2) (B) the same material heated for 25 min in the absence of GUITAR starting material and (C) GUITAR-coated graphite felt (geometric area 1 cm^2).

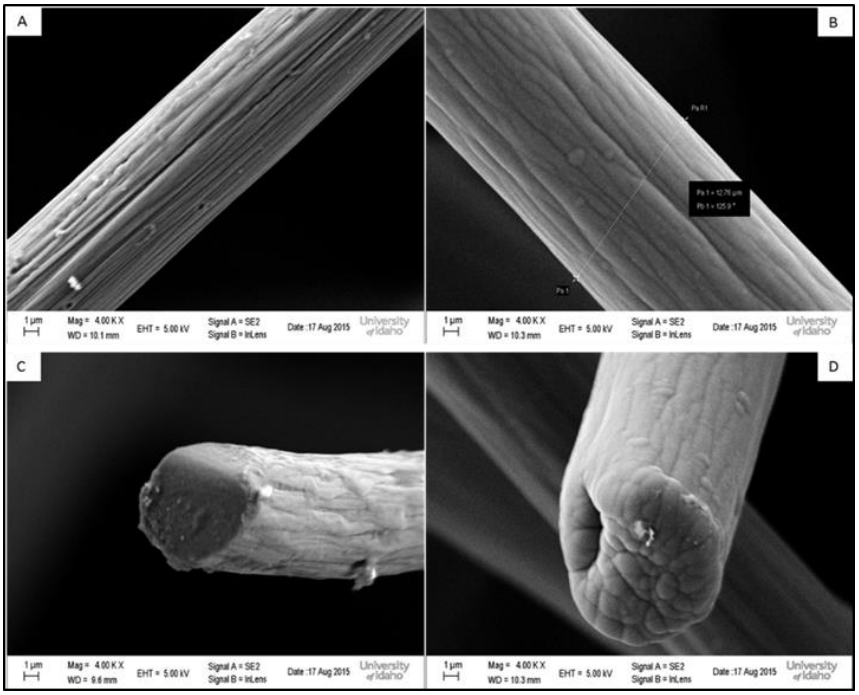

Figure 2.2. Scanning electron micrographs of as-obtained graphite felt (A,C) and GUITAR-coated graphite felt (B,D). Average thicknesses for as-obtained graphite felt (A,C) is obtained as 8.70±0.46 µm (n=10) and for GUITAR-coated graphite felt (B,D) is 12.34±0.34 µm (n=10).

2.2.2. Estimation of Hydrogen Overpotential by Cyclic Voltammetry in 1 M H_2SO_4

Cathodic limits at 200 μA/cm^2 in 1 M H_2SO_4 for graphitic materials lie between -0.3 V to -0.5 V (vs. SHE) (See Table 2.1 and references therein). The cathodic limit for a flat GUITAR electrode is -0.9 V (vs. SHE) as obtained from the cyclic voltammogram. This is similar to a previous study with GUITAR electrodes [22]. On the graphite felt electrode of this study, the hydrogen wave onset is estimated at -0.4 V (vs. SHE) at 200 μA/cm^2 and lies within the range of literature graphitic materials. It is important to note that the cathodic limit of the felt electrodes, both bare and GUITAR-coated is calculated based on the true surface area. On the GUITAR-coated graphite felt electrode, the hydrogen wave onset potential is -0.75 V (vs. SHE), a 350 mV increase in overpotential relative to the bare felt.

Table 2.1. Cathodic potential limits (vs. SHE) at 200 μA/cm^2 for various carbon materials in 1M H_2SO_4 as measure by cyclic voltammetry at 50 mV/s. The number of runs (n) and the standard deviations are also reported.

Material	Cathodic Limit (V) vs. SHE	Reference
GUITAR	−0.90 ± 0.07 (n = 5)	This work
GUITAR/KFD graphite felt	−0.75 ± 0.05 (n = 5)	This work
Pyrolytic Graphite	−0.52 ± 0.06	[22]
KFD Graphite felt	−0.40 ± 0.05 (n = 5)	This work
Graphite*	−0.4 to −0.5	[3–5]
Glassy carbon	−0.3 to −0.5	[3–5]

* Graphite includes highly ordered pyrolytic graphite (HOPG) and exfoliated graphite.

2.2.3. Estimation of $V^{3+/2+}$ HET Rates by Cyclic Voltammetry (CV)

The HET rates of $V^{3+/2+}$ redox couple is relatively slow on most graphitic materials (see Table 2.2). The sequence of CV curves for the $V^{3+/2+}$ (0.050 M VCl_3, 1 M H_2SO_4) redox couple on flat

GUITAR flake, bare KFD graphite felt, and GUITAR-coated graphite felt electrodes are shown in Figure 2.3A-C, respectively. Scan rate variation on KFD graphite felt and GUITAR/KFD felt electrode in 1 mM $Fe(CN)_6^{3-/4-}$ (in 1 M KCl) showed semi-infinite diffusion behavior (where peak current is proportional to the square root of scan rate) at and above 75 mV/s (Figures 2.S1 and 2.S2). Cyclic voltammograms were recorded at a scan rate of 200 mV/s to avoid the thin layer voltammetry (where peak current is directly proportional to the scan rate) [37]. The cathodic peak current density is 25±2 mA/cm^2 (n=3) on the flat GUITAR electrode (Figure 2.3A) at -1.2 V (vs. Ag/AgCl). The peak current density is measured based on geometric area of the electrode. This corresponds to a standard rate constant (k^0) of 4.8×10^{-6} cm/s when modelled through Digisim software. For the bare KFD felt electrode, the cathodic peak current density is 150±10 mA/cm^2 (n=3) (Figure 2.3B) at -1.2 V (vs. Ag/AgCl) which corresponds to a modelled standard rate constant (k^0) of 8.2×10^{-7} cm/s. For the GUITAR-coated KFD felt electrode, the cathodic peak current density is 420±20 mA/cm^2 (n=3) at -1.2 V (vs. Ag/AgCl) which corresponds to a modelled standard rate constant (k^0) of 8.6×10^{-6} cm/s that is 10 times faster than the k^0 for the bare KFD graphite felt system (Figure 2.3C). This is despite the apparent decrease in true surface area with GUITAR-coated KFD electrodes (61.6 cm^2/cm^2 geometric area). HET rates are much faster than the bare KFD graphite felt systems (64.4 cm^2/cm^2 geometric area). The GUITAR-coated KFD electrode exhibits significantly higher current density over the bare KFD felt (Figure 2.3B and C). This improvement in HET rates with GUITAR/KFD electrodes was discussed in a previous publication [22].

Graphitic materials have a well-known anisotropy in HET rates between the basal and edge planes. In general, the edge plane (EP) is much faster at these rates by several orders of magnitude over the basal plane (BP) [38,39]. This is very acute in crystalline graphites where the density of electronic states near the Fermi level is very low [38]. Also noteworthy is that the majority of exposed graphitic surface of KFD fibers is expected to be basal plane in nature. In previous investigations, the BP-GUITAR was found to have HET rates for $Fe(CN)_6^{4-/3-}$ similar to those of its EP-GUITAR and EP-graphites. The k^0 rates for BP-GUITAR (10^{-2} cm/s) surpasses those for BP-highly oriented pyrolytic graphite (HOPG) and BP-graphene by five or more orders of magnitude [1,22]. The $V^{3+/2+}$ redox couple does not exhibit enhanced HET kinetics on the BP-GUITAR as opposed to literature BP-HOPG (Table 2.2), with both being about 10^{-6} cm/s. McCreery classifies the $V^{3+/2+}$ as a redox species whose HET rates are catalyzed by surface oxides [40]. Elemental analysis of GUITAR by XPS reveals that it has a low surface oxygen content [30]. Modification of the GUITAR surface with oxide group for improved HET rates will be a focus of future investigations.

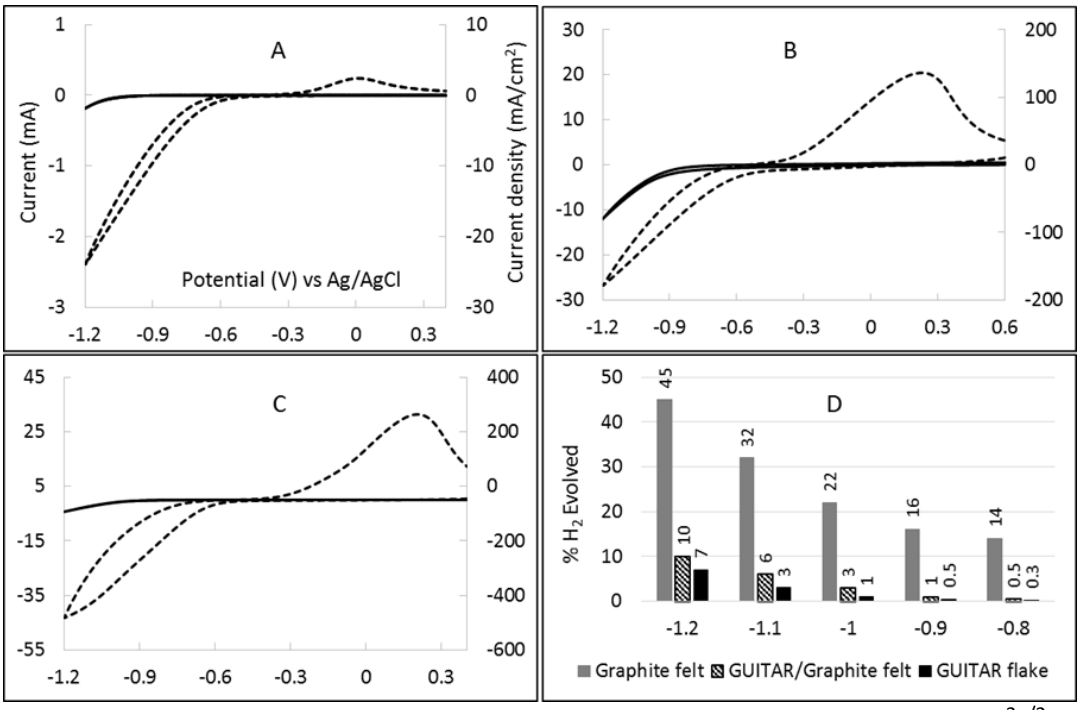

Figure 2.3. Cyclic voltammograms of background (in 1 M H_2SO_4, solid line) and $V^{3+/2+}$ (0.05 M in 1 M H_2SO_4 dashed lines) obtained at the (A) flat GUITAR electrode (0.10 cm^2), (B) KFD graphite felt electrode (geometric area 0.16 cm^2), and (C) GUITAR/KFD graphite felt electrode (geometric area 0.10 cm^2). All cyclic voltammograms were obtained at a scan rate of 200 mV/s. The percentage H_2 evolutions on different electrodes at different potentials (V) are shown in (D).

2.2.4. Percentage Hydrogen Evolution

Figure 2.3D shows hydrogen production as a percentage of total current. The percent of hydrogen evolution was calculated as the ratio of background current (in 1 M H_2SO_4) to V^{3+} reduction current (0.05 M V^{3+} in 1 M H_2SO_4) at a scan rate of 200 mV/s on three electrodes. These are estimated from the cyclic voltammetric waves in Figure 2.3. At −1.0 V, the percentage of hydrogen evolution on flat GUITAR and GUITAR/KFD graphite felt electrodes are observed as 1% and 3%, respectively. On bare KFD graphite felt, 22% of the total current is attributable to hydrogen production (Figure 2.3D and Table 2.3). When compared to literature, GUITAR flake and GUITAR-coated KFD graphite felt electrodes are the lowest

reported for the fraction of the total cathodic current diverted to hydrogen evolution. This high overpotential for hydrogen evolution is not well understood and was reported in a previous publication [22]. The hydrophobicity of GUITAR may diminish proton adsorption on its surface. The detailed mechanism of this behavior, however, is not well understood and is a subject of future study. Table 2.3 highlights the relevant literature. The fraction (as percent) of the total current that evolves hydrogen ranges from a few % to greater than 50%. These values are stated within the publication or calculated from the data in the respective figure mentioned in the table. No other materials approach GUITAR's performance of 1% hydrogen current at -1.0 V (vs. Ag/AgCl) in 1 M H_2SO_4.

Table 2.2. Comparison of standard heterogeneous electron transfer rate constants for $V^{3+/2+}$ redox at various carbon materials. See Figure 2.3 for corresponding cyclic voltammograms.

Material	**Geometric Surface Area (cm^2)**	**True Surface Area (cm^2)**	**HET rate constant (k^o) for $V^{3+/2+}$ (cm/s)**	**Ref.**
GUITAR/KFD graphite felt	0.10	6.1	8.6×10^{-6}	This work
GUITAR flake	0.10	0.10	4.8×10^{-6}	
KFD graphite felt	0.16	10.3	8.2×10^{-7}	
Non-porous flat electrodes				
Edge plane pyrolytic graphite			3.5×10^{-5}-5.5×10^{-4}	[21,41]
Glassy carbon	0.07		1.7×10^{-5}-5.4×10^{-5}	[21,41]
Basal plane highly ordered pyrolytic graphite	0.02		$<3.0\times10^{-6}$	[42]
High surface area electrodes				
Graphite reinforcement carbon	0.08		4.8×10^{-3}-9.7×10^{-3}	[26]
Plastic formed carbon			5.3×10^{-4}	[41]
Carbon felt	3.0		1.5×10^{-7}	[14]
Carbon paper	0.13	128	1.07×10^{-3}-3.28×10^{-3}	[21]

Table 2.3. Comparison of H_2 evolution as a percentage of total current at different carbon electrodes. See Figure 2.3 for the corresponding cyclic voltammograms. The specific potentials and V^{3+} and H_2SO_4 concentrations are noted.

Material	**% H_2**	**Potential (V) vs. Ag/AgCl**	**Conditions**	**How Calculated? and Ref.**
GUITAR flake	1	−1.0	0.05 M V^{3+} 1 M H_2SO_4	Figure 3 This work
	0.3	−0.8		
GUITAR coated KFD graphite felt	3	−1.0		
	0.5	−0.8		
KFD graphite felt	22	−1.0		
	14	−0.8		
Graphite	78	−1.0 vs. SCE	0.1 M V^{3+} 2 M H_2SO_4	Stated [17] Fig. 2b
	22	−0.8 vs. SCE		
Graphite	20	−0.65 vs. SCE	1 M V^{3+} 5 M H_2SO_4	Calculated [43] Fig. 1a,b
Graphite felt	5–8	−0.65	0.05 M V^{3+} 1 M H_2SO_4	Calculated [19] Fig. 2b,4
Carbon felt	20		2 M V^{3+} 2.5 M H_2SO_4	Stated [44] Fig. 6b
Glassy carbon	80	−1.0 vs. SCE	0.08 M V^{3+} 1.8 M H_2SO_4	Calculated [45] Fig. 2
Porous carbon paper	10–22		1 M V^{3+} H_2SO_4:HNO_3=3:1	Stated [46] Table 5
Carbon nanotubes	15	−0.65 vs. SCE	1 M V^{3+} 5 M H_2SO_4	Calculated [44] Fig. 1a,b
WO_3/ASC/CP*	5–9		0.05 M V^{3+} 3 M H_2SO_4	Stated [47] Table 3
Titanium nitride/Carbon paper	12	−0.7 vs. SCE	0.1 M V^{3+}, 1 M H_2SO_4	Calculated [33] Fig. 2
Graphite plate	10	−0.75 vs. SCE	1.6 M V^{3+} 3 M H_2SO_4	Calculated [32] Fig. 3,6

* Carbon paper coated with super activated carbon supported tungsten trioxide.

2.3. Materials and Methods

Materials and chemicals: Graphite felt (KFD 2.5 EA type, with a thickness of 2.5 mm) was donated by SGL Carbon Company (St. Marys, PA, USA). Sulfuric acid (96.3%) was obtained from the J.T Baker Chemical Co. (Phillipsburg, NJ, USA). Vanadium (III) chloride (97%) was obtained from Sigma-Aldrich (St. Louis, MO, USA). Ethyl alcohol (99.5%) was obtained from Pharmco Products Inc. (Brookfield, CT, USA). Potassium chloride was obtained from Fisher Scientific (Waltham, NJ, USA) and potassium ferricyanide was obtained from Acros Organics (Morris Plains, NJ, USA). Black-Jack All Weather Roof Cement (Gardner-Gibson, Inc. Tampa, FL, USA) was used as GUITAR precursor. A quartz tube was obtained from Technical Glass Products, Inc. (Painesville Twp., OH, USA), cut into small wafers (approximately 20 mm × 6 mm), and used as GUITAR deposition substrate. Copper alligator clips (model: CTM-34C) were obtained from Cal Test Electronics (Yorba Linda, CA, USA). Paraffin wax (Gulf wax) was obtained from Royal Oak Enterprises (Roswell, GA, USA). All aqueous solutions were prepared with deionized water which was purified by passage through an activated carbon purification cartridge (Barnstead, model D8922, Dubuque, IA, USA).

Electrode fabrication and electrochemical cell setup: GUITAR was synthesized as described by previous procedures through the thermolyzed asphalt reaction (TAR) [2,30,48]. Deposition of GUITAR onto graphite felt was achieved by this method [30,48]. Graphite felt strips were placed into the crucible prior to the TAR method which allowed GUITAR deposition on the felt fibers. An aliquot of 30 g of roofing tar was used to coat a single batch of graphite felt (3 pieces, each of 15mm×5 mm). The coating process took 30-35 min. Both the KFD felt and GUITAR/KFD felt electrodes were encased with paraffin wax in order to obtain a specific

geometric area. Ohmic contact was made with a copper alligator clip (Figure 2.S2). Electrodes were then made hydrophilic prior to any voltammetric measurements. This was achieved by washing in ethanol, rinsing with deionized water, followed by agitation in the electrochemical cell solution as proposed by Smith et al. [35]. All electrochemical studies were conducted in a three-electrode undivided cell with a reticulated vitreous carbon basket counter electrode (Bioanalytical Systems, Inc. West Lafayette, IN, USA) and an Ag/AgCl/3M NaCl (aq) (0.209 V vs. SHE) reference electrode. Cyclic voltammetry (CV) was carried out using a Bioanalytical Systems CV-50W potentiostat (West Lafayette, IN, USA). The supporting electrolytes (1 M H_2SO_4) were de-aerated by bubbling with N_2 (g) for 15 min before addition of VCl_3. All the solutions were de-aerated by purging with N_2 (g) for at least 15 min before recording cyclic voltammograms.

Modelling of Cyclic Voltammetric Curves: The standard rate constants (k^0, cm/s) were determined by modeling experimental voltammograms with Digisim version 3.03b software (Bioanalytical Systems, Inc. West Lafayette, IN, USA). All CVs were corrected for background hydrogen waves. The transfer coefficient (α) is assumed as 0.5 as used in modelling of $V^{3+/2+}$ HET rates in literature [21,49]. The modeling software converged on a diffusion coefficient of 6×10^{-6} cm^2/s which is also within the range reported in literatures (1.4×10^{-6} to 8.4×10^{-6} cm^2/s) [21,45,49]. Semi-infinite linear diffusion system was considered during the simulation. The half wave potential ($E_{1/2}$ = ½ (E_{pc} + E_{pa})) was calculated as -0.490 V. Scan rate and concentrations (for V^{3+}) used were 0.2 V/s and 0.05 M, respectively. The uncompensated solution resistances were considered as 1.0 Ω for both the KFD felt and the GUITAR/KFD felt and 15.0 Ω for GUITAR flake during the simulation and were measured using the potentiostat.

2.4. Conclusions

This investigation indicates that the application of GUITAR coatings to existing carbon materials for the negative electrode of the VRFB is a viable method for the reduction of parasitic hydrogen gassing as well as increasing the slow HET rates for $V^{3+/2+}$. The HET rate for $V^{3+/2+}$ (0.05 M V^{3+} in 1 M H_2SO_4) on GUITAR-coated KFD felt is 10 times faster than that of the bare KFD graphite felt with a total current that contributes only 3% hydrogen evolution at -1.0 V (vs. Ag/AgCl). Future endeavors will examine the mechanism for V^{3+} reduction, the observed decrement of hydrogen evolution at the negative electrode, as well as the positive ($V^{5+/4+}$) electrode reactions on GUITAR surface.

2.5 References

1) Gyan, I.O.; Cheng, I.F. Electrochemical study of biologically relevant molecules at electrodes constructed from GUITAR, a new carbon allotrope. Microchem. J. 2015, 122, 39–44.

2) Cheng, I.F.; Xie, Y.; Gyan, I.O.; Nicholas, N.W. Highest measured anodic stability in aqueous solutions: Graphenic electrodes from the thermolyzed asphalt reaction. RSC Adv. 2013, 3, 2379–2384.

3) Tanaka, Y.; Furuta, M.; Kuriyama, K.; Kuwabara, R.; Katsuki, Y.; Kondo, T.; Fujishima, A.; Honda, K. Electrochemical properties of N-doped hydrogenated amorphous carbon films fabricated by plasma-enhanced chemical vapor deposition methods. Electrochim. Acta 2011, 56, 1172–1181.

4) Martin, H.B.; Argoitia, A.; Landau, U.; Anderson, A.B.; Angus, J.C. Hydrogen and Oxygen Evolution on Boron-Doped Diamond Electrodes. J. Electrochem. Soc. 1996, 143, L133–L136.

5) Ndlovu, T.; Sampath, O.A.A.S.; Krause, R.W.; Mamba, B.B. Reactivities of Modified and Unmodified Exfoliated Graphite Electrodes in Selected Redox Systems. Int. J. Electrochem. Sci. 2012, 7, 9441–9453.

6) Li, L.; Kim, S.; Wang,W.; Vijayakumar, M.; Nie, Z.; Chen, B.; Zhang, J.; Xia, G.; Hu, J.; Graff, G.; et al. A Stable Vanadium Redox-Flow Battery with High Energy Density for Large-Scale Energy Storage. Adv. Energy Mater. 2011, 1, 394–400.

7) Li, W.; Liu, J.; Yan, C. Graphite-graphite oxide composite electrode for vanadium redox flow battery. Electrochim. Acta 2011, 56, 5290–5294.

8) Joerissen, L.; Garche, J.; Fabjan, C.; Tomazic, G. Possible use of vanadium redox-flow batteries for energy storage in small grids and stand-alone photovoltaic systems. J. Power Sources 2004, 127, 98–104.

9) Fetyan, A.; Derr, I.; Kayarkatte, M.K.; Langner, J.; Bernsmeier, D.; Kraehnert, R.; Roth, C. Electrospun Carbon Nanofibers as Alternative Electrode Materials for Vanadium Redox Flow Batteries. ChemElectroChem 2015, 2, 2055-2060.

10) Xi, J.; Wu, Z.; Teng, X.; Zhao, Y.; Chen, L.; Qiu, X. Self-assembled polyelectrolyte multilayer modified Nafion membrane with suppressed vanadium ion crossover for vanadium redox flow batteries. J. Mater. Chem. 2008, 18, 1232–1238.

11) Kear, G.; Shah, A.A.;Walsh, F.C. Development of the all-vanadium redox flow battery for energy storage: A review of technological, financial and policy aspects. Int. J. Energy Res. 2012, 36, 1105–1120.

12) Weber, A.Z.; Mench, M.M.; Meyers, J.P.; Ross, P.N.; Gostick, J.T.; Liu, Q.H. Redox flow batteries: A review. J. Appl. Electrochem. 2011, 41, 1137–1164.

13) Yang, Z.; Zhang, J.L.; Kintner-Meyer, M.C.W.; Lu, X.; Choi, D.; Lemmon, J.P.; Liu, J. Electrochemical Energy Storage for Green Grid. Chem. Rev. 2011, 111, 3577–3613.

14) Agar, E.; Dennison, C.R.; Knehr, K.W.; Kumbur, E.C. Identification of performance limiting electrode using asymmetric cell configuration in vanadium redox flow batteries. J. Power Sources 2013, 225, 89–94.

15) Aaron, D.; Sun, C.; Bright, M.; Papandrew, A.B.; Mench, M.M.; Zawodzinski, T.A. In Situ Kinetics Studies in All-Vanadium Redox Flow Batteries. ECS Electrochem. Lett. 2013, 2, A1–A3.

16) Agar, E.; Dennison, C.R.; Knehr, K.W.; Kumbur, E.C. Asymmetric performance testing of carbon felt electrodes to identify the limiting electrode in vanadium redox flow batteries. ECS Trans. 2013, 53, 69–73.

17) Chen, F.; L, J.; Chen, H.; Yan, C. Study on Hydrogen Evolution Reaction at a Graphite Electrode in the All-Vanadium Redox Flow Battery. Int. J. Electrochem. Sci. 2012, 7, 3750–3764.

18) Sun, C.; Delnick, F.M.; Baggetto, L.; Veith, G.M.; Zawodzinski, T.A. Hydrogen evolution at the negative electrode of the all-vanadium redox flow batteries. J. Power Sources 2014, 248, 560–564.

19) Surez, D.J.; Gonzlez, Z.; Blanco, C.; Granda, M.; Menndez, R.; Santamara, R. Graphite Felt Modified with Bismuth Nanoparticles as Negative Electrode in a Vanadium Redox Flow Battery. ChemSusChem 2014, 7, 914–918.

20) Parasuraman, A.; Lim, T.M.; Menictas, C.; Skyllas-Kazacos, M. Review of material research and development for vanadium redox flow battery applications. Electrochim. Acta 2013, 101, 27–40.

21) Wu, X.W.; Tomoo, Y.; Suguru, O.; Zhang, Q.X.; Lv, F.C.; Liu, C.M.; Shirasaki, K.; Satoh, I.; Shikama, T.; Lu, D. Acceleration of the redox kinetics of VO^{2+}/VO_2^{+} and V^{3+}/V^{2+} couples on carbon paper. J. Appl. Electrochem. 2011, 41, 1183–1190.

22) Gyan, I.O.; Wojcik, P.M.; Aston, D.E.; McIlroy, D.N.; Cheng, I.F. A Study of the Electrochemical Properties of a New Graphitic Material: GUITAR. ChemElectroChem 2015, 2, 700–706.

23) Li, X.; Zhang, H.; Mai, Z.; Zhang, H.; Vankelecom, I. Ion exchange membranes for vanadium redox flow battery (VRB) applications. Energy Environ. Sci. 2011, 4, 1147–1160.

24) Huang, K.-L.; Li, X.-G.; Liu, S.-Q.; Tan, N.; Chen, L.-Q. Research progress of vanadium redox flow battery for energy storage in China. Renew. Energy 2008, 33, 186–192.

25) Zhong, S.; Kazacos, P.M.; Skyllas-Kazacos, M. Comparison of the physical, chemical and electrochemical properties of rayon and polyacrylonitrile-based graphite felt electrodes. J. Power Sources 1993, 45, 29–41.

26) Kaneko, H.; Nozaki, K.; Wada, Y.; Aoki, T.; Negishi, A.; Kamimoto, M. Vanadium redox reactions and carbon electrodes for vanadium redox flow battery. Electrochim. Acta 1991, 36, 1191–1196.

27) Sun, B.; Skyllas-Kazakos, M. Chemical modification and electrochemical behaviour of graphite fibre in acidic vanadium solution. Electrochim. Acta 1991, 36, 513–517.

28) Lee, H.; Kim, H. Development of nitrogen-doped carbons using the hydrothermal method as electrode materials for vanadium redox flow batteries. J. Appl. Electrochem. 2013, 43, 553–557.

29) Han, P.; Yue, Y.; Liu, Z.; Xu,W.; Zhang, L.; Xu, H.; Dong, S.; Cui, G. Graphene oxide nanosheets/multi-walled carbon nanotubes hybrid as an excellent electrocatalytic material towards VO^{2+}/VO_2^{+} redox couples for vanadium redox flow batteries. Energy Environ. Sci. 2011, 4, 4710–4717.

30) Cheng, I.F.; Xie, Y.; Gonzales, R.A.; Gonzales, P.R.; Sundararajan, J.P.; Fouetio Kengne, B.A.; Aston, D.E.;McIlroy, D.N.; Foutch, J.D.; Griffiths, P.R. Synthesis of graphene paper from pyrolyzed asphalt. Carbon 2011, 49, 2852–2861.

31) Ding, C.; Zhang, H.; Li, X.; Liu, T.; Xing, F. Vanadium Flow Battery for Energy Storage: Prospects and Challenges. J. Phys. Chem. Lett. 2013, 4, 1281–1294.

32) Shen, J.; Liu, S.; He, Z.; Shi, L. Influence of antimony ions in negative electrolyte on the electrochemical performance of vanadium redox flow batteries. Electrochim. Acta 2015, 151, 297–305.

33) Yang, C.; Wang, H.; Lu, S.; Wu, C.; Liu, Y.; Tan, Q.; Liang, D.; Xiang, Y. Titanium nitride as an electrocatalyst for V(II)/V(III) redox couples in all-vanadium redox flow batteries. Electrochim. Acta 2015, 182, 834–840.

34) Huang, X. Fabrication and Properties of Carbon Fibers. Materials 2009, 2, 2369–2403.

35) Smith, R.E.G.; Davies, T.J.; Baynes, N.B.; Nichols, R.J. The electrochemical characterisation of graphite felts. J. Electroanal. Chem. 2015, 747, 29–38.

36) Flox, C.; Rubio-Garcia, J.; Nafria, R.; Zamani, R.; Skoumal, M.; Andreu, T.; Arbiol, J.; Cabot, A.; Morante, J.R. Active nano-$CuPt_3$ electrocatalyst supported on graphene for enhancing reactions at the cathode in all-vanadium redox flow batteries. Carbon 2012, 50, 2347–2374.

37) Bard, A.J.; Faulkner, L.R. Electrochemical Methods: Fundamentals and Applications, 2nd ed.; Wiley: New York, NY, USA, 2000; p. 455.

38) Rice, R.J.; McCreery, R.L. Quantitative Relationship between Electron Transfer Rate and Surface Microstructure of Laser-Modified Graphite Electrodes. Anal. Chem. 1989, 61, 1637–1641.

39) Pour, N.; Kwabi, D.G.; Carney, T.; Darling, R.M.; Perry, M.L.; Shao-Horn, Y. Influence of Edge- and Basal-Plane Sites on the Vanadium Redox Kinetics for Flow Batteries. J. Phys. Chem. C 2015, 119, 5311–5318.

40) Smith, R.E.G.; Davies, T.J.; de B. Baynes, N.; Nichols, R.J. The electrochemical characterisation of graphite felts. J. Electroanal. Chem. 2015, 747, 29–38.

41) McCreery, R.L. Advanced Carbon Electrode Materials for Molecular Electrochemistry. Chem. Rev. 2008, 108, 2646–2687.

42) Yamamura, T.; Watanabe, N.; Yano, T.; Shiokawa, Y. Electron-Transfer Kinetics of Np^{3+}/Np^{4+}, NpO_2^{+}/NpO_2^{2+}, V^{2+}/V^{3+}, and VO^{2+}/VO_2^{+} at Carbon Electrodes. J. Electrochem. Soc. 2005, 152, A830–A836.

43) McDermott, C.A.; Kneten, K.R.; McCreery, R.L. Electron Transfer Kinetics of Aquated $Fe^{+3/+2}$, $Eu^{+3/+2}$, and $V^{+3/+2}$ at Carbon Electrodes: Inner Sphere Catalysis by Surface Oxides. J. Electrochem. Soc. 1993, 140, 2593–2599.

44) Zhu, H.Q.; Zhang, Y.M.; Yue, L.; Li, W.S.; Li, G.L.; Shu, D.; Chen, H.Y. Graphite-carbon nanotube composite electrodes for all vanadium redox flow battery. J. Power Sources 2008, 184, 637–640.

45) Kim, K.J.; Kim, Y.-J.; Kim, J.-H.; Park, M.-S. The effects of surface modification on carbon felt electrodes for use in vanadium redox flow batteries. Mater. Chem. Phys. 2011, 131, 547–553.

46) Sum, E.; Skyllas-kazacos, M. A study of the V(II)/V(III) redox couple for redox flow cell applications. J. Power Sources 1985, 15, 179–190.

47) Yue, L.; Li, W.; Sun, F.; Zhao, L.; Xing, L. Highly hydroxylated carbon fibers as electrode materials of all-vanadium redox flow battery. Carbon 2010, 48, 3079–3090.

48) Yao, C.; Zhang, H.; Liu, T.; Li, X.; Liu, Z. Carbon paper coated with supported tungsten trioxide as novel electrode for all-vanadium flow battery. J. Power Sources 2012, 218, 455–461.

49) Xie, Y.; McAllister, S.D.; Hyde, S.A.; Sundararajan, J.P.; FouetioKengne, B.A.; McIlroy, D.N.; Cheng, I.F. Sulfur as an important co-factor in the formation of multilayer graphene in the thermolyzed asphalt reaction. J. Mater. Chem. 2012, 22, 5723–5729.

Supporting Information

Calculation of "smooth" (or true) surface area of KFD graphite felt and GUITAR/KFD felt:

In regard to the Smith et al [1] calculation method (equation 1 to 3 therein) our values are given in the table below-

Table 2.S1: Values for calculation of "smooth" (or true) surface area of KFD graphite felt and GUITAR/KFD felt.

	KFD graphite felt	**GUITAR/KFD felt**
Density of the felt (g/cm^3)	1.8 [Ref. 1]	1.8 [Ref. 1]
Radius of the graphite fiber (μm)	4.35	6.17
Areal weight of the felt (g/cm^2)	0.025[a]	0.034[b]
Total volume of the graphite fiber (cm^3) ($V_{gf} = m/d_{gf}$)	0.014	0.019
The equivalent length of the graphite fiber (cm) ($V_{gf} = \pi r^2 L_{gf}$)	23562.4	15894.7
"Smooth" surface area of the felt (cm^2) ($A_{gf} = 2\pi r L_{gf}$)	64.4	61.6

a = Reported by SGL Group, b = Measured

Determination of electrochemical surface area of KFD graphite felt and GUITAR/KFD felt using Randles–Sevcik equation:

Randles-Sevcik equation for a reversible process is $I_p = 268{,}600\ n^{3/2} A C \sqrt{(Dv)}$

Where, I_p = Peak current (A)

n = # of electron transferred in the redox process

A = Electrochemical surface area of the electrode (cm^2)

C = Concentration of the redox species (mol/cm^3)

D = Diffusion constant of the redox species (cm^2/s)

v = Scan rate (V/s)

A plot of I_p vs √v gives slope which is equal to 268,600 $n^{3/2}ACvD$ from which the electrochemical surface area (A) of the electrode can be calculated and shown in table 2.S2. The I_p vs √v for both the KFD graphite felt and GUITAR coated KFD graphite felt electrode are shown in figure 2.S1 (in 1 mM $Fe(CN)_6^{3-/4-}$ in + 1 M KCl). For $Fe(CN)_6^{3-/4-}$, n = 1, C= 1×10^{-6} mol/cm^3 and D = 7.26×10^{-6} cm^2/s [2]. Both the felts were made hydrophilic using ethanol as described in Smith et al before use.

Table 2.S2: Values for determination of electrochemical surface area of KFD graphite felt and GUITAR/KFD felt using Randles-Sevcik equation.

	KFD graphite felt	**GUITAR/KFD felt**
Slope of the I_p vs √v plot	0.0089	0.0055
Electrochemical surface area of the felt (cm^2) (slope = $I_p/\sqrt{v}$ = 268,600 $n^{3/2}ACvD$)	12.3	7.6
Geometric area of the felt (cm^2)	0.20	0.15
Electrochemical surface area of the felt/cm^2 of geometric area (cm^2)	61.5	50.6

Scan rate variations on KFD graphite felt and GUITAR/KFD felt:

To distinguish between finite-length (thin-layer) and semi-infinite diffusion behavior on the felt electrodes. Cyclic voltammetry of 1 mM $Fe(CN)_6^{3-/4-}$ (in 1 M KCl) was performed at potential sweep rates (v) between 0.01 to 0.6 V/s (Figure 2.S1). Figure 2.S2 provides the analysis. Thin-layer behavior gives peak current (Ip) α v (see Equation 11.7.17 Ref. [3]), whereas semi-infinite linear diffusion gives Ip α $v^{1/2}$ (Equation 6.3.8 Ref. [3]). At 200 mV/s the current was found to be within the v region where semi-infinite linear diffusion predominates to the electrode surface.

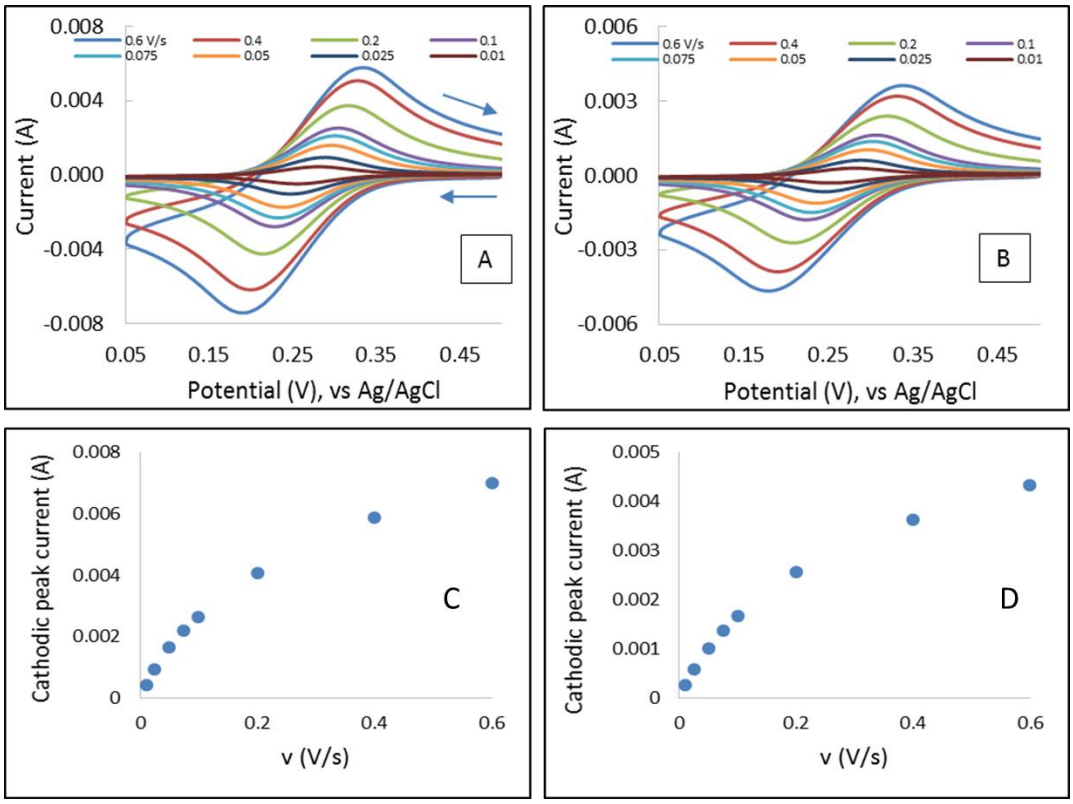

Figure 2.S1. Cyclic Voltammetric scan rate variation on in 1 mM $Fe(CN)_6^{3-/4-}$ (in 1 M KCl) at 0.6, 0.4, 0.2, 0.1, 0.075, 0.05, 0.025 and 0.01 V/s. (A) on KFD felt electrode and the corresponding Ip vs v (C). (B) on GUITAR/KFD felt electrode and the corresponding Ip vs v (D)

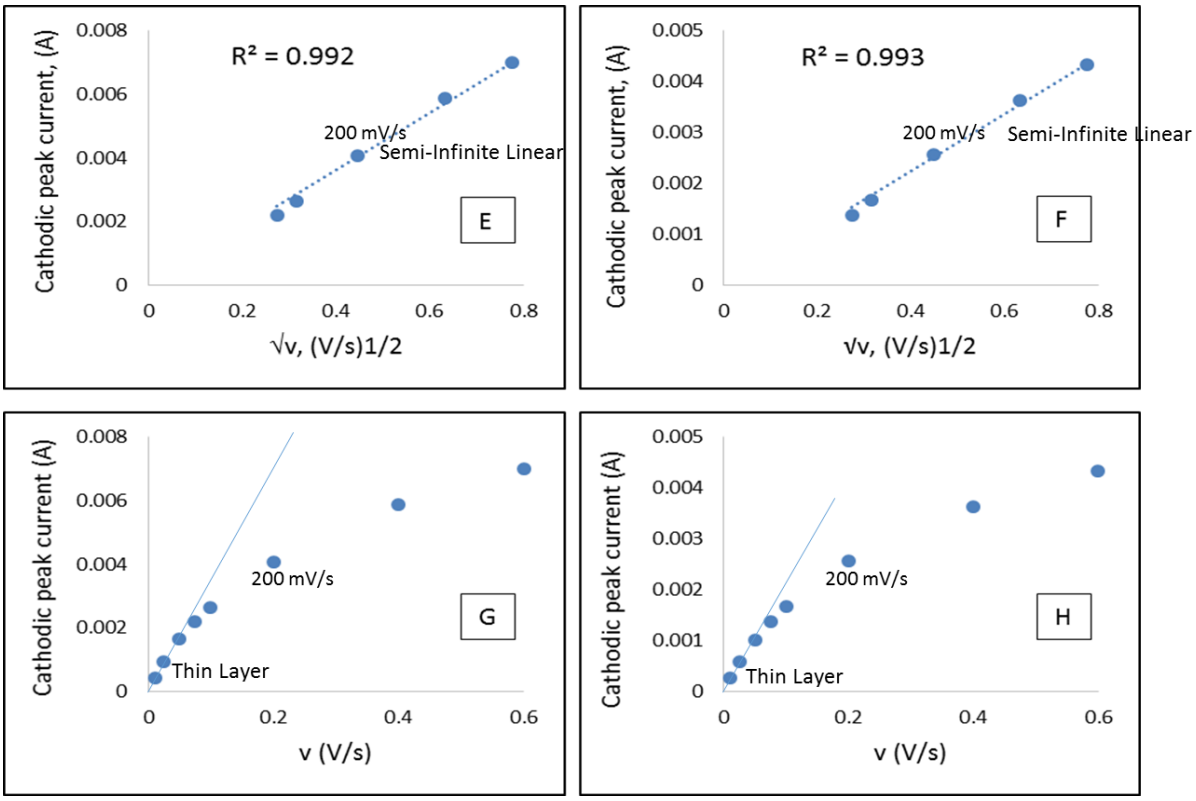

Figure 2.S2. Analysis of cyclic voltammetric peak currents of Figure 2.S1 for thin layer vs. semi-infinite linear diffusion characteristics. (E) Ip vs. $v^{1/2}$ on KFD felt electrode, (F) Ip vs. $v^{1/2}$ on GUITAR/KFD felt. (G) Ip vs. v on KFD felt electrode, (H) Ip vs. v on GUITAR/KFD felt. Thin-layer cell characteristics were found to predominate below 50 mV/s (see Plots G and H). Semi-infinite linear diffusion was found to predominate over 0.075 V/s (see Plots E and F)

Working electrode set-up:

Figure 2.S3 shows the working electrode set-up

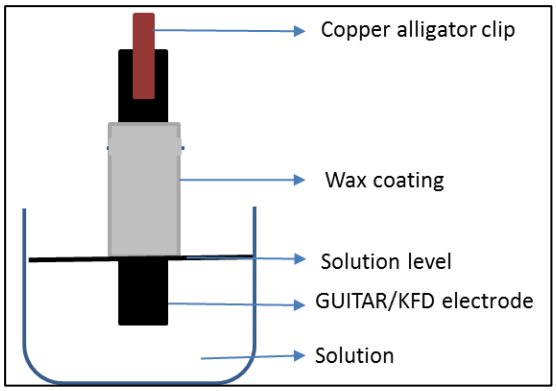

Figure 2.S3. Working electrode set up.

References:

1. Robert E.G. Smith, Trevor J. Davies, Nicholas de B. Baynes, Richard J. Nichols The electrochemical characterization of graphite felts. Journal of Electroanalytical Chemistry 2015, 747, 29–38.

2. S. J. Konopka and Bruce McDuffie. Diffusion Coefficients of Ferri- and Ferrocyanide Ions in Aqueous Media, Using Twin-Electrode Thin-layer Electrochemistry. Analytical Chemistry, 1970, 42 (14), 1741-1746.

3. Allen J. Bard, Larry R. Faulkner, Electrochemical Methods: Fundamentals and Applications, 2nd Ed., John Wiley and Sons 2001, New York.

Chapter 3: Application of GUITAR in Anodic Sensing

"Electrochemical Determination of Chemical Oxygen Demand (COD) on Functionalized Nanocrystalline Graphite Electrodes (GUITAR)." Talanta 2019 (To be submitted).

Abstract

A modified form of nanocrystalline-graphite electrodes from the University of Idaho thermolyzed asphalt reaction (GUITAR) with quinone-like surface functionalities (q-GUITAR) was examined as an anode for the sensing of chemical oxygen demand (COD). These quinone groups were verified by FT-IR and XPS along with cyclic voltammetry (CV). The XPS analysis indicated that the C/O atomic ratio of q-GUITAR is 1.4/1. This is one of the highest abundances of oxygen on the surface of a carbon material reported in literature. The apparent capacitance as measured by CV of q-GUITAR is 170 times greater in 1.0 M H_2SO_4 than the pristine material. This is attributed to the more complete wetting of the porosity of the surface of q-GUITAR relative to the unmodified form. The $Fe(CN)_6^{3-/4-}$ redox probe was used to assess the effects of the quinone groups on heterogeneous electron transfer at the surfaces of the pristine material and q-GUITAR. The CV peak potential differences of 75 mV on GUITAR and 90 mV on q-GUITAR indicates a slightly higher barrier to electron transfer with this inner-sphere couple on the modified surface. The COD sensing performance of q-GUITAR was quantified with glucose, potassium hydrogen phthalate, lactic acid, and sodium dodecyl benzenesulfonate. At a constant potential of 1.6 V vs. Ag/AgCl q-GUITAR anodes have the largest linear range of 0-10000 ppm (as glucose) reported in literature. The limit of detection (40 ppm) and sensitivity are competitive with other electrode systems.

3.1 Introduction

Nanocrystalline-Graphite from the University of Idaho Thermolyzed Asphalt Reaction (GUITAR) is a hypothesized new form of carbon [1,2,3,4,5,6,7,8]. While having morphological and spectroscopic similarities with graphites it differs in the electrochemical properties. These include fast heterogeneous electron transfer (HET) at the basal plane and excellent resistance to corrosion [1,4,5]. With $Fe(CN)_6^{4-/3-}$ redox probe, the basal plane (BP) of GUITAR has a standard rate constant ($k^0 \approx 10^{-2}$ cm/s) that surpasses graphene, graphites, carbon nanotubes (CNT), boron-doped diamond (BDD) and diamond-like carbon (DLC) by 1 to 8 orders of magnitude [1,6]. In 1 M H_2SO_4 the sp^2 hybridized carbon material GUITAR has comparable anodic limits with sp^3 boron-doped diamond [1,5]. In these aspects GUITAR has possible applications as electrochemical sensors especially those requiring anodic stability.

Chemical oxygen demand (COD) is defined as the number of oxygen equivalents consumed in the oxidation of organic compounds [9]. Determination of COD is important for water quality assessment and pollution control [10]. To meet environmental protection regulations, wastewater treatment plants as well as other industries (e.g., textiles, pharmaceutical, dairy, cosmetic, wood, paper, leather, food, etc.) are required to monitor COD levels of their effluents in a timely and accurate fashion [11,12]. The traditional technique determines COD by oxidative degradation of organics through volumetric redox titration with strong oxidizing agents such as dichromate or permanganate [9,10]. However, this method has some intrinsic drawbacks including large sample volumes, time-consuming reflux process (2-4 h), complicated handling, incomplete oxidation of volatile compounds, expensive reagents (Ag_2SO_4), corrosive (concentrated H_2SO_4) and toxic (Hg and Cr) chemicals along with health

and safety concerns [9,10]. Additionally, the reproducibility of results is heavily dependent on operator skill.

Numerous efforts have been made to overcome these disadvantages by developing simple and rapid analytical approaches [9,10,11]. Emerging techniques for COD determination include electrochemical methods [14,15], photocatalytic method [11], and ultraviolet [16], fluorescence [17], chemiluminescence [18], and photoelectrochemical [19] spectroscopies. Electrochemical methods have received much attention due to the promise of a cost effective, portable, and rapid detector with continuous monitoring abilities and little or no sample preparation. This is through direct oxidation of the organics in aqueous electrolyte at an electrode via Reaction 3.1.

$$C_xH_yN_zO_w + {}^{(n-y)}/_2\, H_2O \rightarrow xCO_2 + zNO_2 + nH^+ + ne^- \qquad (3.1)$$

This process requires a corrosion resistant anode. As a result, present efforts have examined sensing electrodes based on boron doped diamond [15], copper [9], nickel [20], cobalt [21], titanium [22], and lead [23]. However, in most instances problems such as narrow linear range, material expense, and/or surface fouling were encountered. Inexpensive graphitic electrodes do not offer enough stability for anodic COD sensing as they are subject to corrosion at the electrochemical potentials for Reaction 3.1 [10]. For this study, the applicability of corrosion resistant GUITAR as an anode for electrochemical COD sensing was examined. This feature along with fast HET rates at its basal planes indicate strong possibilities for the continuous determination of COD.

3.2 Experimental

Chemicals and Materials. Sodium sulfate (anhydrous) and potassium hydrogen phthalate were obtained from EMD Chemicals (Gibbstown, NJ, USA). D-glucose (anhydrous, granular) was obtained from Macron Fine Chemicals (Center Valley, PA, USA). Lactic acid solution (≥85% in H_2O) and Sodium dodecyl benzenesulfonate were obtained from Sigma-Aldrich (St. Louis, MO, USA). Sulfuric acid (96.3%) was obtained from the J.T Baker Chemical Co. (Phillipsburg, NJ, USA). Potassium chloride was obtained from Fisher Chemical (Fair Lawn, NJ, USA). Potassium ferricyanide was obtained from Acros Organics (Morris Plains, NJ, USA). Graphite foils were obtained from John Crane Inc. (Chicago, IL, USA). Quartz tubes obtained from Technical Glass Products Inc. (Painesville Twp., OH, USA) were used as substrate for GUITAR synthesis. All aqueous solutions were prepared with deionized water purified by passage through an activated carbon purification cartridge obtained from Barnstead - model D8922 (IA, USA).

Electrode Fabrication and Electrochemical Setup: GUITAR samples were synthesized as described in previous studies [1]. Electrode fabrication and geometric area isolation were performed as described previously [1]. All electrochemical studies were conducted in a three-electrode undivided cell with graphite rod counter electrode and Ag/AgCl/3M NaCl (aq) (0.209 V vs SHE) reference electrode. Cyclic voltammetry (CV) was carried out using a Bioanalytical Systems (BAS) CV-50W potentiostat (West Lafayette, IN, USA).

Electrode Characterization: IR spectra were recorded using Thermo Fisher Scientific Nicolet-iS10 FT-IR spectrometer. The X-ray photoelectron spectroscopy (XPS) apparatus was built in-house at the University of Idaho. XPS was performed in a vacuum chamber with a base

pressure of 1×10^{-10} torr. Measurements were made with the Al Kα emission line (1486.6 eV) and a hemispherical energy analyzer with a resolution of 0.025 eV. During spectral acquisition the samples were grounded and exposed to a 500 eV electron beam to eliminate spurious charging. All spectra were acquired at room temperature. The XPS peaks were fitted to the Gaussian curve after performing a Shirley background subtraction. For all the fitted peaks, the FWHM were kept to the same value.

3.3 Results and Discussion

Two different surfaces were examined for chronoamperometric COD sensing. These include pristine and electrochemically modified GUITAR surfaces. For the latter, this was conducted by application of +2.1 V for 150 sec followed by 15 cyclic voltammetric cycles from -0.7 V to +1.0 V at 50 mV/s in 1.0 M H_2SO_4. This procedure functionalized the surface of GUITAR with quinone-like moieties (q-GUITAR). This modification as well as optimization of q-GUITAR synthesis potential are described in detail in the Supplementary Information (Figure S1). The q-GUITAR surface has a bluish hue relative to the metallic appearance of GUITAR (see photographs in Figure 5). It is noteworthy that attempts at making quinone functionalized graphite under the same conditions for q-GUITAR fails as it gives mechanically unstable expanded layers that exfoliate in solution (see Figure S2). Unlike graphites, GUITAR does not undergo a dimensional expansion by electrochemical oxidation. The basal planes of graphites is penetrated by electrolytes which under oxidative potentials evolve CO_2 and O_2 gases which cause blistering, expansion, and pit corrosion [24].

3.3.1 Characterization of q-GUITAR

Infrared and x-ray photoelectron spectroscopy (XPS) analyses indicate the attachment of oxygen containing functional groups on the surface of GUITAR by the electrochemical treatment. The FT-IR spectra of GUITAR and q-GUITAR are shown in Figure 1. The pristine material shows no discernable peaks while q-GUITAR has features indicating broad signals at 3700-3000 cm^{-1} and peaks at 1726, 1620, 1185 and 1063 cm^{-1}. These are attributed to C-O-H, C=O, aromatic C=C and C-O (1185 and 1063 cm^{-1}) respectively [25]. An earlier study reveals that GUITAR contains 88% carbon and 12% hydrogen [1]. The XPS analysis on pristine GUITAR is discussed in a previous study. Only a C1s peak with two components, C=C at 284.2 eV (85%) and C-C at 285.4 eV (15%) is observed [1]. This material conforms to XPS of graphitic materials in the literature (See Table 3.1). The XPS spectrum on q-GUITAR is shown in Figure 2. The wide scan XPS spectrum on q-GUITAR shows O1s peak along with the C1s peak (Figure 2A). The deconvolved components of C1s peak in Figure 2B indicates a surface that consists of 41% oxides (19% C-O at 285.9 eV, 11.8% C=O at 287.4 eV and 10.2% COOH at 288.8 eV). The total oxide concentrations of 41% (C:O atomic ratio 1.4:1) for q-GUITAR is one of the highest for a sp^2 carbon material. In a previous study, q-GUITAR synthesized at 2.0 V (vs Ag/AgCl) for 150 seconds followed by 15 cyclic voltammetric scans from -0.7 to 1.0 V at 50 mV/s in 1.0 M H_2SO_4 contained a total oxide concentrations of 34% (17.5% C-O, 9.1% C=O and 7.0% COOH) [26]. Literature graphene oxides (GO) range from 25 to 44% (see Table 3.1 and references therein). It is important to note that GO materials are formed by the chemical oxidation of graphite which delaminates into separated oxidized graphene layers. This is from the electrolyte intercalation mechanism described above. These layers are reassembled by

filtration forming layered graphene oxides. On the other hand, q-GUITAR maintains its dimensional integrity during oxidation. This feature along with resistance to corrosion and fast HET rates at the BP are indicators that GUITAR is a carbon form distinct from graphite.

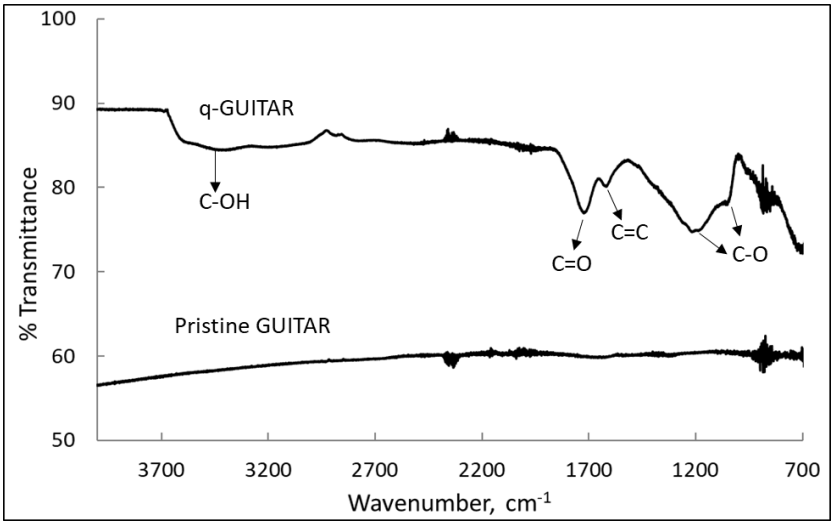

Figure 3.1. FT-IR spectra on pristine (bottom) and q-GUITAR (top). The peak assignments at 3700-3000, 1726, 1620, 1185 and 1063 cm^{-1} are indicated in the figure.

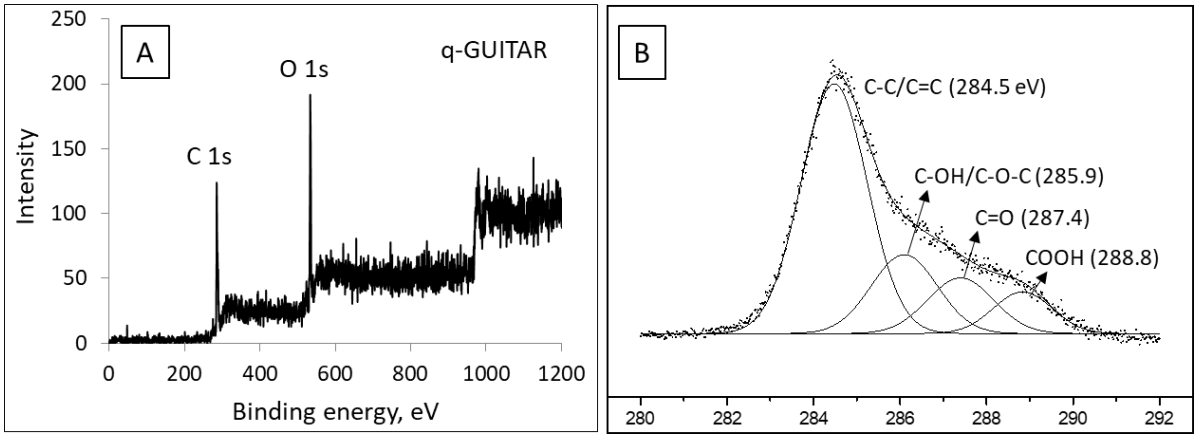

Figure 3.2. Wide scan XPS spectrum on q-GUITAR (A). Deconvolved components of C1s peak (B).

Table 3.1. Comparison of surface oxides content of GUITAR and q-GUITAR with graphite, reduced graphene and graphene oxides as measured by XPS.

Material	Oxygen (%)	Carbon (%)			C/O atomic ratio	Ref.
		Total Carbon (%)	sp^2 (%)	sp^3 (%)		
GUITAR	-	88.0 (12.0% H)	85.0	15.0	N/A	1
q-GUITAR	41.0	59.0	-	-	1.4/1	This work
	34.0	66.0	-	-	1.9/1	26
Graphite	3.4	96.6	80.0	20.0	28.4/1	27
Reduced Graphene	3.0	97.0	75.0	25.0	32.3/1	27
	8.8	91.2	90.0	10.0	10.3/1	28
	16.6	83.4	-	-	5/1	29
	20.0	80.0	70.0	30.0	4/1	30
Graphene Oxide	25.6	74.4	77.8	22.2	2.9/1	31
	27.0	73.0	70.0	30.0	2.7/1	28
	32.5	67.5	40.0	60.0	2.1/1	27
	33.3	66.7	46.0	54.0	2/1	30
	43.8	56.2	-	-	1.3/1	29

3.3.2 Surface Capacitance of q-GUITAR Relative to GUITAR

In general, double layer capacitance is proportional to electrode surface area [32]. This quantity was measured for pristine and q-GUITAR in 1.0 M H_2SO_4 by cyclic voltammetry (Figure 3.3A). Non-faradaic current (i) gives capacitance (C) through C = i/v, (where v is potential sweep rate). At 50 mV/sec, pristine GUITAR has a double layer capacitance of 15 $\mu F/cm^2$, a value that is close to other graphitic materials [33,34]. On the other hand, q-GUITAR has a double layer capacitance of 2,600 $\mu F/cm^2$ at +0.1 V, corresponding to an increase of 170

times in surface area relative to pristine GUITAR. Potentials above +0.2 V in Figure 3.3A contains the quinone group faradaic current and was not considered in the calculation for capacitance. As discussed above, GUITAR is not subject to the corrosion mechanism endemic to graphites, therefore the increase in capacitance cannot be attributed to the exposure of the subsurface graphene planes.

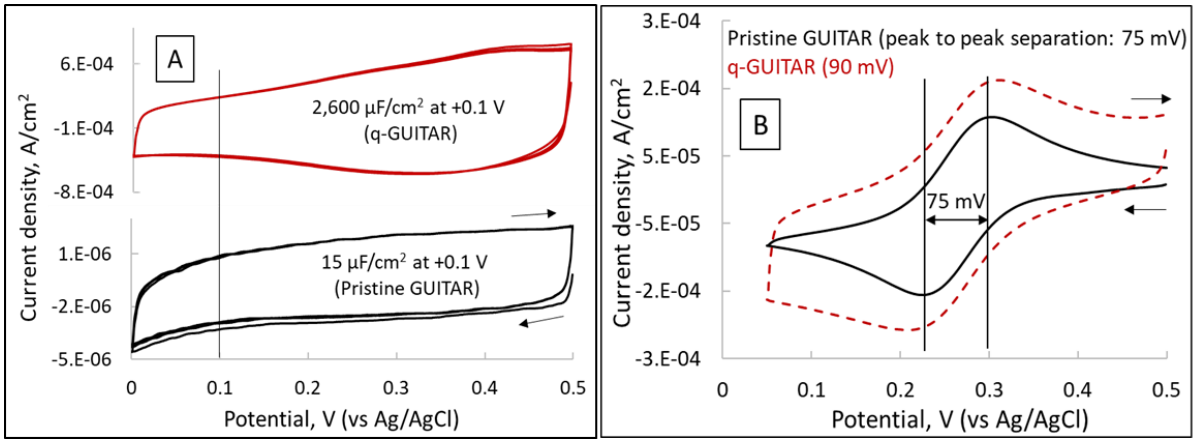

Figure 3.3. (A) Electrochemical double layer capacitance in 1.0 M H_2SO_4 and (B) peak to peak separation in 1.0 mM $Fe(CN)_6^{3-/4-}$ (in 1.0 M KCl) on pristine and q-GUITAR surfaces at 50 mV/s.

An atomic forces microscopy investigation of the basal plane of GUITAR in a previous study indicates a wavy surface with random distribution of pores 10-50 nm in diameter and an amplitude of 20 nm [2]. It is likely that insertion of oxygen containing groups on the surface of basal plane of GUITAR increases hydrophilicity and allows aqueous electrolyte to fully wet these pores on q-GUITAR.

3.3.3 Heterogeneous Electron Transfer Kinetics

The COD sensing scheme relies on HET via Reaction 3.1. In general, the basal plane of GUITAR has excellent HET rates for $Fe(CN)_6^{3-/4-}$ which matches those of the edge plane graphitic materials [1,6]. In order to assess how the formation of quinone functionalities affect HET

rates, cyclic voltammetric (CV) studies with $Fe(CN)_6^{3-/4-}$ on q-GUITAR electrodes were conducted. Figure 3.3B illustrates the CV studies. The potential peak to peak (ΔEp) separations of 75±10 mV (n=20) and 90±10 mV (n=10) correspond to the basal planes of GUITAR and q-GUITAR respectively. These values are statistically different at the 95% confidence level by the t-test. The pristine material behaves as previously described [1,2]. The ΔEp for q-GUITAR at its basal plane is indicating slightly slower HET rates for the $Fe(CN)_6^{3-/4-}$ redox couple. On other graphitic electrodes, this species is described as being insensitive to surface oxides and not requiring adsorption [35]. On the other hand, Ji et al suggest that $Fe(CN)_6^{3-/4-}$ is an inner-sphere which is dependent on surface functionalities of graphite electrode [36]. The authors also observed that outer-sphere redox couples were largely unaffected by the presence of surface oxides.

3.3.4 Determination of Chemical Oxygen Demand (COD) on Pristine and q-GUITAR

Four surrogates for chemical oxygen demand (COD) were investigated. These included glucoses, potassium hydrogen phthalate (KHP), lactic acid, and sodium dodecyl benzenesulfonate (SDBS). All were selected based on their common usage in the literature [15,37,38,39,40]. Chronoamperometric studies via Reaction 3.1 were conducted at +1.6 V in 0.1 M Na_2SO_4 solution on the pristine and q-GUITAR surfaces. The responses are shown in Figure 3.4 (A and B) and a family of chronoamperometric responses with glucose on q-GUITAR is shown in Figure 3.S3. The optimization of electrode potential is explained in the Supplementary Information (Figure 3.S4). In short, chronoamperometric responses were measured at 1.5, 1.6, 1.8 and 2.0 V. The optimal electrode potential was selected based on

background signal and sensitivity considerations. In Figure 3.4C it is evident that q-GUITAR has a more sensitive current response for glucose at 1.6 V over the unmodified electrode. The current signal at 10 seconds is approximately 85% greater (from 140 to 260 $\mu A/cm^2$) for 4000 mg/L COD (Glucose). The balance of the investigation was therefore concentrated on q-GUITAR. Although the HET rate for q-GUITAR was found to be slower for $Fe(CN)_6^{4-/3-}$ than unmodified GUITAR, complete wetting of the surface may have an important role for adsorption and electro-oxidation of organics via Reaction 3.1. Surface fouling and signal loss is associated with the adsorption of organics [41]. This is evident with q-GUITAR by the subsequent re-measurement with the same surface which shows a decayed response of 170 from 260 $\mu A/cm^2$ (Figure 3.4D). Pristine GUITAR surfaces experienced a similar fouling phenomenon. Regeneration was conducted by application of +1.6 V for 2 minutes followed by -0.7 V for 3 minutes in 0.1 M Na_2SO_4. The optimization of this process is explained in the Supplementary Information (Figure 3.S5). This procedure is necessary to produce the calibration curves of all four COD surrogates in Figure 3.4A (pristine) and B (q-GUITAR). From Figure 3.4A it is evident that the sensitivities (slopes) of the response of each surrogate differs on the pristine GUITAR. This problematic feature is observed with other electrochemical COD detectors in the literature [22,39,42,43]. On the other hand, differences in the sensitivities between each of the four COD surrogates (Figure 3.4B) is somewhat alleviated with the use of q-GUITAR. The slopes varied from 0.046 (μA.mg COD/cm^2L) for lactic acid to 0.032 for glucose. Figure 3.5 illustrates the sequence for q-GUITAR sensor formation to COD sensing to surface regeneration. The stability of the q-GUITAR electrodes is found stable up to 10 measurements, after which a failure in COD measurement is noticed. Table 3.2 summarizes

the results of COD detection with q-GUITAR and those in literature. It is apparent from that table that the linear range of the q-GUITAR anode is among the highest in literature. This adds flexibility in applications as COD concentrations for industrial and domestic effluents vary from 400-65,700 and 300-1000 mg/L, respectively [44,45]. Depending on the country and industry the COD limit in the industrial discharged wastewater is 75-34,000 mg/L [46,47]. The limit of detection (LOD) of the q-GUITAR anode of 40 ppm for glucose is therefore competitive in the literature and applicable to monitoring COD.

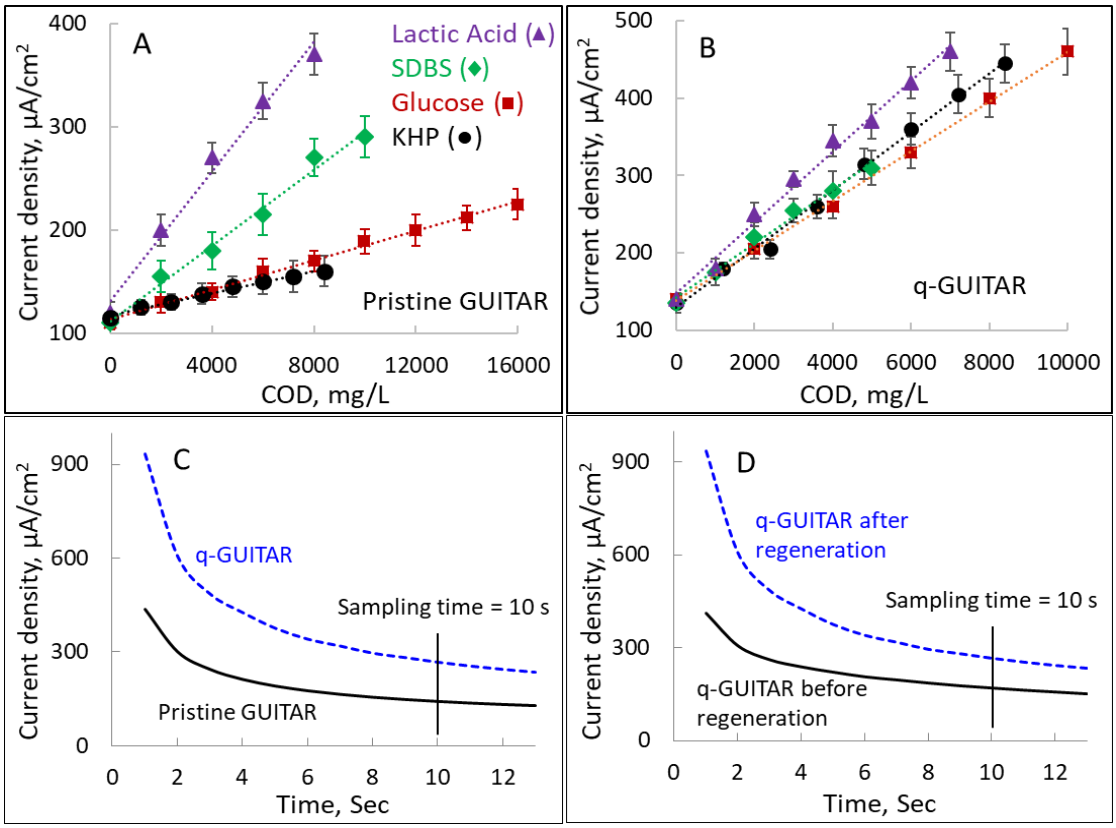

Figure 3.4. Determination of chemical oxygen demand (COD) with glucose, potassium hydrogen phthalate (KHP), lactic acid, and sodium dodecyl benzenesulfonate (SDBS) on (A) pristine and (B) q-GUITAR at +1.6 V in 0.1 M Na_2SO_4 (n=5). Amperometric responses of 4000 mg/L COD (Glucose) on (C) pristine and q-GUITAR and (D) aged (black) and regenerated (blue) q-GUITAR at +1.6 V in 0.1 M Na_2SO_4.

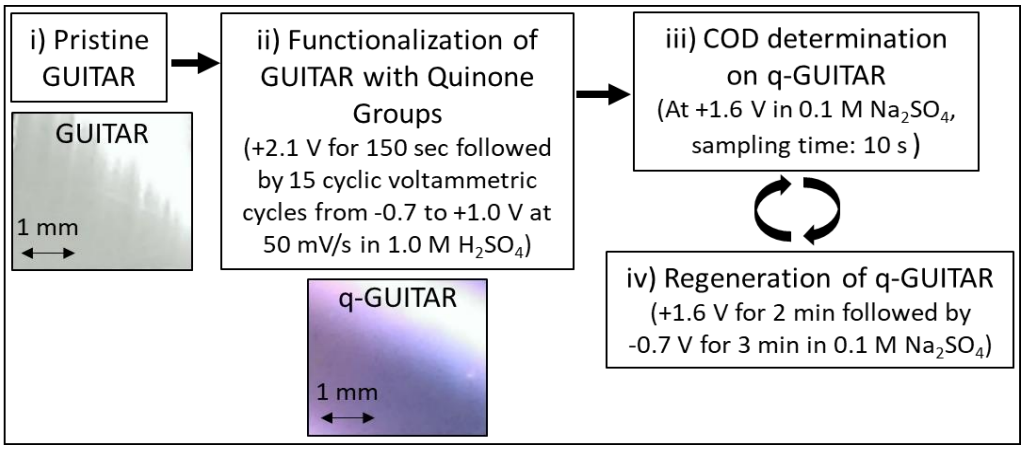

Figure 3.5. Flow chart showing the generation of q-GUITAR and their optical images, COD analysis and surface regeneration.

Table 3.2. Comparison of linear range, limit of detection (LOD), sensitivity, stability (number of measurements, n) and Cl^- tolerance of q-GUITAR with literature COD sensor electrodes.

Material	Analyte	Potential* (V)	Linear range (mg/L)	LOD (mg/L)	Sensitivity (μA-L/mg-cm^2)	n	Cl^- tolerance (mg/L)	Ref.
q-GUITAR	Glucose	1.6	0-10000	40	0.032	≈ 10	100	This Work
	KHP		0-9000	33	0.038			
	SDBS		0-5000	36	0.035			
	Lactic acid		0-7000	27	0.046			
Boron doped diamond (BDD)	Mixture of Glucose, KHP, Ethanol, 4-Hydroxybenzoic acid, Glutamic acid, Acetic acid, Acetone, Sucrose, Phenol	2.8	2-175	1	0.5	500	0	36
	Glucose, KHP, Glutamic acid, Phenol, Oxalic acid, p-Nitrophenol, Acetic acid, Cysteamine, Salicylic acid	2.5	20-9000	7.5	7.6	400	-	11,43
	KHP, Glucose	1.6	0-232	0.2	1.5	-	-	44
Ti/TiO_2	KHP, Phenol	2.0	25-530		0.1		-	18
PbO_2/ graphite	Glucose, KHP	1.5	200-6000		0.005		-	33
F-PbO_2/	Glucose	1.3	100-1200	15	0.008	650	C_{Cl^-}/COD	19

Pt							<2.5	
Cu NPs/ Cu disk	Glycine	0.8	4.8 600	3.6	6.4		700	5
CoO/glassy carbon		0.8	17-170	1.1	14.2	1	700	17
Cu-Ni NPS/ MWCNT	Glucose	0.75	106-1292	21	0.91		-	16
CuO-AgO NPs/ MWCNT				28	0.027			
CoO NPs/ MWCNT				36	0.61			
Ni NPs/ MWCNT				58	0.16			
Cu/CuO	Glucose	0.7	53-2800	20.3	4.8	150	-	45
Cu-Co NPs/Au	Glucose	0.6	2-768	0.6	12.6		700	46
Ni NPs/ glassy carbon	Glucose, Phenol, Lactose, Citric acid, Aniline, Ethanol, Glycose, Pyrrole	0.5	10- 533	1.1	0.8	35	700	6
	Glycine	0.4	0.2-480	0.14	16.3		3500	47

*COD determining potential vs. Ag/AgCl.

NPs - Nanoparticles, MWCNT - Multiwall carbon nanotube, KHP - Potassium hydrogen phthalate, SDBS - Sodium dodecyl benzenesulfonate, F-PbO_2 - Fluorinated PbO_2.

3.3.5 Chloride Interference

Chloride is an interference in the classical titration method and with the newer emerging anode-based sensors for COD measurements [10,23,41,52]. This effect is based on the oxidation of these ions at the prevailing potentials of the sensors (see Reaction 3.2).

$$Cl_2(aq) + 2e^- \rightleftarrows 2Cl^-(aq) \qquad E^0 = 1.396\ V \qquad (3.2)$$

This is of concern as chloride content in domestic and industrial effluents varies within the range of 20-300 and 100-4500 mg/L respectively [53,54]. Figure 3.6 compares the chronoamperometric responses (at 1.6 V) of 2000 mg/L COD (glucose) and 350 mg/L Cl^- injections at 120 and 210 seconds respectively. This indicates that Cl^- is indeed an interference at the q-GUITAR anode.

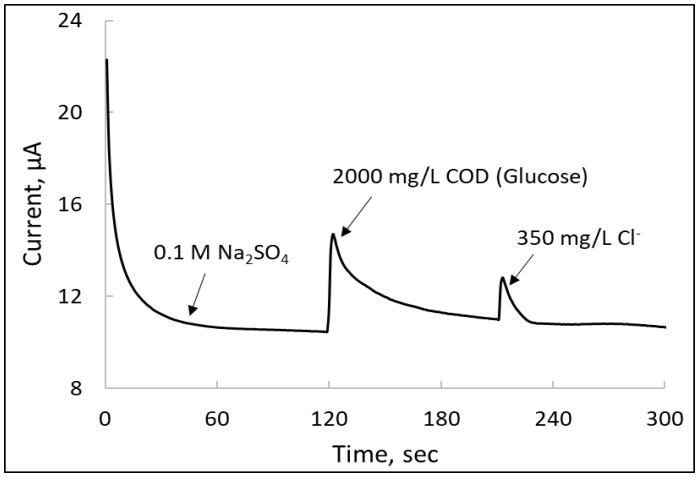

Figure 3.6. Interference of chloride on COD detection with q-GUITAR anodes held at +1.6 V in 0.1 M Na_2SO_4.

We expect that chloride will be of concern to the q-GUITAR COD detector, as well as the other carbon-based sensors. The maximum Cl^- tolerance level for q-GUITAR anode is found to be 100 mg/L, above which the Cl^- interference becomes noticeable (see Figure 3.S6). While chloride can be precipitated out using $HgSO_4$ or $AgNO_3$ prior to the determination of COD

[10,52], the development of strategies aimed at mitigating this interference is underway and will be reported in future publications.

3.4 Conclusions

The q-GUITAR anode exhibits excellent linear ranges (0-10,000 ppm as glucose) for COD analysis and surpasses most other electrode sensors. The LOD (40 ppm) and sensitivity are competitive albeit with the Cl^- interference that is evident with conventional titration and most of other electrochemical sensors. It is expected that GUITAR anodes will be inexpensive relative to other materials and offer the strong possibility of a disposable test strip configuration for portability.

3.5 References

1) Kabir, H.; Zhu, H.; May, J.; Hamal, K.; Kan, Y.; Williams, T.; Echeverria, E.; McIlroy, D. N.; Estrada, D.; Davis, P. H.; Pandhi, T.; Yocham, K.; Higginbotham, K.; Clearfield, A.; Cheng, I. F. CARBON 2019, 144, 831-840.

2) Cheng, I. F.; Xie, Y. Q.; Gonzales, R. A.; Brejna, P. R.; Sundararajan, J. P.; Kengne, B. A. F.; Aston, D. E.; McIlroy, D. N.; Foutch, J. D.; Griffiths, P. R. CARBON 2011, 49(8), 2852-2861.

3) Gyan, I. O.; Wojcik, P. M.; Aston, E. D.; McIlroy, D. N.; Cheng, I. F. ChemElectroChem 2015, 2, 700-706.

4) Gyan, I. O.; Cheng, I. F. Microchemical Journal 2015, 122, 39-44.

5) Kabir, H.; Gyan, I. O.; Foutch, J. D.; Zhu, H.; Cheng, I. F. C - Journal of Carbon Research 2016, 2, 13.

6) Villarreal, C. C.; Pham, T.; Ramnani, P.; Mulchandani, A. Current Opinion in Electrochemistry 2017, 3(1), 106-113.

7) Xie, Y.; McAllister, S. D.; Hyde, S. A.; Sundararajan, J. P.; Kengne, B. A. F.; McIlroy, D. N.; Cheng, I. F. Journal of Materials Chemistry 2012, 22, 5723-5729.

8) Kabir, H.; Ma, P. Y.; Renn, N.; Nicholas, N. W.; Cheng, I. F. Analytical Chemistry 2019 (Submitted).

9) Yang, J.; Chen, J.; Zhou, Y.; Wu, K. Sensors and Actuators B 2011, 153, 78–82.

10) Jing, T.; Zhou, Y.; Hao, Q.; Zhou, Y.; Mei, S. Analytical Methods 2012, 4, 1155-1159.

11) Zhao, H.; Jiang, D.; Zhang, S.; John, R. Analytical Chemistry 2004, 76, 155−160.

12) Brillas, E.; Huitle, C. A. M. Applied Catalysis B: Environmental 2015, 166–167, 603–643.

13) Moore, W. A.; Walker, W. W. Analytical Chemistry 1956, 28, 164–167.

14) Bogdanowicz, R.; Czupryniak, J.; Gnyba, M.; Ryl, J.; Ossowski, T.; Sobaszek, M.; Siedlecka, E. M.; Darowicki, K. Sensors and Actuators B 2013, 189, 30-36.

15) Kondo, T.; Tamura, Y.; Hoshino, M.; Watanabe, T.; Aikawa, T.; Yuasa, M.; Einaga, Y. Analytical Chemistry 2014, 86, 8066−8072.

16) Kong, H.; Wu, H. Water Environment Research 2009, 81, 2381–2386.

17) Hur, J.; Lee, B. M.; Lee. T. H.; Park, D. H. Sensors 2010, 10, 2460–2471.

18) Yao, H.; Wu, B.; Qu, H.; Cheng, Y. Analytica Chimica Acta 2009, 633, 76–80.

19) Zhang, S.; Li, L.; Zhao, H. Environmental Science & Technology 2009, 43, 7810-7815.

20) Capitán, M. G.; Baldi, A.; Gómez, R.; García, V.; Jorquera, C. J.; Sánchez, C. F. Analytical Chemistry 2015, 87, 2152−2160.

21) Wang, J.; Wu, C.; Wu, K.; Cheng, Q.; Zhou, Y. Analytica Chimica Acta 2012, 736, 55-61.

22) Ge, Y.; Zhai, Y.; Niu, D.; Wang, Y.; Fernandez, C.; Ramakrishnappa, T.; Hu, X.; Wang, L. International Journal of Electrochemical Science 2016, 11, 9812-9821.

23) Li, J.; Li, L.; Zheng, L.; Xian, Y.; Ai, S.; Jin, L. Analytica Chimica Acta 2005, 548, 199–204.

24) Goss, C. A.; Brumfield, J. C.; Irene, E. A.; Murray, R. W. Analytical Chemistry 1993, 65, 1378-1389.

25) Kabir, H.; Gyan, I. O.; Cheng, I. F. Journal of Power Sources 2017, 342, 31-37.

26) Zhu, H.; Kabir, H.; Lopez, R.; Smith, H. J.; Nicholas, N. W.; Sankaran, P.; McIlroy, D. N.; Cheng, I. F. Analytical Chemistry 2019 (Submitted).

27) Ganguly, A.; Sharma, S.; Papakonstantinou, P.; Hamilton, J. Journal of Physical Chemistry C
2011, 115, 17009–17019.

28) Dreyer, D. R.; Park, S.; Bielawski, C. W.; Ruoff, R. S. Chemical Society Reviews 2010, 39, 228-240.

29) Khan, M.; Al-Marri, A. H.; Khan, M.; Shaik, M. R.; Mohri, N.; Adil, S. F.; Kuniyil, M.; Alkhathlan, H. J.; Warthan, A. A.; Tremel, W.; Tahir, M. N.; Siddiqui, M. R. H. Nanoscale Research Letters 2015, 10, 281.

30) Chang, H.; Sun, Z.; Saito, M.; Yuan, Q.; Zhang, H.; Li, J.; Wang, Z.; Fujita, T.; Ding, F.; Zheng, Z.; Yan, F.; Wu, H.; Chen, M.; Ikuhara, Y. ACS Nano 2013, 7(7), 6310–6320.

31) Moraesa, A. C. M.; Andrade, P. F.; Faria, A. F.; Simões, M. B.; Salomão, F. C. S.; Barros, E. B.; Goncalves, M. C.; Alves, O. L. Carbohydrate Polymers 2015, 123, 217–227.

32) Hengxing; Zhao, X.; Qiao, Z.; Jung, J.; Zhu, Y.; Lu, Y.; Zhang, L.; MacDonald, A. H.; Ruoff, R. S. Nature Communications 2014, 5, 3317.

33) Liu, C.; Yu, Z.; Neff, D.; Zhamu, A.; Jang, B. Z. Nano Letters 2010, 10, 4863–4868.

34) Shi, H. Electrochimica Acta 1996, 41(10), 1633-1639.

35) McCreery, R. L. Chemical Reviews 2008, 108, 2646-2687.

36) Ji, X.; Banks, C. E.; Crossley, A.; Compton, R. G. ChemPhysChem 2006, 7, 1337-1344.

37) Wang, J.; Li, K.; Yang, C.; Wang, Y.; Jia, J. Electrochemistry Communications 2012, 18, 51-54.

38) Mo, H.; Wang, X.; Chen, Y.; Sun, Y.; Wan, P. The Electrochemical Society Conference on Energy and the Environment 2014 Abstract #541.

39) Wang, C.; Wu, J.; Wang, P.; Ao, Y.; Hou, J.; Qian, J. Analytica Chimica Acta 2013, 767, 141-147.

40) Kim, Y. C.; Lee, K. H.; Sasaki, S.; Hashimoto, K.; Ikebukuro, K.; Karube, I. Analytical Chemistry 2000, 72, 3379-3382.

41) Yu, H.; Ma, C.; Quan, X.; Chen, S.; Zhao, H. Environmental Science & Technology 2009, 43, 1935-1939.

42) Li, X.; Bai, J.; Liu, Q.; Li, J.; Zhou, B. Sensors 2014, 14, 10680-10690.

43) Zhang, A.; Zhou, M.; Han, L.; Zhou, Q. Electroanalysis 2010, 22(24), 2947-2959.

44) Chan, Y. J.; Chong, M. F.; Law, C. L.; Hassell, D. G. Chemical Engineering Journal 2009, 155, 1-18.

45) U.S. EPA Handbook. Septage treatment and disposal. EPA/625/6-84/009 (NTIS PB88184015), 1984, 27-33.

46) Effluent Limit Development Guidance. Idaho Pollutant Discharge Elimination System, Department of Environmental Quality 2017, State of Idaho, USA.

47) Textile Industry Wastewater Discharge Quality Standards. Literature Review 1 - Zero Discharge of Hazardous Chemicals Programme, 2015.

48) Yu, H.; Wang, H.; Quan, X.; Chen, S.; Zhang, Y. Electrochemistry Communications 2007, 9, 2280-2285.

49) Silva, C. R.; Conceição, C. D. C.; Bonifácio, V. G.; Filho, O. F.; Teixeira, M. F. S. Journal of Solid-State Electrochemistry 2009, 13, 665-669.

50) Wang, J.; Yao, N.; Li, M.; Hu, J.; Chen, J.; Hao, Q.; Wu, K.; Zhou, K. Microchimica Acta 2015, 182, 515–522.

51) Cheng, Q.; Wu, C.; Chen, J.; Zhou, Y.; Wu, K. Journal of Physical Chemistry C 2011, 115, 22845-22850.

52) Ma, C.; Tan, F.; Zhao, H.; Chen, S.; Quan, X. Sensors and Actuators B 2011, 155, 114–119.

53) Rajkumar, D.; Palanivelu, K. Journal of Hazardous Materials B 2004, 113, 123-129.

54) Szpyrkowicz, L.; Naumczyk, J.; Grandi, F. G. Water Research 1995, 29(2), 517-524.

Supplementary Information

Electrochemical Modification of GUITAR

Electrochemical modification of GUITAR to q-GUITAR was conducted by application of +2.1 V vs. Ag/AgCl for 150 sec followed by 15 cyclic voltammetric (CV) scans from -0.7 V to +1.0 V at 50 mV/s in 1.0 M H_2SO_4. The corresponding chronoamperograms at 1.8 to 2.1 V are shown in Figure 3.S1.

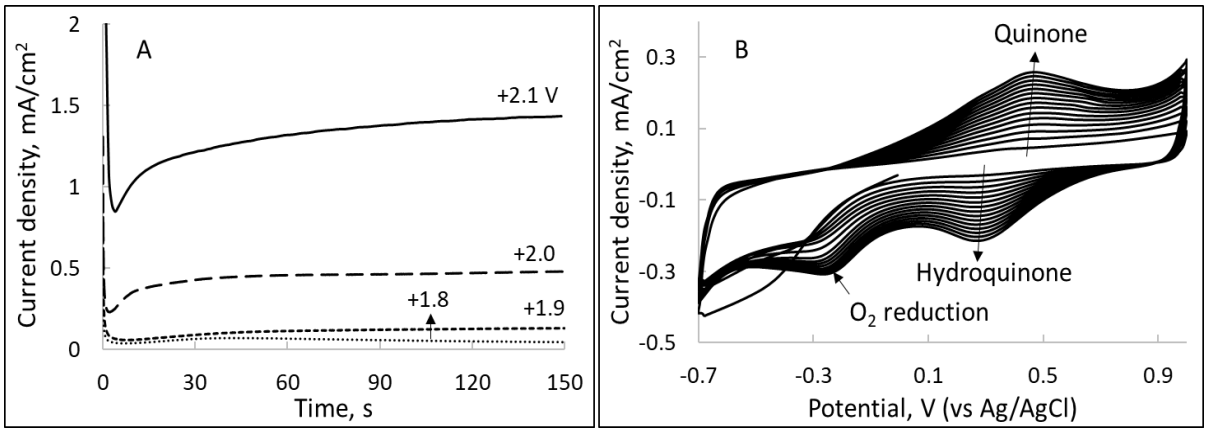

Figure 3.S1. (A) Chronoamperograms of GUITAR modification by application of indicated electrode potential vs. Ag/AgCl and (B) 15 cyclic voltammetric cycles from -0.7 V to +1.0 V at 50 mV/s in 1.0 M H_2SO_4.

Chronoamperometric modification was explored at different potentials (1.8 to 2.1 V) as shown in Figure 3.S1A. The application of 1.8 and 1.9 V vs. Ag/AgCl consists of a current signal decay indicative of capacitive charging. At 2.0 and 2.1 V a faradaic process is observed with increase in current until the end of the run at 150 seconds. Above 2.1 and/or beyond 150 seconds the GUITAR electrodes fail. The potential of 2.1 V vs. Ag/AgCl was therefore selected for the formation of q-GUITAR. Electrode conditioning was required to obtain the quinone functional groups after chronoamperometry at 2.1 V. This was conducted by 15 CV scans from

-0.7 V to +1.0 V at 50 mV/s in 1.0 M H_2SO_4. Figure 3.S1B shows the growth of the hydroquinone/quinone through successive CV scans. A total of 15 cycles was required for complete formation of the quinone moiety on GUITAR.

Attempted Synthesis of q-Graphite

Synthesis of quinone functionalized graphite under the same conditions as q-GUITAR fails as it gives mechanically unstable expanded layers. Figure 3.S2 shows the top and side views for as obtained and the expanded graphite foils after applying same conditions as q-GUITAR.

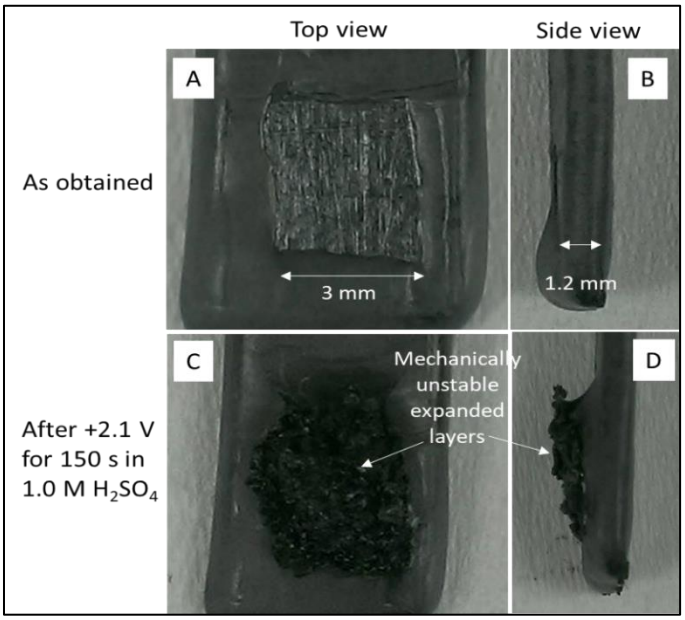

Figure 3.S2. Top view (A & C) and side view (B & D) of as obtained and expanded graphite foil.

Chronoamperometric Responses with Glucose on q-GUITAR

A representative series of amperograms for the determination of COD values with glucose solution on q-GUITAR at +1.6 V is shown in Figure 3.S3. Amperogram-a recorded in 0 mg/L COD (in 0.1 M Na_2SO_4) and b-f are recorded in 2,000-10,000 mg/L COD. Data are collected at

10 sec to construct the calibration curves. A surface regenerative treatment of +1.6 V for 2 min followed by -0.7 V for 3 min in 0.1 M Na_2SO_4 was applied on the q-GUITAR between each amperogram to avoid the signal loss from the surface fouling during oxidation of organics at +1.6 V.

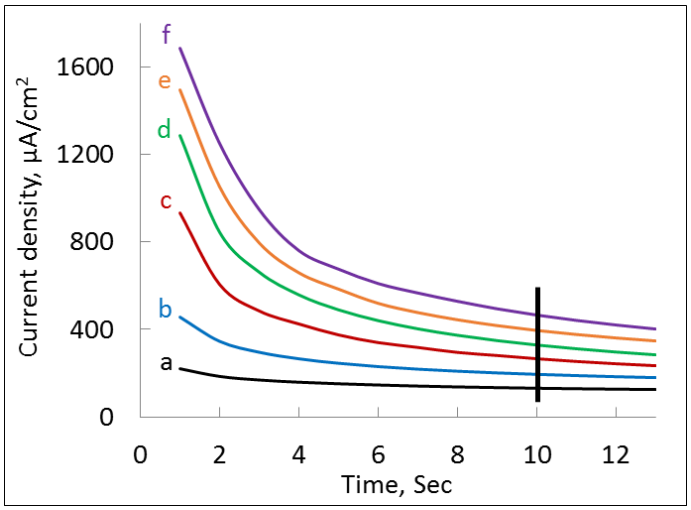

Figure 3.S3. Amperometric response of 0, 2000, 4000, 6000, 8000, and 10000 mg/L COD (a to f respectively) with Glucose in 0.1 M Na_2SO_4 at +1.6 V (vs Ag/AgCl) on q-GUITAR at a sampling time of 10 sec.

Optimization of Working Potential for COD Detection on q-GUITAR

Different working potentials (1.5, 1.6, 1.8 and 2.0 V) were applied on q-GUITAR to determine the COD values with glucose in 0.1 M Na_2SO_4 (Figure 3.S4). Surface regenerative treatment (+1.6 V applied for 2 min followed by -0.7 V applied for 3 min in 0.1 M Na_2SO_4) was applied between each sampling point. 1.8 and 2.0 V showed higher background currents due to both for the corrosion of GUITAR and O_2 evolution. A potential of 1.5 V showed lower sensitivity, therefore 1.6 V was selected as optimum working potential.

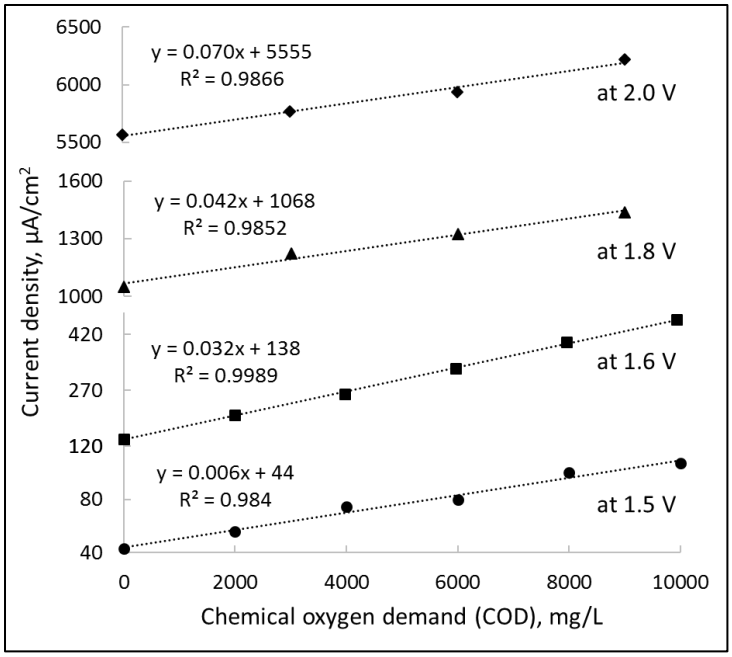

Figure 3.S4. Optimization of working potential for chemical oxygen demand (COD) measurement with glucose in 0.1 M Na_2SO_4 on q-GUITAR.

Optimization of Regeneration of q-GUITAR

The calibration curve of Figure 3.4 on GUITAR and q-GUITAR COD sensing electrodes require surface between each COD measurement. This treatment is conducted in 0.1 M Na_2SO_4. Four regenerative pulses were examined. These include (i) an initial potential of +1.6 V for 2 min followed by -0.7 V for 3 min, (ii) -0.7 V for 3 min followed by +1.6 V for 2 min, (iii) +1.6 V for 2 min and (iv) -0.7 V for 3 min. The best surface regenerative condition was found with (i) which gives the maximum linear range for COD determination as illustrated in Figure 3.S5.

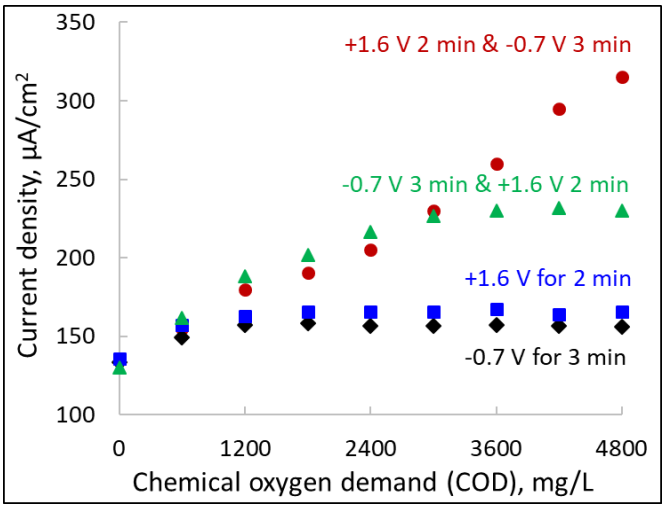

Figure 3.S5. Optimization of surface regenerative treatment on q-GUITAR with methods described above. Potassium hydrogen phthalate was the COD surrogate. The analyses were conducted in 0.1 M Na_2SO_4 at +1.6 V (vs Ag/AgCl).

Chloride Interference

Chloride interferences were studied on q-GUITAR with KCl using chronoamperometric (CA) method at 1.6 V in 0.1 M Na_2SO_4. Figure 3.S6 shows the current densities collected from the CA responses at 10 sec. Up to 100 mg/L of Cl^- no noticeable current increments were observed. Above 100 mg/L Cl^-, CA current gave linear response with chloride concentration.

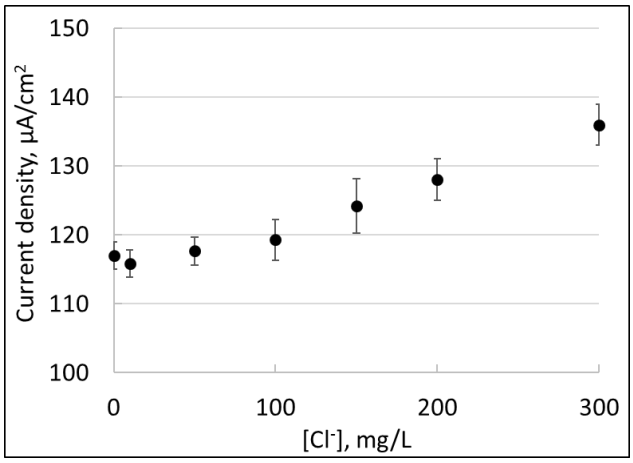

Figure 3.S6. Determination of Cl^- tolerance level for q-GUITAR in 0.1 M Na_2SO_4 at +1.6 V (n=3).

Chapter 4: Application of GUITAR in Cathodic Sensing

"Electrochemical Determination of Free Chlorine on Nanocrystalline Graphite Electrodes (GUITAR)." Talanta 2019 (To be submitted).

Abstract

Nanocrystalline graphite from the University of Idaho Thermolyzed Asphalt Reaction (GUITAR) is a hypothesized new form of carbon. It shares morphological features with graphites, including basal and edge planes. Unlike graphites and other sp^2-hybridized carbons, GUITAR has fast heterogeneous electron transfer across its basal planes and resistance to corrosion similar to boron-doped diamond electrodes. In this contribution GUITAR electrodes were examined as sensors for aqueous free chlorine (HOCl and OCl^-) at pH 7.0 with cyclic voltammetric (CV) and chronoamperometric (CA) methods. Using CV at 50 mV/s GUITAR has a limit of detection of 1.0 µM, linear range of 0-5,000 µM, sensitivity of 215.8 µA/mM-cm^2 and a signal stability of 4 days in constant exposure to 1 mM free chlorine in pH 7.0, 0.1 M phosphate buffer system. After 7 days of exposure GUITAR electrodes lost 37% of the former sensitivity, which was recovered by an *in-situ* regeneration procedure. The common aqueous ions, Ca^{2+}, Na^+, NO_3^-, SO_4^{2-}, Cl^-, CO_3^{2-} and dissolved oxygen did not affect the response of the GUITAR-based sensor. The combination of limit of detection, linear range, sensitivity, sensor lifetime and its relative lack of interferences indicate that GUITAR is one of the best performers in free chlorine sensors.

4.1 Introduction

Nanocrystalline graphite from the University of Idaho Thermolyzed Asphalt Reaction (GUITAR) is a hypothesized new form of carbon. In electrochemical applications it offers many advantages over other carbons. [1,2,3,4,5,6] Its appearance is similar to a crystalline graphite but differs in that both the basal and edge planes (EP) have facile heterogeneous electron transfer (HET) kinetics. [1,2] The basal plane (BP) of graphites have a barrier to HET as these materials are zero-band gap semiconductors. On the other hand, structural defects within the molecular planes of BP-GUITAR increases density of electronic states (DOS) near the Fermi-level with corresponding HET rates. [1,2] With the $Fe(CN)_6^{3-/4-}$ redox probe BP and EP-GUITAR achieve a standard HET rate (k^0) of 10^{-2} cm/s. Electrodes based on BP of graphene and highly oriented pyrolytic graphite (HOPG) have k^0 between 10^{-10} to 10^{-6} cm/s whereas the EP-GUITAR is about 10^{-2} cm/s. [7,8,9,10] Other distinguishing features are slow hydrogen evolution kinetics and that the molecular planes of GUITAR are impervious to sub-surface electrolyte intercalation making it more resistant to corrosion than graphites. [1,3,4,11,12,13] This results in wide electrochemical potential window of 3 V at 200 μA/cm^2 in 1 M H_2SO_4. This surpasses other sp^2 carbon electrodes by 1 V and places it alongside with boron doped diamond. [1,2] These properties make GUITAR suited for applications including electrochemical sensors, batteries, fuel cells, ultracapacitors and water purification. [3,4] Sensing of strongly oxidizing species, e.g. free chlorine, requires resistance to corrosion along with fast HET rates. With those properties in mind, this study examines the application of the unique properties of GUITAR to the electrochemical sensing of free chlorine (sum of dissolved HClO and ClO^-).

Free chlorine is widely used in water disinfection in order to inactivate pathogenic microorganisms such as *Escherichia coli* and *Cryptosporidium*. [14,15,16] It is also used in a variety of other applications spanning from household to the agriculture and food industries. In water treatment, concentration of free chlorine must fall within the range of 20-100 μM according to WHO (World Health Organization) standards. [17,18,19,20,21] In case of industrial processes the concentration tends to fall within 0.01 - 10 mM. [1] Analytical techniques for free chlorine sensing include spectrophotometry, iodimetry, chemiluminiscence, catalyst-assisted flow injection and electrochemistry. [16,22,23,24] The most widely used technique for municipal water samples is colorimetry based on N,N'-diethyl-p-phenylenediamine (DPD) which has narrow concentration linear range and cannot be applied in continuous on-line monitoring systems. [20,25,26,27] In contrast, electrochemical methods offer the promise of a cost effective, portable and rapid detector with continuous monitoring and little or no sample preparation. [28] However, at present electrode materials suitable for chlorine monitoring are expensive and have one or more of the following problems of short lifetime from surface fouling, insufficient limit of detection, narrow linear range or low sensitivity. [23,24,29,30] Present efforts have examined composite materials based on graphene, carbon nanotube, boron doped diamond, platinum, gold and glassy carbon. [19,31,32,33,34,35] In this study, we investigate GUITAR electrodes for free chlorine sensing. Its relative robustness to corrosion and fast HET rates at its basal planes indicates strong possibilities for the continuous detection of strong oxidizing species.

4.2 Experimental Section

Materials and Chemicals: Sodium hypochlorite (5% m/m) was obtained from Acros Organics (NJ, USA). Potassium iodide (99.6%), potassium iodate (99.6%), sodium thiosulfate (99.5-101.0%), glacial acetic acid (99.9%) and starch (1% w/v) were obtained from J. T. Baker (PA, USA) for standardization of sodium hypochlorite. Potassium monophosphate (99.6%), potassium diphosphate (99.8%) and potassium chloride (99.7%) were obtained from Fisher Scientific (Waltham, NJ, USA). All aqueous solutions were prepared with deionized water purified by passage through an activated carbon purification cartridge obtained from Barnstead-model D8922 (IA, USA). GUITAR deposition targets were constructed from quartz tubes (Technical Glass Products, Inc., Painesville Twp., OH, USA) cut into 2cm×0.5cm wafers. Hypochlorite solutions were standardized by iodometric titration and used within three days. [16]

Electrode Fabrication and Electrochemical Setup: GUITAR electrodes were synthesized as described in previous study. [1] Electrode fabrication and geometric area isolation were performed as described previously. [1] All electrochemical studies were conducted in a three-electrode undivided cell with graphite rod counter electrode and Ag/AgCl/3M NaCl (aq) (0.209 V vs SHE) reference electrode and using a Bioanalytical Systems (BAS) CV-50W potentiostat (West Lafayette, IN, USA). Chronoamperometric studies at -0.15 V vs. Ag/AgCl were conducted under mass transport aided conditions by stirring at 800 rpm with a BAS Controlled Growth Mercury Electrode cell stand.

4.3 Results and Discussion

4.3.1 Determination of Free Chlorine on GUITAR Electrodes

The reduction of free chlorine proceeds as Equation 1. [28]

$$ClO^- + 2e^- + 2H^+ = Cl^- + H_2O \qquad E^{0\prime} = 1.49 \text{ (vs SHE) at pH 7} \qquad (4.1)$$

This reaction was examined by both chronoamperometric (CA) (at -0.15 V) and cyclic voltammetric (CV) (at 50 mV/s) methods on GUITAR electrodes (Figure 4.1A and B) at pH 7.0 in various concentrations of free chlorine. The CV peak potential (E_p) appears at -0.15 V (vs Ag/AgCl) in 1 mM free chlorine (Figure 4.1B). The corresponding calibration curves are shown in Figure 4.2. For that figure the CA (Figure 4.2A) current densities were collected from Figure 4.1A at 120 seconds. For the CV calibration curve (Figure 4.2B) E_p current densities are considered. The CA and CV linear ranges are 0.2 - 2.2 and 0 - 5 mM respectively and the sensitivities are 55.24 and 215.83 μA/mM-cm^2 respectively (n=5). The CA and CV limit of detections (S/N = 3) of free chlorine are 0.5 and 1.0 μM respectively.

A comparison of LOD, linear range and sensitivity for free chlorine determination on different materials is shown in Table 4.1. Overall, GUITAR has a good combination of LOD, linear range and sensitivity relative to other electrode materials. The LOD and the linear range of the GUITAR-based sensor gives it more flexibility in use relative to other sensors. It is also noteworthy that GUITAR is expected to be a much lower cost material than the others mentioned in Table 4.1.

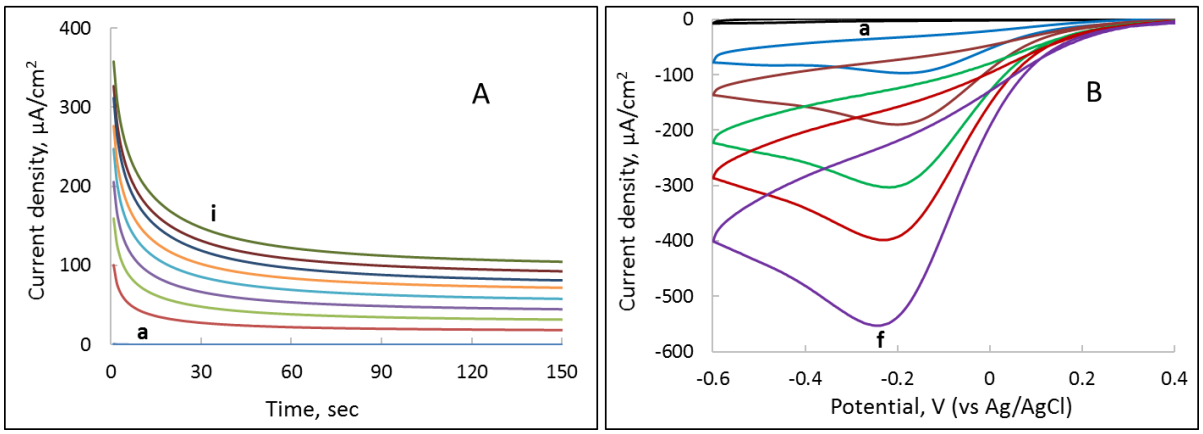

Figure 4.1. Chronoamperometric and cyclic voltammetric responses of flat GUITAR electrode (geometric area 0.10 cm^2) for different concentrations of free chlorine in 0.1 M phosphate buffer solution, pH=7.0, N_2 saturated. A) Chronoamperograms of 0, 0.2, 0.4, 0.6, 0.8, 1.0, 1.2, 1.4 and 1.6 mM free chlorine (a to i respectively) at -0.15 V. B) Cyclic voltammograms of 0, 0.5, 1.0, 1.5, 2.0 and 2.5 mM free chlorine (a to f respectively) at 50 mV/s.

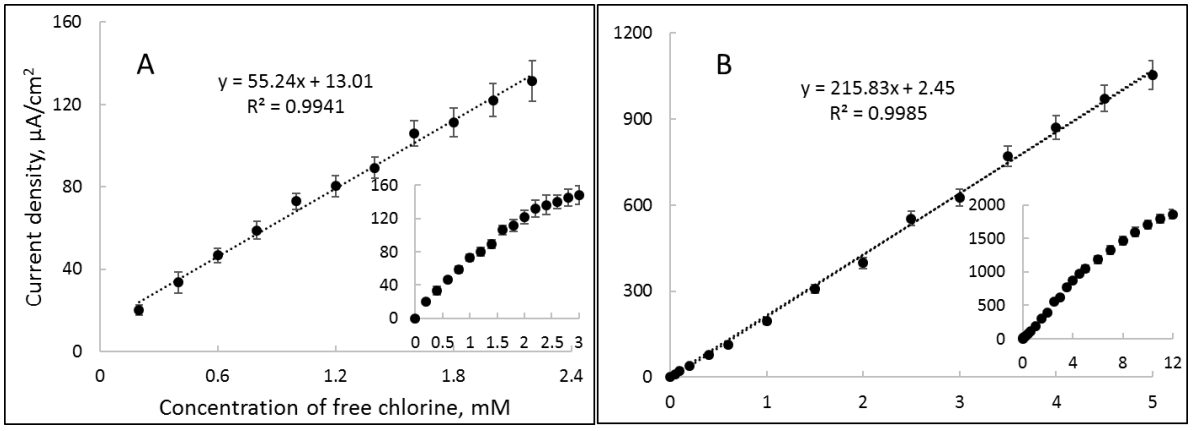

Figure 4.2. Chronomperometric (A) and cyclic voltammetric (B) calibration curves (n = 5) for free chlorine determination on GUITAR in 0.1 M phosphate buffer solution, pH=7.0, under N_2 saturation. The insets show the corresponding entire concentration range responses of this study.

Table 4.1. Comparison of cyclic voltammetric (CV) and chronoamperometric (CA) LOD, linear range, sensitivity, and signal stability for free chlorine sensor electrodes.

Material	LOD (µM)	Linear range (µM)	Sensitivity (µA/mM-cm^2)	Stability
GUITAR (CV)[This work]	1.0	0-5000	215.8	> 7 days[d]
GUITAR (CA)[This work]	0.5	200-2200	55.2	> 7 days[d]
CuO-NPs/MWCNT/epoxy resin[a] [36]	0.085	N/A	17	7 days[d]
Boron doped diamond [19]	0.16	400-2000	38	3 months[d]
Au [34,35,37]	0.2 - 0.4	0.2-300	720	2 days [35] > 7 days [34]
Pt [28,34,38]	0.2 - 1.4	2.8-60	670	6 days [28] 7 days [34]
Carbon nanotube/epoxy resin [29]	0.4	0.4-80	75	30 days
AuNPs-PEDOT/GC[b] [39]	1.0	1-932	200	N/A
Au micro electrode [30]	1.5	0-80	278	N/A
Carbon fiber [40]	1.9	15-800		N/A
Aminated-glassy carbon [41]	1.55	200-2000	283	N/A
Polymelamine modified screen-printed carbon electrode [20]	5.5	10-7000	210	7 days
AuNPs/poly-MnTAPP/GC[c] [24]	24.7	N/A	5	3 days
Aminated-pencil graphite [14]	N/A	0.8-116	15	N/A
Glassy carbon [41]	N/A	0-2000	230	N/A

[a]Copper (II) oxide nanoparticles deposited on multiwall carbon nanotube/epoxy resin
[b]Au nanoparticles-poly(3,4-ethylenedioxythiophene) modified glassy carbon
[c]Poly Manganese tetra (o-amino phenyl) porphyrin-nano Au film modified glassy carbon
[d]With periodic surface cleaning or reactivation
N/A - Not Measured or Not Available

4.3.2 Sensor Performance in the Presence of Possible Interferences

Dissolved oxygen is a possible interference for free chlorine detection as indicated by the formal potential for its reduction. [42]

$$O_2 + 4H^+ + 4e^- \rightarrow 2H_2O \qquad E^{0\prime} = 0.816 \text{ V (vs SHE) at pH 7}$$

Figure 4.3A shows that that the CV reduction peak for dissolved oxygen (air saturation) its -0.45 V which is separated by 300 mV from free chlorine (E_p = -0.15 V). Table 4.2, Rows I and II highlight the results of the CA calibration curve for free chlorine determination in presence of dissolved O_2 (Figure 4.3B) and under N_2 purge (Figure 4.2A). Both have the same slopes and intercept demonstrating that O_2(aq) is not an interference with this sensor.

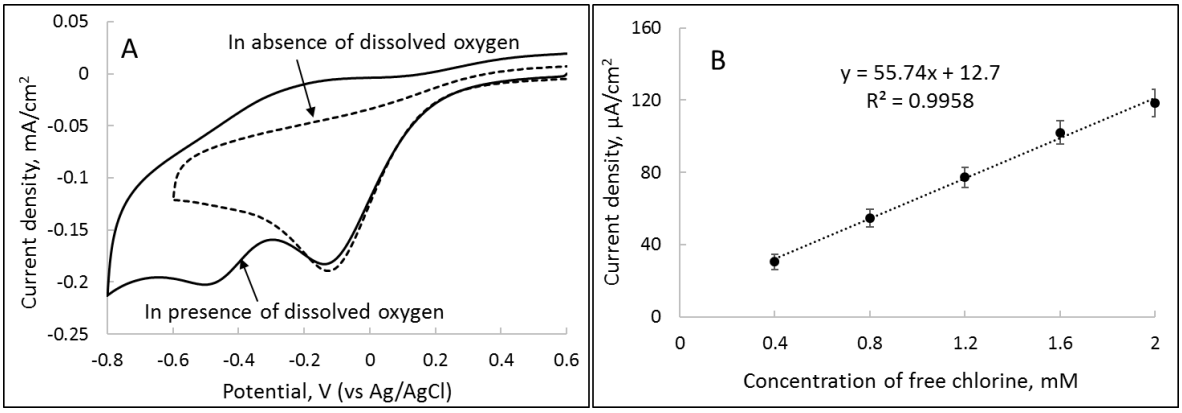

Figure 4.3. (A) CV's of 1 mM free chlorine on GUITAR electrode in presence (solid line) and absence (dashed line) of dissolved oxygen, scan rate 50 mV/s and (B) calibration curve (chronoamperometric) for free chlorine determination in presence of dissolved O_2 at -0.15 V (n=3) in 0.1 M phosphate buffer solution, pH=7.0.

Figure 4.4 shows the effects of other potential interferences. In that study the effects of 100 µL spikes from 10 mM of free chlorine (NaOCl), $NaNO_3$, Na_2SO_4, NaCl and $CaCO_3$ are measured by chronoamperometry. The first two spikes of free chlorine solutions (at 120 and 240 seconds) give proportional responses via Reaction 4.1. The GUITAR electrode did not respond

to the introduction of the other salts. The spike at 840 seconds indicates that the electrode still gives a proportional response to free chlorine.

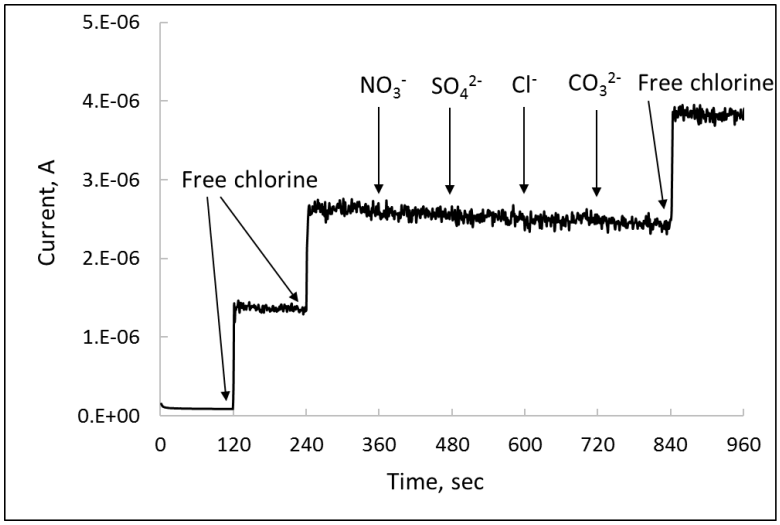

Figure 4.4. Chronoamperometric study of common ions. NO_3^-, SO_4^{2-}, Cl^- and CO_3^{2-} effects on the free chlorine response. Each arrow is an injection of 100 µL from 10 mM of the respective solution (NaOCl, $NaNO_3$, Na_2SO_4, NaCl and $CaCO_3$ respectively) in 10 ml 0.1 M phosphate buffer solution, pH=7.0. None of the ions affected the response of the final free chlorine injection at 840 seconds.

4.3.3 Sensor Stability and Regeneration

The response of GUITAR electrode is found stable after 4 days of continuous exposure to 1 mM free chlorine solution in 0.1 M phosphate buffer solution at pH 7.0 (Figure 4.S2, see supporting information). Table 4.2, Row III shows the sensitivity (slope), intercept and correlation values for each day obtained by chronoamperometry at -0.15 V. After 7 days of continuous exposure in free chlorine solution GUITAR electrodes experience a 37% loss in sensitivity (from 56.8 to 35.7 µA/mM-cm^2) as shown in Figure 4.S3 and summarized in Table 4.2, Row III. This signal loss is associated with the passivation of GUITAR surface during exposure to hypochlorite and dissolve oxygen, and electrochemical reduction of hypochlorite. This passivation effect is also experienced on other literature materials.

[19,28,34,35,43,44] An *in-situ* regeneration protocol was developed to extend the lifetime of this sensor. This process applied -1.6 V (vs Ag/AgCl) for 10 min in 0.1 M phosphate buffer solution, pH=7.0 and and was able to clean GUITAR surface by reducing the passivation layer. The regenerated GUITAR electrode recovered 94% of the initial sensitivity (Figure 4.S3 and Table 4.2 Row IV). No attempts were made at extending the lifetime of GUITAR-based sensors beyond one week, but it is reasonable to expect that the electrode will undergo several regeneration cycles as demonstrated in a previous investigation. [2] Literature reports free chlorine sensor electrodes with signal stabilities from hours to several months (see Table 4.1). Again, when considering LOD, linear range, sensitivity along with sensor lifetime, GUITAR electrodes are very competitive with literature.

Table 4.2. Summary of chronoamperometric sensing of free chlorine at GUITAR electrodes highlighting sensitivities, intercept and r^2 of the calibration curves obtained under the specified conditions.

Row			Sensitivity (μA/mM-cm^2)	Intercept	r^2	Number of electrode samples, n
I under N_2	Figure 2A		55.2	13.0	0.99	5
II under air	Figure 3B		55.7	12.7	0.99	3
III	Stability Tests	Day				
		1	56.8	12.1	0.99	3
		2	56.2	12.5	0.99	3
		3	53.0	14.0	0.98	3
		4	55.5	12.8	0.98	3
		7	35.7	6.5	0.98	3
IV	Regenerated		53.5	11.8	0.99	3

4.4 Conclusions

The focus on electrochemical free chlorine sensors have been with materials of relatively high costs. It is expected that GUITAR will be inexpensive relative to these materials (see Table 4.1) with competitive detection limit, linear range, and sensitivity. Furthermore, GUITAR is not affected from possible common aqueous interferences O_2, Ca^{2+}, Na^{+}, NO_3^{-}, SO_4^{2-}, Cl^{-} and CO_3^{2-}. A significant feature of GUITAR is long term signal stability and the ability to recover sensitivity with the eventual fouling of the electrode surface. Relative to recent advances in fluorescence method and classical colorimetric method (N,N-diethyl-p-phenylenediamine), the presented technique of this study has much wider linear range (0.05-15 vs. 0-5000 µM). Furthermore, the GUITAR-based method is more rapid and offers continuous monitoring capabilities. Another feature is that GUITAR electrodes can be fabricated into a variety of geometries including micron and smaller dimensions. These qualities indicate possible application ranging from home use to embedded sensors where durability and continuous monitoring is required.

4.5 Reference

1) Kabir, H.; Zhu, H.; May, J.; Hamal, K.; Kan, Y.; Williams, T.; Echeverria, E.; McIlroy, D. N.; Estrada, D.; Davis, P. H.; Pandhi, T.; Yocham, K.; Higginbotham, K.; Clearfield, A.; Cheng, I. F. CARBON 2019, 144, 831-840.

2) Gyan, I. O.; Wojcik, P. M.; Aston, D. E.; Mcllroy, D. N.; Cheng, I. F. ChemElectroChem 2015, 2(5), 700–706.

3) Gyan, I. O.; Cheng, I. F. Microchemical Journal 2015, 122, 39–44.

4) Kabir, H.; Gyan, I. O.; Foutch, J. D.; Zhu, H.; Cheng, I. F. C - Journal of Carbon Research 2016, 2, 13.

5) Xie, Y.; McAllister, S. D.; Hyde, S. A.; Sundararajan, J. P.; Kengne, B. A. F.; McIlroy, D. N.; Cheng, I. F. Journal of Materials Chemistry 2012, 22, 5723.

6) Cheng, I. F.; Xie, Y.; Gonzales, R. A.; Brejna, P. R.; Sundararajan, J. P.; Kengne, B. A. F.; Aston, D. E.; McIlroy, D. N.; Foutch, J. D.; Griffiths, P. R. CARBON 2011, 49, 2852-2861.

7) Cline, K. K.; McDermott, M. T.; McCreery, R. L. Journal of Physical Chemistry 1994, 98, 5314-5319.

8) Ambrosi, A.; Pumera, M. Journal of Physical Chemistry C 2013, 117, 2053-2058.

9) Brownson, D. A. C.; Munro, L. J.; Kampouris, D. K.; Banks, C. E.; RSC Advances 2011, 1, 978-988.

10) Henstridge, M. C.; Shao, L.; Wildgoose, G. G.; Compton, R. G.; Tobias, G.; Green, M. L. H. Electroanalysis 2008, 20, 498-506.

11) Hathcock, K. W.; Brumfield, J. C.; Goss, C. A.; Irene, E. A.; Murray, R. W. Analytical Chemistry 1995, 67, 2201-2206.

12) Alsmeyer, D. C.; McCreery, R L. Analytical Chemistry 1992, 64, 1528-1533.

13) Kabir, H.; Gyan, I. O.; Cheng, I. F. Journal of Power Sources 2017, 342, 31-37.

14) Pan, S; Deen, M. J.; Ghosh, R. Analytical Chemistry 2015, 87, 10734−10737.

15) Lu, T.; Zhang, L.; Sun, M.; Deng, D.; Su, Y.; Lv, Yi. Analytical Chemistry 2016, 88, 3413−3420.

16) Wang, B.; Anzai, J. International Journal of Electrochemical Science 2015, 10, 3260-3268.

17) Fayer, R. Applied and Environmental Microbiology 1995, 61(2), 844−846.

18) Venczel, L. V.; Arrowood, M.; Hurd, M. Applied and Environmental Microbiology 1997, 63(4), 1598−1601.

19) Murata, M.; Ivandini, T. A.; Shibata, M.; Nomura, S.; Fujishima, A.; Einaga, Y. Journal of Electroanalytical Chemistry 2008, 612, 29–36.

20) Senthilkumar, K.; Zen, J. M. Electrochemistry Communications 2014, 46, 87–90.

21) Simpson, K. L.; Hayes, K. P. Water Research 1998, 32, 1522−1528.

22) Soldatkin, A. P.; Gorchkov, D. V.; Martelet, C.; Renault, N. Sensors and Actuators B 1997, 43, 99.

23) Zhu, Z.; Xu, Y.; Liu, W.; Shao, C.; Wu, H.; Jiang, H.; Du, B.; Zhang, X. Sensors and Actuators B 2014, 191, 473.

24) Thiagarajan, S.; Wu, Z. Y.; Chen, S. M. Journal of Electroanalytical Chemistry 2011, 661, 322–328.

25) Hu, H. C. Journal of American Water Works Association 1981, 73(3), 150-153.

26) Moberg, L.; Karlberg, B. Analytica Chimica Acta 2000, 407, 127−133.

27) White, G. C. Handbook of Chlorination and Alternative Disinfectants, 5th ed.; Wiley: New York, 2010.

28) Ordeig, O.; Mas, R.; Gonzalo, J.; Campo, F. J. D.; Muñoz, F. Electroanalysis 2005, 17(18), 1641-1648.

29) Monllau, R. O.; Pereira, A.; Bartrolí, J.; Baeza, M.; Céspedes, F. Talanta 2010, 81, 1593–1598.

30) Lee, W. H.; Ma, X. M. Austin Journal of Biosensors and Bioelectronics 2015, 1(2), 1006.

31) Salazar, P.; Martin, M.; Garcia, F. J. G.; Mora, J. L. G.; Elipe, A. R. G. Sensors and Actuators B 2015, 213, 116−123.

32) Dong, Y.; Li, G.; Zhou, N.; Wang, R.; Chi, Y.; Chen, G. Analytical Chemistry 2012, 84(19), 8378−8382.

33) Hsu, L. H. H.; Hoque, E.; Kruse, P.; Ravi S. P. Applied Physics Letters 2015, 106(6), 63102.

34) Campo, F. F. D.; Ordeig, O.; Muñoz, F. Analytica Chimica Acta 2005, 554, 98–104.

35) Monllau, R. O.; Orozco, J.; Sánchez, C. F.; Baeza, M.; Bartrolí, J.; Jorquera, C. J.; Céspedes, F. Talanta 2009, 77(5), 1739−1744.

36) Munoz, J.; Cespedes F.; Baeza, M. Microchemical Journal 2015, 122, 189–196.

37) Tsaousis, A. N.; Huber, C. O. Analytica Chimica Acta 1985, 178, 319-323.

38) Awad, M. I.; Sata, S.; Ohsaka, T. Electroanalysis 2005, 17(9), 769–775.

39) Tsai, T. H.; Lin, T. K. C.; Chen, S. M. International Journal of Electrochemical Science 2011, 6, 2672-2687.

40) Li, X. A.; Zhou, D. M.; Xu, J. J.; Chen, H. Y. Talanta 2008, 75, 157–162.

41) Watanabe, H.; Uchiyama, S. Bunseki Kagaku 2007, 56(6), 433-437.

42) Ishii, S.; Watanabe, K.; Yabuki, S.; Logan, B. E.; Sekiguchi, Y. Applied and Environmental Microbiology 2008, 74(23), 7348-7355.

43) Kozin, L. F.; Prokopenko, V. A.; Bogdanova, A. K. Protection of Metals 2005, 41(1), 22–29.

44) Qin, Y.; Kwon, H. J.; Howlader, M. M. R.; Deen, M. J. RSC Advances 2015, 5, 69086-69109.

Supporting Information

Stability of the GUITAR Electrode Signal in Free Chlorine: The response of GUITAR electrode is found stable after 4 days of continuous exposure to 1 mM free chlorine.

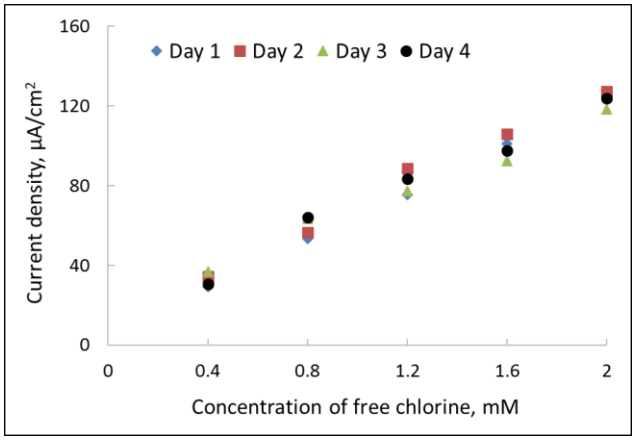

Figure 4.S1. Amperometric calibration curves on GUITAR electrode in 1 mM free chlorine (in 0.1 M PBS, pH=7.0) at -0.15 V for 4 consecutive days. GUITAR electrode was stored in free chlorine solution and no surface regeneration treatment was applied in between.

Regeneration of GUITAR Electrode: GUITAR electrode can be regenerated after signal loss by applying -1.6 V (vs Ag/AgCl) for 10 min in 0.1 M phosphate buffer solution, pH=7.0.

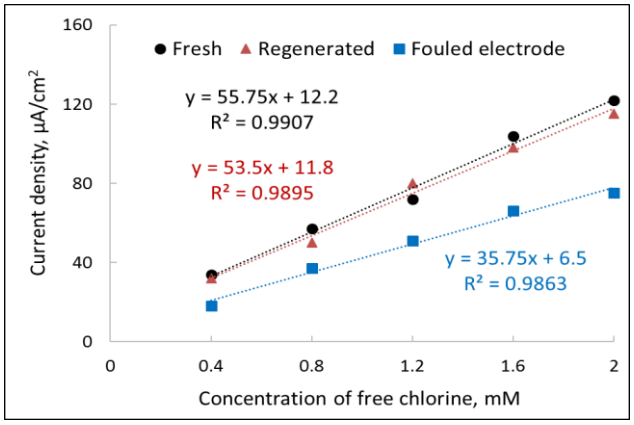

Figure 4.S2. Amperometric calibration curves for free chlorine determination on fresh, fouled and regenerated GUITAR electrodes in 0.1 M PBS, pH=7.0 at -0.15 V. Fouled electrode: 7 days of continuous exposure in free chlorine. Electrode regeneration: -1.6 V (vs Ag/AgCl) for 10 min in 0.1 M PBS, pH=7.0.

Chapter 5: Conclusions

GUITAR is one of the purest carbon forms grown by chemical vapor deposition (CVD) method. While other CVD deposited carbon materials contain different contaminations and high oxygen content, GUITAR contains no such contamination as well as no oxygen groups. GUITAR synthesis method is less expensive, much safer and simpler. It is expected that GUITAR will prove to be more economically viable for large-scale implementation relative to other expensive carbon materials, like as boron-doped diamond, glassy carbon, graphene, carbon nanotubes, etc. Another feature is that GUITAR electrodes can be fabricated into a variety of geometries including micron and nano dimensions. GUITAR is characterized by different techniques over the past couple of years including SEM, TEM, AFM, elemental analyzer, XPS, Raman spectrometer, TGA, XRD, and electrochemical analyzer. As a summary of these characterization, it can be mentioned that GUITAR contains classical basal and edge plane morphology like as graphite, but the surface topography is noticed atomically rough. GUITAR contains 88% carbon (with a sp^2/sp^3 ration of 85/15) and 12% hydrogen. GUITAR is nanocrystalline with average grain size 1.6 nm and has high defect density. These high defect densities provide a higher density of electronic states at the Fermi-level and eventually makes GUITAR electrochemically more active. Therefore, GUITAR possesses high heterogeneous electron transfer rate. GUITAR also has wide potential window and high corrosion resistance which might be associated with the interconnection between GUITAR layers, which blocks the intercalation of ions into the GUITAR layers. The interlayer distance in GUITAR (0.350 nm) appears little wider than in classical graphite (0.335 nm). The overall performance of GUITAR

in electrochemical energy storage (VRFB) and sensing (COD and ClO^-) is obtained as one of the top performers when compared with other literature reported materials. These qualities indicate potential application of GUITAR based electrodes in different fields ranging from domestic to industrial use.